Mechanisms of heat-induced lifespan extension in Saccharomyces cerevisiae and Caenorhabditis elegans

Musa, Marina

FACULTY OF SCIENCE

Postgraduate University Study of Biophysics

Doctoral thesis

Mechanisms of heat-induced lifespan extension in *Saccharomyces cerevisiae* and *Caenorhabditis elegans*

Marina Musa

Split, October 2019

BASIC DOCUMENTATION CARD

University of Split
Faculty of Science

PhD. thesis

Mechanisms of heat-induced lifespan extension in *Saccharomyces cerevisiae* and *Caenorhabditis elegans*

Marina Musa

Mediterranean Institute for Life Science

Abstract

Aging is a process almost all known organisms undergo and it is accompanied by a general loss of function of all important physiological processes, including reduced resistance to cellular stress. While different stresses such as heat or oxidative stress are generally detrimental to the cell and the organism, if they are short and mild enough, they can benefit the organism and confer increased stress resistance later in life and prolong lifespan. This phenomenon is known as hormesis. By studying and comparing the response of the cell to heat stress in *S. cerevisiae* and *C. elegans*, we wanted to better understand what is necessary for the stress to produce a hormetic effect. Research into the molecular mechanisms of hormesis can give us a better picture of the processes required for the maintenance of stress resistance in cells, how it can be preserved or restored in aging cells, and its effects in lifespan.

(110 pages, 52 figures, 7 tables, 212 references, original in English)
Thesis deposited in National and University Library in Zagreb, University Library in Split, Library of the Faculty of Science, University of Split.

Keywords: aging, chaperones, heat shock response, homeostasis, lifespan

Supervisor: dr. sc. Anita Kriško, group leader
Co-supervisor: prof. Miroslav Radman

Reviewers: 1. dr.sc. Sandra Sobočanec
2. dr.sc. Katarina Vukojević
3. prof.dr.sc. Irena Drmić Hofman

Thesis accepted: September 18th, 2019

TEMELJNA DOKUMENTACIJSKA KARTICA

Sveučilište u Splitu
Prirodoslovno-matematički fakultet Doktorski rad

Mehanizmi produljenja života uslijed toplinskog šoka u *Saccharomyces cerevisiae* i *Caenorhabditis elegans*

Marina Musa

Mediteranski institut za istraživanje života

Sažetak

Starenje je proces koji se događa u skoro svim poznatim organizmima, a prati ga opći gubitak funkcije svih značajnih fizioloških procesa, uključujući otpornost na stanični stres. Dok različiti stresori poput visoke temperature ili oksidativnog stresa su generalno pogubni za stanicu i organizam, ako je stres dovoljno kratak i blag, može imati pozitivan utjecaj na organizam, učiniti ga otpornijim na stres kasnije u životu, te produžiti životni vijek. Ovaj fenomen se naziva hormeza. Istražujući i uspoređujući stanični odgovor na toplinski stres u *S. cerevisiae* i *C. elegans*, željeli smo bolje razumjeti što je potrebno da stres proizvede hormetski efekt. Istraživanje molekularnih mehanizama hormeze nam može dati bolji uvid u procese koji su potrebni da bi stanica održala otpornost na stres, kako se otpornost na stres može održati ili čak povratiti u starijim stanicama, te njen utjecaj na životni vijek.

(110 stranica, 52 slike, 7 tablica, 212 literaturnih navoda, 1 prilog, izvornik napisan na engleskom jeziku)
Rad je pohranjen u Nacionalnoj sveučilišnoj knjižnici u Zagrebu, Sveučilišnoj knjižnici u Splitu, knjižnici Prirodoslovno-matematičkog fakulteta Sveučilišta u Splitu.

Ključne riječi: homeostaza, proteinski šaperoni, stanični odgovor na stres, starenje, životni vijek

Mentori: Dr.sc. Anita Kriško
Prof.dr.sc. Miroslav Radman

Ocjenjivači: 1. Dr.sc. Sandra Sobočanec
2. Izv.prof.dr.sc. Katarina Vukojević
3. Prof.dr.sc. Irena Drmić Hofman

Rad prihvaćen: 18. rujna 2019.

Acknowledgments

The making of this thesis would not be possible without effort, support and encouragement of a very special group of people.

Firstly, I would like to thank Anita Kriško for years of support and mentoring. Without her this project truly wouldn't be possible.

To Miroslav Radman, thank you for inspiring us and always being open for discussions and sharing your knowledge and experiences.

A special thank you goes to Ira Milošević and Nuno Raimundo, who welcomed me into their labs and without who this thesis would not be what it is today.

I would also like to express gratitude to my labmates and collegues: Marina R, Marina K, Tea, Anita, Andrea, and, last but certainly not the least, Matea. This project was a joint effort and is a joint accomplishment.

Finally, a big thank you to my friends and family for their support and encouragement.

CONTENTS

List of figures

List of tables

Abbreviations

CCCP	carbonyl cyanide m-chlorophenyl hydrazine
DCFDA	2',7'-dichlorodihydrofluorescin
DMSO	Dimethyl sulphoxide
ER	Endoplasmic reticulum
ETC	Electron transport chain
FA	Fatty acid
FUDR	5'-Fluoro-2'-deoxyuridine

UPR	Unfolded protein response
OXPHOS	Oxidative phosphorylation
HGPS	Hutchinson-Gilford progeria syndrome
HS	Heat shock
HSR	Heat shock response
OGT	Optimal growth temperature
ROS	Reactive oxygen species
SOD	Superoxide dismutase

1. INTRODUCTION

1.1. Aging

Aging is a process characterized by an accumulation of changes at all levels of biological organization. As such, aging can refer to single cells, which have stopped dividing i.e. cellular senescence, or to the increasing age of the entire population or cohort. In humans, aging encompasses an array of physical, physiological, and social changes.

1.1.1. Theory of aging

Why do we age to begin with? How did this trait even evolve and was not selected against, being so obviously undesirable? Through evolution, organisms are optimized for survival in order to pass on their genes to the next generation. In nature, where resources are limited, a 'decision' has to be made whether to invest the energy into reproduction or into repair and maintenance mechanisms i.e. longevity. Thus, there is always a trade-off between the two. In youth, selection pressure is high and, consequently, resources are allocated to ensure survival of progeny. Therefore, genes and traits that increase fitness in any given set of conditions will be favoured by strong selection pressure. However, as the organism ages the selection pressure decreases; traits that arise later in life, especially those traits that manifest beyond reproductive period, are subject to practically no selection (Charlesworth, 2000; Hamilton, 1966).

Therefore, if a gene or a trait is beneficial early in life it is strongly favoured, and through genetic drift can become widespread in the population, even if it turns out to be detrimental later in life. By the time the deleterious effects are manifested there is no way to weed the underlaying mutation out from the population as it has most likely already been passed on to the next generation i.e. there is no negative selection pressure. Similarly, aging could be a consequence of new deleterious mutations accumulating as the selection pressure decreases. These ideas are the basis of two mainstream theories of aging: antagonistic pleiotropy theory and disposable soma theory (Figure 1.1.). Both theories emphasize the trade-off between Darwinian fitness and longevity. With the advancements in medicine and overall increase in the standard of living, today humans live longer than our ancestors, with median population age higher than ever, thus experience such deleterious effect more so than previous generations.

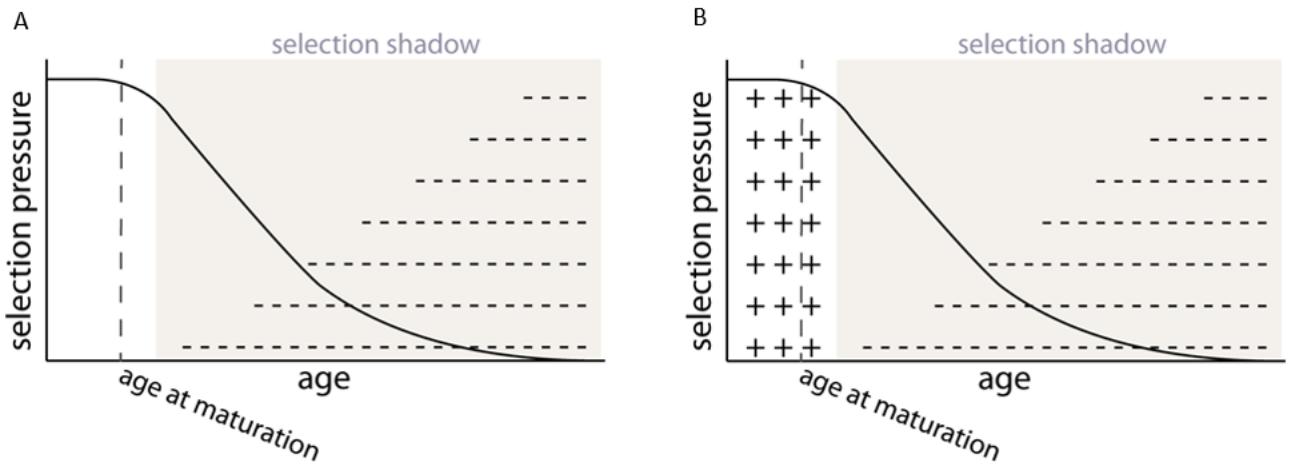

Figure 1.1. Antagonistic pleiotropy and disposable soma theories of aging are based on two main ideas of Darwinian trade-off. These two theories are based on the fact that natural selection is low or non-existent past the reproductive period of the organisms, therefore this period is named ″selection shadow″. In these theories there are two main scenarios which would promote aging: at the onset of the ″selection shadow″ deleterious mutations are allowed to accumulate in the absence of selection pressure (A), or mutations which provided advantage in youth when selection pressure is high but are deleterious later in life are selected for early and cannot be eliminated past the reproductive period (B).

While these theories explain how aging evolved, there is still much to learn about how it progresses. With the increased body of knowledge about aging it has become clear that aging is not a result of one process alone, be it genetic factors or accumulating damage, but that it is influenced by a combination of genetic and environmental factors. The cumulative effect of their influence, as well as their interplay on the cellular level, is most likely to be crucial in driving the aging process. Further, as humans are already defying primary natural selection through leaps in medicine and increased standards of living, the possibility to slow down or alleviate aging has never seemed as feasible as it does today.

1.1.2. Hallmarks of aging

There is a number of changes of cellular content and structure that have been associated with aging and age-related diseases, but which of these changes cause aging and which simply accompany and drive aging once it has already started, is far from well understood. Lopez-Otin and others have defined a list of hallmarks of aging common to different organisms; genomic instability, telomere attrition, epigenetic alterations, loss of proteostasis, deregulated nutrient sensing, mitochondrial dysfunction, cellular senescence, stem cell exhaustion, and altered intercellular communication (Figure 1.2.)(López-Otín, Blasco, Partridge, Serrano, & Kroemer, 2013). These hallmarks are singled out based on the following criteria: they must be present during normal aging, while their worsening should promote, and conversely, their amelioration should impede aging. Of these hallmarks, current understanding is that genomic instability, the shortening of telomeres, changes in epigenetics and proteostasis are likely causative, while senescence, mitochondrial dysfunction and deregulation of nutrient sensing occur as responses to damage, resulting in stem cell exhaustion and changes in intercellular communication (López-Otín et al., 2013). How these hallmarks cause or accompany aging and how they interconnect is still a subject of active research.

Lopez-Otin and collegues also draw an interesting parallel between aging and cancer: while the former is characterized by loss of function and fitness, the latter is a product of aberrant gain of fitness, hyperactivity and overgrowth, but both are simply different manifestations of time dependent accumulation of damage to cellular components. Interestingly, activation of TOR pathway has been associated with aging, meaning that common description of aging as an overall loss of function is not adequate (short of being the loss of negative control of TOR), and it could be more aptly described as loss of homeostasis.

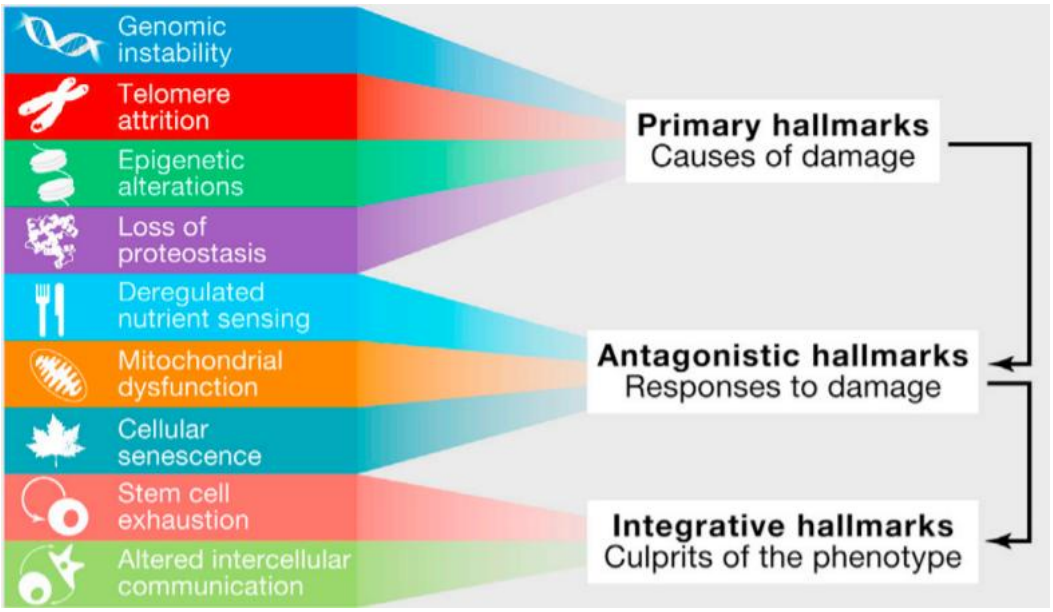

Figure 1.2. Interconnections between the proposed hallmarks of aging and the process of aging. Hallmarks are grouped based on their proposed functional role in aging: cause of damage (top), response to damage (middle) and the phenotype (bottom). Image taken from (López-Otín et al., 2013)

1.1.3. TOR and aging

Target of Rapamycin kinase or TOR (TOR1) is a kinase conserved from yeast to mammals. It is a component of the TOR complex (TORC) as a part of which it regulates a number of vital cellular processes (Figure 1.3.). TORC senses nutrients and oxygen and integrates upstream input from hormone and growth factor signalling. Thus, it is a central metabolic regulator. Drug Rapamycin specifically inhibits TORC1, which has proved beneficial for organism's health; decrease of TOR activity is associated with increased longevity in both yeast and *C. elegans*, as well as in mammals (S. C. Johnson, Rabinovitch, & Kaeberlein, 2013; Kaeberlein et al., 2005; Musa et al., 2018; Perić et al., 2017; Semchyshyn & Valishkevych, 2016; Wei et al., 2009).

TOR pathway is considered to support the antagonistic pleiotropy theory of aging, as loss of TOR early in life causes developmental arrest, while loss of TOR or its inactivation in adulthood is shown to be beneficial across organisms (Gangloff et al., 2004; Murakami et al., 2004; Pan & Shadel, 2009; Wei et al., 2009). TOR inhibits autophagy, stimulates translation and increase translational error rate

(Kamada et al., 2000; Ma & Blenis, 2009), which is conductive to production and aggregation of misfolded proteins, while their clearance is impaired.

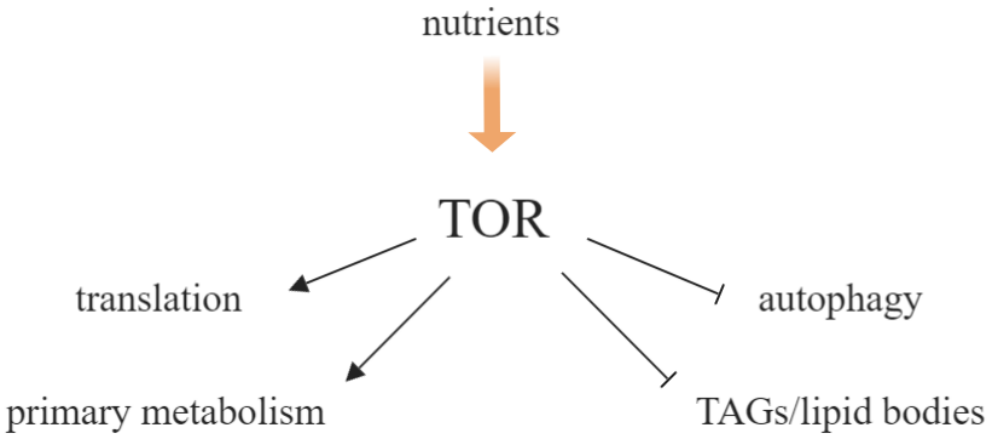

Figure 1.3. TOR is a central metabolic regulator. TOR senses nutrient and energy status of the cell, and modifies metabolism accordingly. While TOR is essential in development, its activity later in life is associated with decreased longevity.

1.2. Proteostasis

Proteins are the work-horse of the cell, having a role in everything from catalysis (synthesis of all cellular molecules, including proteins), cell structure and maintenance, relaying signals inside and between cells, intercellular transport etc. Proteins are also key to DNA replication and maintenance. Therefore, their proper synthesis and maintenance is key cellular life.

Research done on extremophile *Deinoccocus radiodurans*, a bacterium extremely resistant to desiccation and radiation, showed that when irradiated with high doses of gamma radiation, its genome is seemingly irreparably damaged, but the organism is able to repair it and survive regardless. Krisko et al. showed that the *D. radiodurans* DNA itself is not unusually protected in any way, but its proteins are – the proteins of *D. radiodurans* sustain minimal damage following massive doses of radiation, and are therefore able to repair its DNA, thus allowing its successful replication and cell division in the future (Krisko & Radman, 2010). Protein sensitivity to oxidation has been positively correlated to mutation rate (Krisko & Radman, 2013) – therefore proteostasis is key to

both cell survival and maintenance of DNA, errors in which would affect both the current population and future ones if the errors are not lethal.

1.2.1. Homeostasis

Cellular homeostasis refers to the state of equilibrium – all cell processes are maintained at optimum running capacity and adjusted to the current environmental conditions to ensure that the cell maintains its function. Maintenance of cellular homeostasis requires coordination at different levels of organization – disruptions in the DNA likely lead to aberrant translation, therefore changing protein amino acid sequence, and consequently, affecting secondary and tertiary structure. As demonstrated on *D. radiodurans*, damage to DNA can be fixed if the proteins are left intact, but direct damage to proteins, especially ribosomal proteins and rRNA will lead to errors in protein amino acid sequence despite correct DNA template. If proteins are unable to fold to their native conformation, their activity and interaction with both their partner molecules will be compromised, resulting in loss of cellular homeostasis and fitness. To counter environmental insults to homeostasis, diverse cellular mechanisms have evolved to ensure that cellular processes and structures at all levels are properly regulated, located, and coordinated.

1.2.2. Protein folding

To be able to perform their function properly, all proteins must assume a correct tertiary structure or native state. The protein fold is determined by the numerous non-covalent interactions between amino acids in the polypeptide sequence i.e. the protein primary structure. Therefore, each sequence of different amino acids will fold into a specific shape that is associated with a specific function. The native state of the protein is a low energy, stable structure. Proteins are synthesised as long polypeptide chains, which fold into their secondary and tertiary structure after leaving the ribosome. Between the polypeptide chain and the native state there are intermediary structures or folding intermediates which represent local energy minima, thus presenting an energy barrier to native protein folding (Figure 1.4.). Furthermore, misfolded and damaged proteins tend to form aggregates which can be toxic to the cell if accumulated. These protein aggregates are also low energy structures, and thus favoured in absence of a safety mechanism that would challenge their formation. A class of proteins called chaperones assist and facilitate the folding process, ensuring a functional protein conformation, while removing the already damaged proteins from the soluble phase. In other

words, chaperones are essential in maintaining suitable protein folding environment (Hartl & Hayer-Hartl, 2009).

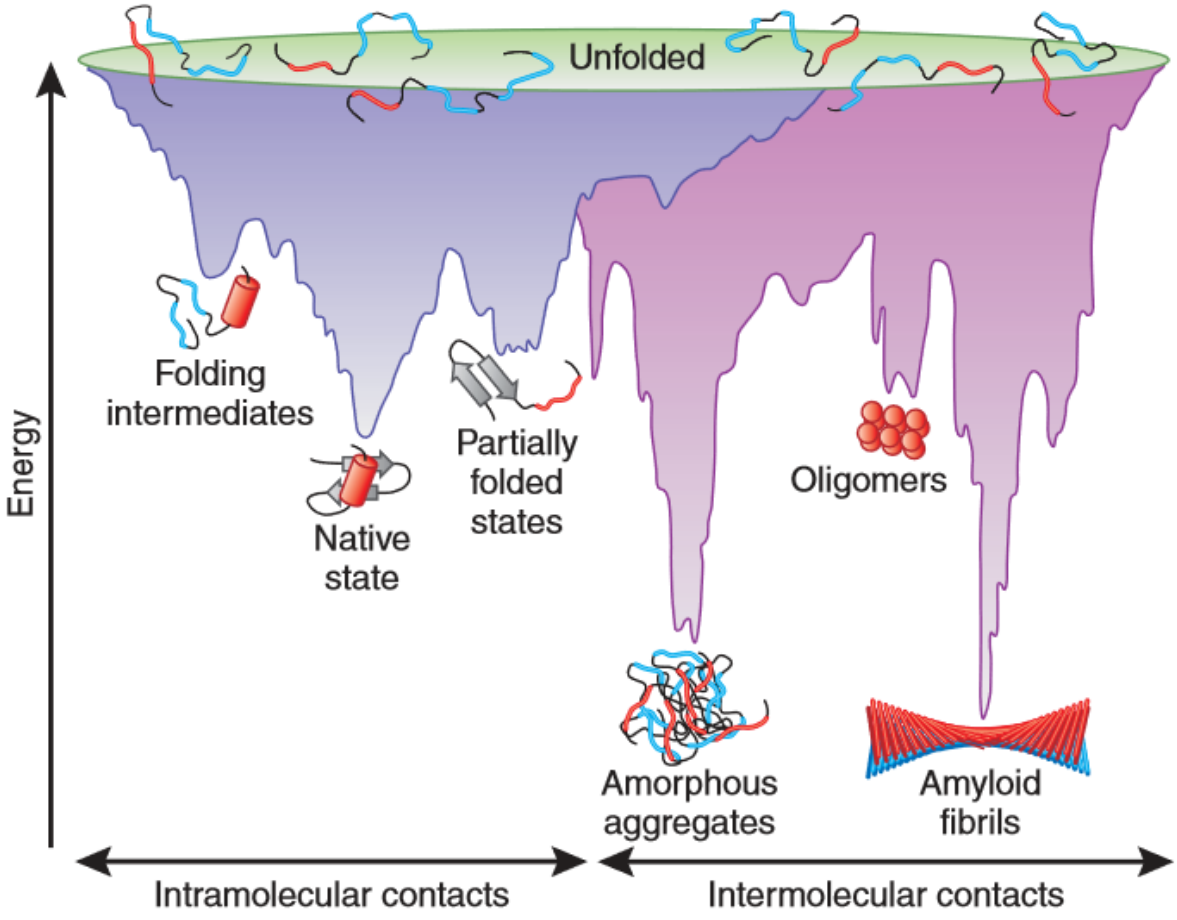

Figure 1.4. Protein folding energy landscape. Various conformations are 'funnelled' towards the native or aggregated state through intramolecular interactions. The blue and purple areas represent folding into native state and aggregated state, respectively; the two energy surfaces are overlapping. Aggregates can be formed both from de novo synthesized proteins and from destabilized native state proteins. Aggregation is countered by molecular chaperones. Image taken from (Hartl & Hayer-Hartl, 2009).

1.2.3. Chaperones

Chaperones oversee maintenance of protein homeostasis or proteostasis, both through ensuring proper folding and by recognizing and removing misfolded and damaged proteins (Koga, Kaushik, & Cuervo, 2011). Proteins can be damaged as a consequence of exogenous cell stress, but also during normal cell function. Conformational changes, for example during translocation, often expose protein hydrophobic regions; chaperones bind to these regions and in that way inhibit unspecific binding with other proteins. Different types of chaperones are summarized in Table 1.1.

Table 1.1. A summary of major chaperone families.

	Function	Notable examples
Chaperonins	Ring shaped chaperones which encapsulate non native proteins up to 60 kDa in size in an ATP dependent manner. Depending on the folding properties of the polypeptide chain, it folds either after being released from the chaperonin or during encapsulation, which provides favourable folding microenvironment, as interaction with other proteins is eliminated.	GroEL, GroES, TRiC
Hsp70	Involved in de novo folding of proteins in physiological conditions, during stress they can refold proteins and help prevent aggregation. Contains ATPase domain and protein binding domain which is composed of seven mainly hydrophobic amino acids in a stretch; the affinity for the substrate is high in the posthydrolysis ADP state. Activity of Hsp70 is regulated by cofactors which bind non-native proteins and deliver it to Hsp70. The cofactors are J-domain containing proteins, and the J domain stimulates the hydrolysis of bound ATP. Hsp70 assists with folding proteins and dissolving aggregates, but the extent of its action is still being researched. It is one of the most conserved chaperones.	DnaK, Hsc70, Hsp70, BiP, Hsp110/Grp170
Hsp100	Subdivided classes 1 and 2 based on the number of AAA	Clp, Hsp104

	domains. Hexameric rings through which protein is unfolded, enabling it to be refolded to native state. Hsp100 class 1 proteins are also able to pull proteins from aggregates and refold them. Hsp100 class 1 proteins are missing in some of the higher eukaryotes like nematodes, arthropods and mammals.	
Small HSPs	Most widely spread but least conserved family; common feature is a conserved α-crystallin domain. sHSPs prevent aggregation of partially folded protein through ATP-independent interaction; sHSPs hold them until they can be refolded by other chaperones. sHSPs can also be sequestered into aggregates, affecting their structure and remodelling by chaperones.	α-crystallin

Chaperones have various functions, all of them ensuring that other proteins maintain proper conformation. Chaperones play a role throughout protein lifespan - for example, chaperones such as the Trigger Factor (TF, tig) help fold nascent proteins as they exit the ribosome, while Hsc70 recognizes KFERQ motif, carried by about a third of cytosolic proteins buried in the protein structure but exposed by misfolding, and passes them on for autophagy. Therefore, there is also a wide range of chaperone specificity; some have a wide clientele and recognize very common motifs, hydrophobic regions and common posttranslational modifications, while others recognize a defined binding region in few proteins.

Once synthesized, proteins will undergo many conformational changes, as constant unfolding and refolding are necessary to function correctly within the cells. For example, translocation from one cellular compartment to a different one usually comprehends protein unfolding for the polypeptide chain to pass the membrane and be refolded on the other side. Therefore, misfolding is not a problem just for nascent proteins. A certain degree of flexibility is innate to all protein, as conformational changes, especially in ligand-binding proteins, are necessary for their function. This is known as marginal protein stability, from which we can infer that a significant proportion of the total proteome can be unfolded with small energy requirements, thus highlighting the importance of

different cellular defences against protein damage and the need to maintain homeostasis (Williams, Pollock, & Goldstein, 2007). Furthermore, proteins also suffer damage from various exogenous and endogenous threats, including heat, irradiation, ROS, etc. Once damaged, proteins become prone to misfolding; changes in primary and secondary structure most often impact tertiary structure as well, meaning that some of the hydrophobic residues which are usually buried in the protein core end up exposed. These exposed hydrophobic residues make the misfolded proteins prone to both damage and aggregation. Some chaperones specifically bind such hydrophobic areas in order to prevent their aggregation. In some cases, it is possible to refold the protein to its native state using chaperones, while in other cases this is not possible, especially when a misfolded protein has been oxidized or otherwise damaged. In this case proteins are sent for degradation by the proteasome or autophagy. Timely removal of damaged proteins from the soluble phase is crucial for proteostasis maintenance. Therefore, various proteases are also upregulated during stress. Some of them, such as bacterial DegP (ClpXP) display dual protease-chaperone function; they are able to refold a protein if it is possible and degrade it if it is damaged beyond repair. In eukaryotes, most of the protein degradation is performed in specialized compartments, vacuoles or lysosomes. These contain organelle specific proteases such as Lon protease. There are differences between higher and lower organisms, with higher eukaryotes seeming to prefer refolding over proteolysis, as fewer proteolytic components are upregulated during stress than in bacteria or yeast (Richter, Haslbeck, & Buchner, 2010; Wong & Houry, 2004).

While refolding proteins does require energy, the energy requirements of removing damaged proteins and synthesising new ones to replace them are far greater. Therefore, maintaining proteostasis economises energy. Loss of chaperone function is associated with many age-related diseases; correspondingly resistance to stress is reduced in aged organisms (Bansal, Zhu, Yen, & Tissenbaum, 2015; Dues et al., 2016; Labbadia & Morimoto, 2015a).

1.2.4. Folding environment influences protein quality and cell fitness

In living cells, the prevailing source of damage to the proteins is oxidative stress, as a consequence of both ROS and intrinsic susceptibility to damage of some proteins. Cells in which this damage has been reduced display higher fitness. This was determined in *E. coli* by their ability to produce λ-phage – higher burst size indicates greater capacity of the cell to produce the virus (Figure 1.5.) (Krisko & Radman, 2013). Importantly, cells which were able to produce more λ-phage showed

reduced total protein carbonylation i.e. less oxidized protein, and displayed lower spontaneous mutation rates (Krisko & Radman, 2013).

This susceptibility of proteins to oxidation has been shown to correlate with the quality of protein biosynthesis; aberrantly folded proteins are more susceptible to carbonylation i.e. irreversible oxidation (Dukan et al., 2000). For example, mutated proteins are more likely to be oxidized due to conformational changes arising from the presence of an otherwise silent mutation. Error rate during translation can be decreased by increasing the rejection rate of near cognate tRNAs. Substituting Asn for Lys at position 42 of the S12 protein of the small subunit achieves exactly this, and has been shown to reduce levels of carbonylation without affecting the levels of ROS (Krisko & Radman, 2013). Proteins produced in bacterial strain carrying this mutation (RpsL) have been shown to be less carbonylated, as well as to be more efficient in performing their function (Musa, Radman, & Krisko, 2016). This illustrates the importance of maintaining the appropriate folding environment through chaperone action and amelioration of the negative effects brought on by the changing environmental conditions such as temperature or food availability.

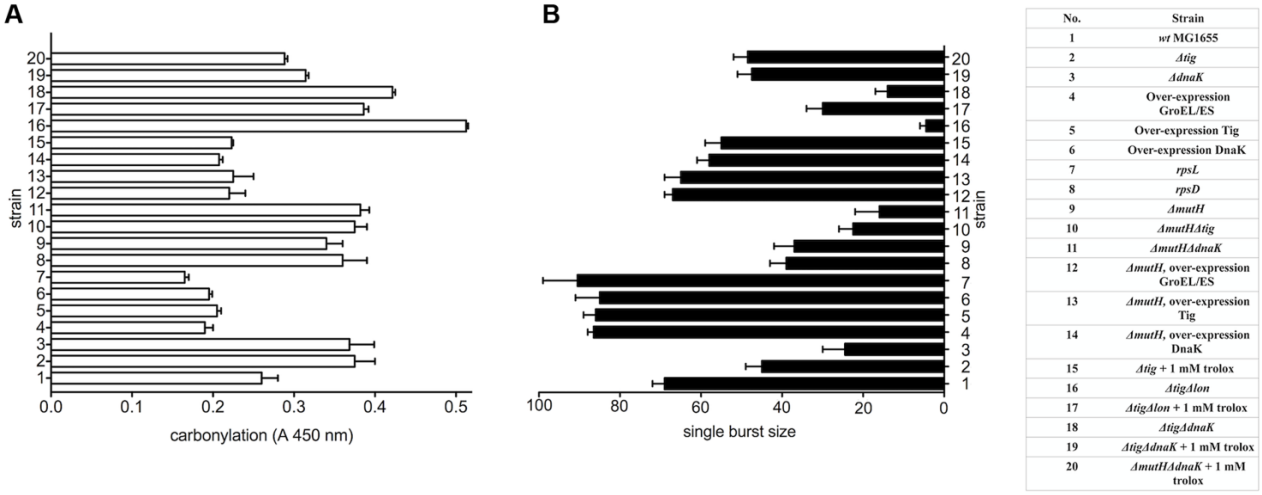

No.	Strain
1	*wt* MG1655
2	*Δtig*
3	*ΔdnaK*
4	Over-expression GroEL/ES
5	Over-expression Tig
6	Over-expression DnaK
7	*rpsL*
8	*rpsD*
9	*ΔmutH*
10	*ΔmutHΔtig*
11	*ΔmutHΔdnaK*
12	*ΔmutH*, over-expression GroEL/ES
13	*ΔmutH*, over-expression Tig
14	*ΔmutH*, over-expression DnaK
15	*Δtig* + 1 mM trolox
16	*ΔtigΔlon*
17	*ΔtigΔlon* + 1 mM trolox
18	*ΔtigΔdnaK*
19	*ΔtigΔdnaK* + 1 mM trolox
20	*ΔmutHΔdnaK* + 1 mM trolox

Figure 1.5. Quality of the proteome correlates with cells biosynthetic capacity. Proteome carbonylation is reduced in bacterial strains over-expressing chaperone coding genes (A) and is inversely proportional to the λ-phage burst size (B). The increased burst size demonstrates that improving the protein folding environment increases cells' biosynthetic capacity (Krisko & Radman, 2013).

1.3. Heat shock response

Heat shock response or HSR is an array of changes that happen in the cell in reaction to stress. The most robust and well-studied feature of HSR is the robust upregulation of heat shock proteins or HSPs following heat stress, dependent on the HSF1 transcription factor. Under normal conditions, HSF1 exists as a hetero-oligomer together with chaperones HSP70 and HSP90, either in the cytoplasm or the nucleus, depending on the organism. When the cell is stressed and misfolded and damaged proteins appear, the HSPs dissociate from the HSF1 and bind to their clients, freeing HSF1 to migrate to the nucleus and form a homo trimer with two other HSF1 molecules. The trimerized HSF1 can then bind to areas of DNA called heat shock elements. Heat shock elements or HSEs consist of three repeats of oppositely oriented nGAAn pentamers; each DNA binding domain of the HSF1 trimer binds one nGAAn sequence in the HSE. HSF1 biding to HSEs drives robust transcription of HSPs. The number and nucleotide composition of HSEs on different loci varies, thereby modulating the affinity of HSF1 to the DNA (Perisic, Xiao, & Lis, 1989; Vihervaara & Sistonen, 2014). Once the HSPs bind to and neutralize all the misfolded proteins and the cell is no longer under stress, the HSPs will bind back to the HSF1. This autoregulatory mechanism allows HSF1 to adjust the stress response to the state of the protein folding environment (Figure 1.6.).

Regulation of HSF1 binding to and away from DNA is done by a complex combination of post-translational modifications. After binding to DNA, HSF1 is phosphorylated at several amino-acids between HR-A/B and HR-C domains. HSF1 hyperphosphorylation is associated with activity. However, only phosphorylation of S230 and S326 has been shown to increase the HSF1 transcriptional activity, while some amino acids are phosphorylated even in absence of stress and repress the activation of HSF1. Therefore, the role of phosphorylation in HSF1 is twofold (Vihervaara & Sistonen, 2014). Sumoylation at K298, dependent on phosphorylation of S303, suppresses the HSF1 transactivational activity. HSF1 disassociation from DNA is facilitated by K80 acetylation, while the binding can be prolonged by SIRT1 which serves as a HSF1 deacetylase. HSF1 is regulated differently during stress and during development, when its function is carried out mainly through HSP-unrelated genes (Vihervaara & Sistonen, 2014). How HSF1 chooses and finds its target loci is still not fully described, as well as the exact mechanism of its activation. Furthermore, there is evidence that HSF-1 works in tandem with cofactors such as HPK-1, which works in both HSF-1 and TORC1 pathway, which are independent but complementary in promoting longevity (Das et al., 2017).

HSR upregulated proteins can be divided into 7 different classes depending on their role; chaperones, components of the proteolytic system, DNA repair enzymes, metabolic enzymes, regulatory elements such as various kinases and transcription factors, cytoskeleton, and membrane modifying proteins (Table 1.2.). Out of these, expression of metabolic enzymes displays biggest variation between species (Richter et al., 2010).

Table 1.2. Overview of different HSR components sorted by their role.

HSPs	Responding to damage
Proteolytic systems	
RNA and DNA modifying enzymes	
Metabolic enzymes	Adaptation and regulation
Transcription factors, kinases	
Cell structure and cytoskeleton	
Transport and membrane modifying proteins	

HSR has been first observed by Ritossa in 1962. Ritossa observed *Drosophila* salivary gland chromosomes and noticed puffing in some chromosomal regions after incubation at an elevated temperature. These areas were later determined to contain HSEs, and the HSPs got their name. It is important to note however, that HSPs are not exclusive to heat stress: HSPs also play a role in responding to proteotoxic stress caused by a stressor other than heat such as irradiation. Moreover, HSPs are widely present during development and tissue reorganization (Kurtz, Rossi, Petko, & Lindquist, 1986). For this reason, many papers refer to HSPs as “stress proteins” or chaperones. As HSPs are present in the cell in the absence of stress, and in significant quantities at that, their robust upregulation in the face of stress mirrors the need for stoichiometric ratios between the chaperones and their clients.

In unicellular organisms, HSR is cell autonomous, while in multicellular organisms such as *C. elegans*, heat stress is sensed, and the response is coordinated through neuronal action. In *C. elegans*, thermo sensory neuron AFD senses the heat stress and regulates the temperature dependent behaviour (Prahlad, Cornelius, & Morimoto, 2008).

While HSR is necessary to endure the stress, its prolonged activation is detrimental to the cell; activation of HSR redirects energy from the metabolism to homeostasis maintenance, which if prolonged interferes with the normal processes such as growth and division (Lindquist, 1980, 1986; Prahlad et al., 2008). Moreover, aberrant activation of HSF1 has been associated with promoting tumorigenesis and cancer, as well as connected with poor prognosis (Dai et al., 2012; Dai, Whitesell, Rogers, & Lindquist, 2007; Mendillo et al., 2012; Santagata et al., 2011; Santagata et al., 2013; Whitesell & Lindquist, 2009; Whitesell et al., 2014). Therefore, the HSR needs to be tightly regulated and triggered accordingly, imposing additional constraints.

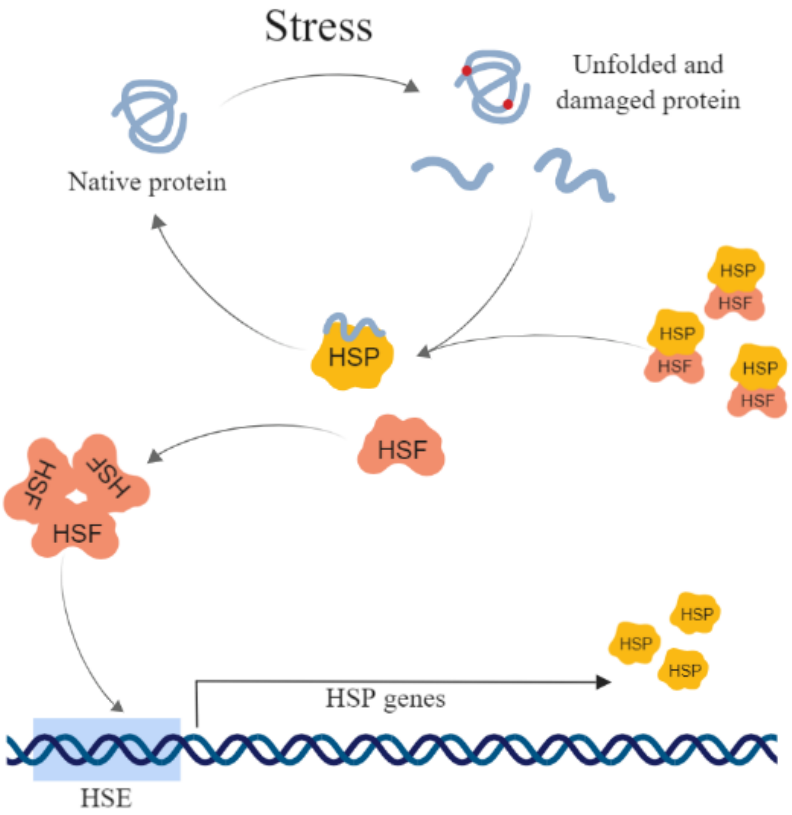

Figure 1.6. A schematic representation of the heat shock response. Stress induced protein misfolding is recognized by chaperones, which bind their clients and, in the process, free the bound HSF-1. The HSF-1 is now free to trimerize and drive transcription of heat shock proteins i.e. chaperones.

1.4. Oxidative stress response

Similarly, changes in cell redox state also illicit a response, dubbed oxidative stress response. The concept of oxidative stress response was first formulated in 1985 as a "disturbance in the prooxidant-antioxidant balance in favour of the former" (Helmut Sies, 1985). It is essential for modulating cellular processes through redox signalling. Oxidative stress response is usually upregulated in oxidizing conditions as a response to either oxygen itself or increased presence of oxidized proteins. It manifests itself as upregulation of antioxidant enzymes and ROS scavengers, such as superoxide dismutases, catalazes, peroxidases, etc., under control of the Nrf2 transcription factor (called SKN-1 in *C. elegans*) from the Nrf/CNC family (Blackwell, Steinbaugh, Hourihan, Ewald, & Isik, 2015). Nrf2 controls both the basal and inducible expression of antioxidant and stress-response proteins. Its transcriptional targets include catalases, superoxide dismutases, glutathione metabolism regulators, and peroxiredoxins.

Oxidative stress is associated with senescence and a number of diseases in humans (Finkel & Holbrook, 2000). Similar to HSR, oxidative stress, can produce a hormetic effect; therefore, its proper activation and management is vital.

1.4.1 Reactive oxygen species (ROS)

As the name suggests, ROS are chemically reactive species that contain oxygen. Aside from oxygen, other elements also form reactive compounds, summarized in Table 1.3. ROS are formed during normal metabolism (Figure 1.7.) and they are important for various cell signalling pathways and homeostasis. Non-radical ROS species have an important role as second messengers, but free radicals can also have useful roles in the cell, such as superoxide's role in defence against microbial infection (Babior, 1984). However, high levels or aberrant localization in the cell can lead to oxidative stress, causing damage to cellular structures. Increased levels of ROS have been associated with aging, but causal relationship was never confirmed; while ROS can be toxic and does increase during aging, levels of ROS do not necessarily correlate with aging, and can be separated from lifespan (Van Raamsdonk & Hekimi, 2009, 2010; Yang, Li, & Hekimi, 2007). Moreover, increased levels of mitochondrial ROS in *C. elegans* have been associated with increased lifespan (Van Raamsdonk & Hekimi, 2009).

Reduction of molecular oxygen produces superoxide, precursor to other ROS. Superoxide production occurs in mitochondria, where in normal conditions most oxygen is reduced to produce

water, but a smaller percentage of electrons passing through the respiratory chain is prematurely and incompletely reduced to superoxide.

$$O_2 + e^- \rightarrow {}^{\bullet}O_2^- \quad (1.1.)$$

Although superoxide is not particularly reactive, in its protonated form (hydroperoxyl: $HO^{\bullet}{}_2$) it can trigger lipid peroxidation and inactivate specific enzymes, thereby causing damage. Damaged mitochondria can trigger apoptosis or programmed cell death. Superoxide can be dismutated by a class of enzymes called superoxide dismutases (SOD) to produce hydrogen peroxide.

$$2H+ + {}^{\bullet}O_2^- + {}^{\bullet}O_2^- \rightarrow H_2O_2 + O_2 \quad (1.2.)$$

Hydrogen peroxide can then be either fully reduced to water or partially reduced to create hydroxyl radical.

$$2H^+ + 2e^- + H_2O_2 \rightarrow 2\,H_2O \quad (1.3.)$$

$$H_2O_2 + e^- \rightarrow HO^- + {}^{\bullet}OH \quad (1.4.)$$

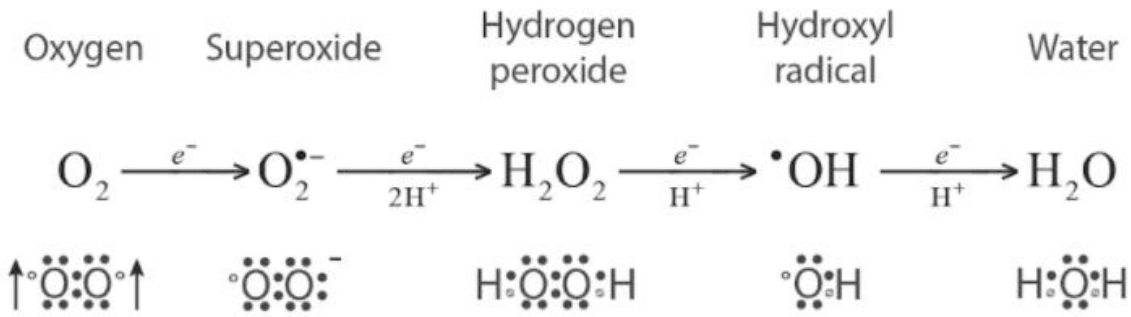

Figure 1.7. Oxygen reduction to different oxygen reactive species or ROS. Image taken from (Ley, 2018).

Hydrogen peroxide is degraded by several classes of enzymes. Catalases, found in peroxisomes and cytoplasm, react with hydrogen peroxide to produce water and oxygen. Sulphur reactive centre of the glutathione peroxidase carries the electrons from the peroxide to a sulphur-containing glutathione. Peroxides are also degraded by peroxiredoxins.

Table 1.3. Chemical diversity of reactive species. From (H. Sies, Berndt, & Jones, 2017).

Free radicals	Nonradicals
Reactive oxygen species	
Superoxide anion radical ($O_2^{-\bullet}$)	Hydrogen peroxide (H_2O_2)
Hydroxyl radical ($OH^\bullet$)	Organic hydroperoxide (ROOH)
Peroxyl radical ($ROO^\bullet$)	Singlet molecular oxygen ($O_2\,^1\Delta_g$)
Alkoxyl radical ($RO^\bullet$)	Electronically excited carbonyls (RCO)[a]
	Ozone (O_3)
Reactive chlorine/bromine species	
Atomic chlorine ($Cl^\bullet$)	Hypochlorite (OCl^-)
Atomic bromine ($Br^\bullet$)	Chloramines (RNHCl)
	Hypobromite (OBr^-)
Reactive nitrogen species	
Nitric oxide = nitrogen monoxide ($NO^\bullet$)	Nitrite (NO_2^-)
Nitrogen dioxide ($NO_2^\bullet$)	Nitroxyl anion (NO^-)
	Peroxynitrite ($ONOO^-$)
	Peroxynitrate (O_2NOO^-)
	Nitrosoperoxycarbonate ($ONOOCO_2^-$)
Reactive sulfur species	
Thiyl radical ($RS^\bullet$)	Thiol (RSH), thiolate (RS^-) [e.g., glutathione (GSH), thioredoxin (Trx)]
	Disulfide (RSSR) [e.g., GSSG, mixed disulfide (protein SSG)]
	Sulfenate (RSO^-)
	Sulfinate (RSO_2^-)
	Sulfonate (RSO_3^-)
	Hydrogen sulfide (H_2S)
	Polysulfide (H_2S_x), x = 2 or higher; RSSH
Reactive carbonyl species	
	Acetaldehyde
	Acrolein
	Methylglyoxal
	4-Hydroxy-nonenal
	Electronically excited (triplet) carbonyls
Reactive selenium species	
	Selenite
	Selenate
	Selenocysteine
	Selenomethionine

1.5. Hormesis

While prolonged stress is toxic, short exposure to stress has been shown to provide benefit to the cell in certain conditions. Generally, benefit from stress has been observed in cases when stress has been administered at the right time of development/life, and has been sufficiently mild and transient (Figure 1.8.). This effect is known as hormesis, and so far has been demonstrated on budding yeast, *C.elegans*, *Drosophila*, and mice (Butov et al., 2001; Cypser & Johnson, 2002; Hercus, Loeschcke, & Rattan, 2003; López-Martínez & Hahn, 2014; Scott, Bruce, Gott, Wilder, & March, 2012).

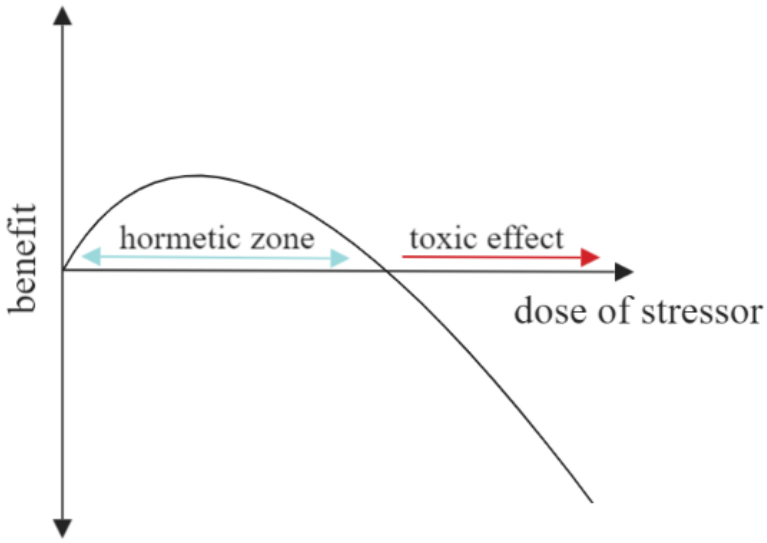

Figure 1.8. Hormetic effect is dose dependent. At very low, sub-toxic doses of stressor, there is a narrow window when the slight increase in stressor dose is beneficial, but after that point the benefit quickly declines, and the stress becomes toxic.

1.6. Proteostasis in aging

Loss of proteostasis is one of the primary hallmarks of aging (López-Otín et al., 2013). As an organism ages, its proteins are progressively more susceptible to damage as a result of folding defects, which occur due to errors in transcription and translation, the chance of which increases with age (Dukan et al., 2000). It is well documented that damaged protein clearance decreases with aging as well, and many age-associated diseases are proteinopathies characterized by accumulation and aggregation of aberrant protein variants (Andersson, Hanzén, Liu, Molin, & Nyström, 2013; Cuervo, 2008; Ferrington, Husom, & Thompson, 2005; Grune, Jung, Merker, & Davies, 2004; Lee,

Klopp, Weindruch, & Prolla, 1999; Vernace, Arnaud, Schmidt-Glenewinkel, & Figueiredo-Pereira, 2007). Furthermore, protein aggregate formation is found not only in the context of disease, but during healthy aging as well, making it an intrinsic part of the aging process (David et al., 2010). Proteostasis collapse has been shown to correlate with onset of aging, and long-lived *C. elegans* strains exhibit increased proteasome activity and delayed collapse of HSR and proteostasis (Shemesh, Shai, & Ben-Zvi, 2013), while failure to clear misfolded and damaged proteins causes short lived and prematurely aged phenotype across species (Ben-Zvi, Miller, & Morimoto, 2009; Hars et al., 2007; Janssens & Veenhoff, 2016; Labbadia & Morimoto, 2015b; Matecic et al., 2010; Simonsen et al., 2008; Tomaru et al., 2012; Tóth et al., 2008).

Proteostasis is achieved through response and maintenance mechanisms that prevent and fix damage that arises due to stress. These mechanisms are regulated by stress response pathways: heat shock response, unfolded protein response, and oxidative stress response. The inducibility of HSR and oxidative stress response is reduced in old organisms (Blake, Fargnoli, Gershon, & Holbrook, 1991; Labbadia & Morimoto, 2014; Rahman, Sykiotis, Nishimura, Bodmer, & Bohmann, 2013; Westerheide, Anckar, Stevens, Sistonen, & Morimoto, 2009), and the induced chaperones can be overwhelmed by the increased amounts of aberrant proteins (Csermely, 2001). On the other hand, overexpression of HSF1 or FOXO suppresses proteostasis collapse and promotes longevity (Shore, Carr, & Ruvkun, 2012). Furthermore, as UPR and HSR disruption precedes proteostasis collapse and is associated with decreased stress resistance, it hints that the loss of UPR and HSR is at the root of the proteostasis collapse (Labbadia & Morimoto, 2014). Thus, stress response pathways are essential for proteostasis maintenance, and therefore for delay of aging.

In humans, the age associated decline in proteostasis manifests itself most prominently as increased risk of development of neurodegenerative diseases and conditions. Alzheimer's disease (AD) is caused by aggregation of misfolded amyloid peptides β and tau. Once aggregated, these proteins cause formation of neuronal plaques and neurofibrillary tangles, respectively. In inborn predisposition, Parkinson's disease (PD) is caused by point mutations in α-synuclein, a presynaptic terminal protein, which promote its misfolding and aggregation, leading to creation of inclusions called Lewy bodies, characteristic of PD. The time of PD onset correlates with increase in intrinsic α-synuclein oxidability due to predisposing mutation (Krisko & Radman, 2019). Although exact causes of amyotrophic lateral sclerosis (ALS) are unknown, it is associated with accumulation of

insoluble inclusions and mutations in main components of protein quality control, including point mutations in cytosolic SOD1 antioxidant enzyme, which catalyses the conversion of superoxide to hydrogen peroxide (Figure 1.9.).

Although different proteins are involved in their onset, these neurological conditions are all characterized by accumulation of aberrant proteins in the neurons (Cohen & Dillin, 2008; Saez & Vilchez, 2015). Furthermore, the protein inclusions associated with AD, PD, and ALS all contain abnormal amounts of ubiquitin, suggesting accumulation of proteins marked for clearance (Nixon, 2013; Tanaka & Matsuda, 2014). This suggests a strong connection between neurodegenerative disease and accumulation of aberrant proteins.

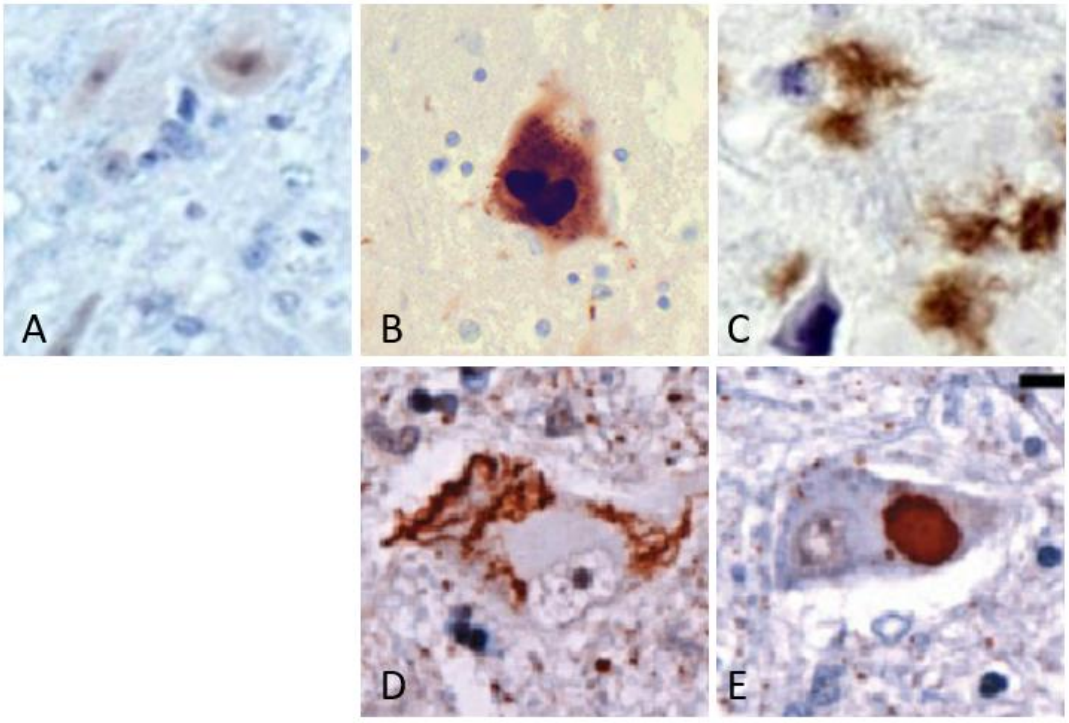

Figure 1.9. Aberrant protein accumulation is associated with the most widespread age-related diseases. Micrographs of healthy brain tissue (A), Lewy body inclusion in substantia negra of a Parkinson's disease patient (B), and amyloid beta plaques of an Alzheimer's disease patient (C). ALS patients display different types of protein inclusions, ranging from protein tangles (D) to large aggregates (E). Images taken from Novus biological, Parkinson's foundation, and (Mackenzie et al., 2007).

1.7. Cross-organelle communication

Traditionally, researchers focused on signalling pathways and organelles individually, with little focus to their interactions. However, organelles and cellular pathways do not function independently – studies of various processes involved in stress response and aging suggest a great deal of coordination and highlight the need to study their interactions. Many signalling pathways show overlaps in metabolites or share enzymes. Organelles, on the other hand, can also share both enzymes and host the same metabolic processes. For example, fatty acids are oxidized in both mitochondria and peroxisomes, but only peroxisomes are able to oxidize VLCFAs. After the VLCFAs are shortened in the peroxisomes, they can be either stored as triglycerides or shuttled to mitochondria, which is an example of their interaction. Organelles can also interact physically with one another through contact sites, such as those between mitochondria and the ER. These interactions in the context of aging are still relatively unexplored. Data suggests that mitochondrial and metabolic activity can be coordinated with the chaperone networks in different cellular compartments (Kim et al., 2016; Perić et al., 2016; Perić et al., 2017). Mitochondria in particular are responsive to the changes in the cellular environment (Kim et al., 2016), and have been shown to be in a redox sensitive relationship with peroxisomes (Fransen, Nordgren, Wang, & Apanasets, 2012).

1.7.1. Mitochondria

Mitochondria are double membrane bound organelles found in most eukaryotic cells. They generate the majority of the cellular energy supply in the form of ATP (Figure 1.10.). In postmitotic cells, along with lysosomes i.e. clearance of aberrant proteins, mitochondria display the most pronounced age-associated changes (Brunk & Terman, 2002), possibly because mitochondrial respiration is the major source of ROS in the cell (Cadenas & Davies, 2000; Sohal & Brunk, 1992; Sohal & Sohal, 1991).

Mitochondria have a central role in the cell as one of the main signalling hubs; they regulate everything from cell differentiation, growth, cell cycle, and cell death. Therefore, they are able to communicate to other cellular compartments, including the nucleus, endoplasmic reticulum, and peroxisomes. Their numbers vary greatly between different cell types, and their morphology is subject to change corresponding to the growth conditions and cell status. Defects in mitochondria are associated with a number of human health conditions and disorders, and are often lethal. With increasing age of the organism, mitochondria undergo various morphological changes associated

with decreased capacity for energy production (Brunk & Terman, 2002; Ozawa, 1997; Vanneste & van den Bosch de Aguilar, 1981).

Mutations in mitochondrial DNA have been shown to increase with age in humans (Cortopassi & Arnheim, 1990), and age related decline in function is most apparent on complexes with greater proportion of mitochondrially encoded genes i.e. complexes I and IV, which have 7 out of 44 and 3 out of 13 mitochondrially encoded proteins, respectively. In comparison, all 4 complex II proteins are encoded in the nucleus, while only 1 out of 11 complex III proteins is encoded in the mitochondrial DNA (Brunk & Terman, 2002; Takasawa et al., 1993). However, these are not believed to be a driving agent of aging, as more recent studies showed the majority of cells would need to harbour pathological mutations on the mitochondrial DNA in order to cause a measurable effect (Jang, Blum, Liu, & Finkel, 2018; Kauppila, Kauppila, & Larsson, 2017).

Although mitochondrial dysfunction is lethal, disruption of mitochondria can have a hormetic effect, and several studies have shown that increase in mitochondrial levels of ROS are beneficial for the cell and increase longevity (Bonawitz, Chatenay-Lapointe, Pan, & Shadel, 2007; Van Raamsdonk & Hekimi, 2009; Yang & Hekimi, 2010).

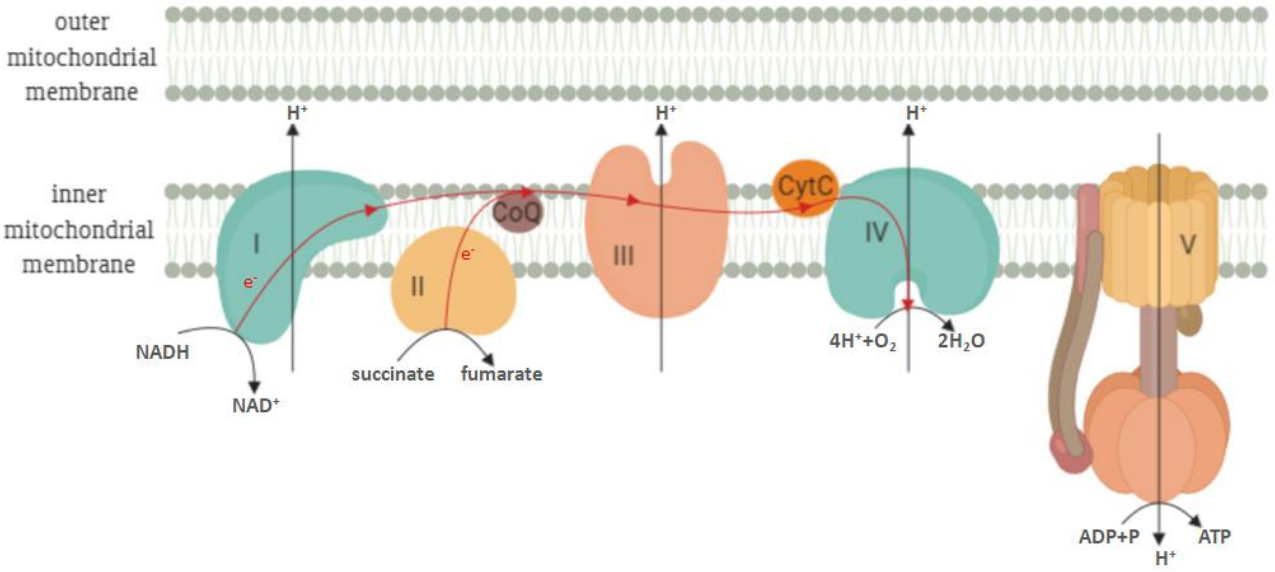

Figure 1.10. Schematic representation of the electron transport chain. NADH and succinate from the citric acid cycle are oxidized at complexes I and II, respectively, providing electrons for the Q-cycle, the sequential reduction and oxidation of coenzyme Q. The Q-cycle contributes to the proton gradient by absorbing and releasing electrons in complex III. Complex III may leak electrons

when respiration is inhibited or the membrane potential is high, producing superoxide. Complex IV is cytochrome C oxidase, which removes electrons from the cytochrome C and produces water. Removal of protons from the mitochondrial matrix by complexes I, III and IV contributes to the proton gradient. The proton gradient is used by the ATP synthase or complex V for ATP production via oxidative phosphorylation.

1.7.2. Peroxisomes

Peroxisomes are small, single membrane bound organelles found in all eukaryotic cells. They participate in a number of vital cellular functions, lipid and hydrogen peroxide metabolism being the most prominent. New peroxisomes are formed by budding from the ER or by fission of existing peroxisomes. While peroxisomes in general are able to also fuse, in *C. elegans* fusion has not been observed thus far. Defects in peroxisomal structure, number, or composition cause a wide array of disorders and clinical symptoms, and disturbances in the peroxisomal redox metabolism are associated with increased sensitivity to oxidative stress (Fransen et al., 2012). Peroxisome biogenesis disorders have been associated with an array of pathologies including Parkinson's disease, Alzheimer's disease, cancer, diabetes and heart failure (Di Cara, Sheshachalam, Braverman, Rachubinski, & Simmonds, 2017; Fransen, Nordgren, Wang, Apanasets, & Van Veldhoven, 2013).

Aside from their role in hydrogen peroxide metabolism, peroxisomes also play a key role in metabolism of lipids (Figure 1.11.). Peroxisomes house enzymes necessary for the metabolism of very long chain fatty acids (VLCFAs). VLCFAs are fatty acids with 20 or more carbons in the backbone, and can only be oxidized i.e. shortened in the peroxisomes. There, the VLCFAs go through the process of β-oxidation, which shortens by two carbons in each reaction. The resulting medium chain fatty acids serve as precursors for production of acetyl-CoA or can exported from the peroxisomes and shuttled to mitochondria where they are broken down to carbon dioxide and water. In yeast and plant cells, however, VLCFAs are processed entirely in peroxisomes. Furthermore, peroxisomes are sites of α-oxidation of 3-methyl branched FAs, as well as synthesis hubs for ether lipids. Their role in lipid metabolism makes them vital for survival of heat stress, as different lipid species incorporation into the membrane determines its physical properties and oxidability (Fransen et al., 2013; Perluigi, Coccia, & Butterfield, 2012).

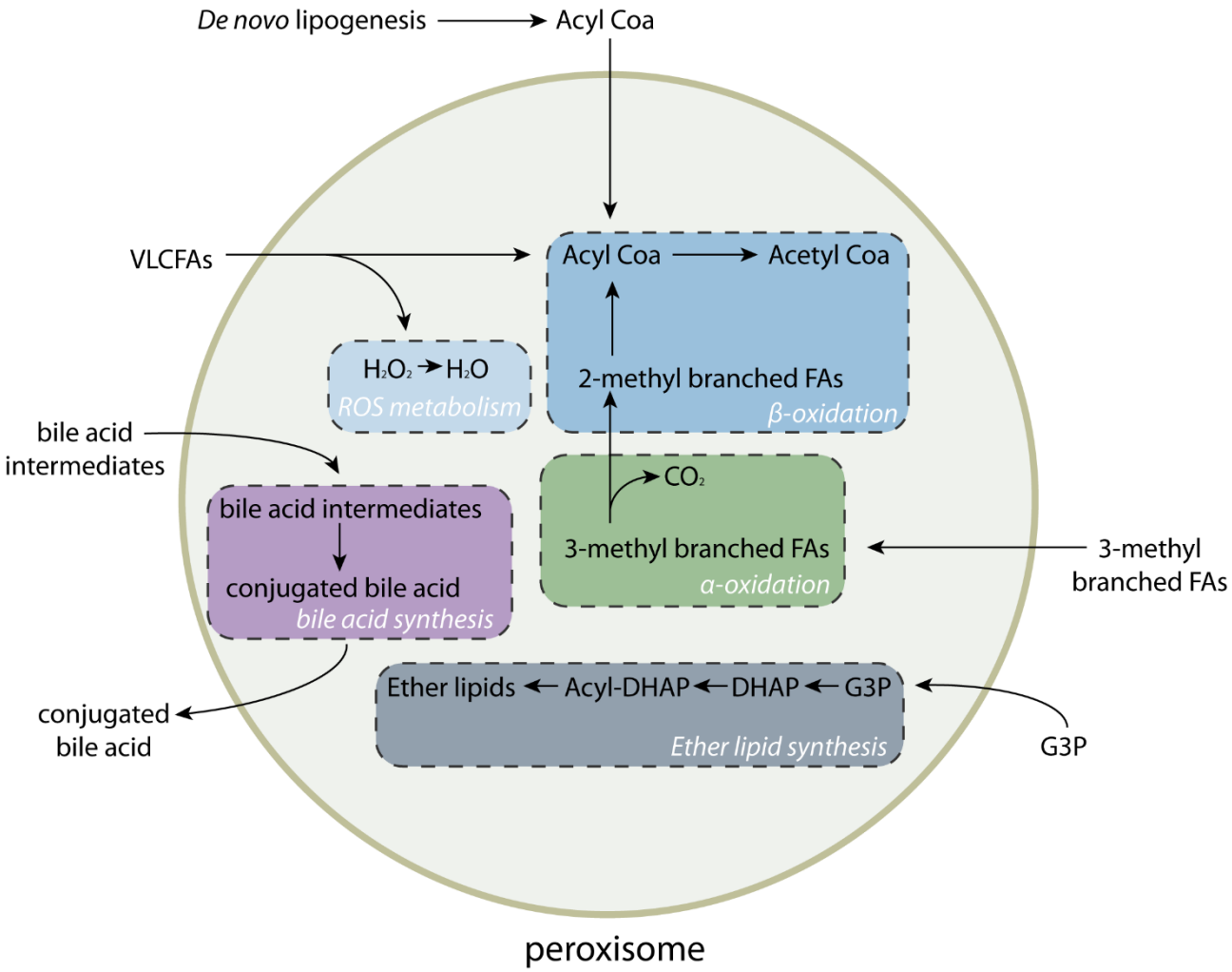

Figure 1.11. Overview of peroxisomal metabolism. Peroxisomes were named for their role in ROS metabolism, most notably of hydrogen peroxide. However, their importance is wider than that, and they house many lipid metabolism related processes, some of which, such as VLCFA β-oxidation, are exclusive to peroxisomes.

1.8. Lipid metabolism

One of important aspects of energy homeostasis is fat metabolism. Changes in fat composition and metabolism can be observed during aging, as well as differences between fat stores in long lived and short-lived *C. elegans* strains (Papsdorf & Brunet, 2018). In humans, during aging, as well as in Hutchinson-Gilford progeria syndrome (HGPS) and similar conditions such as Marfan syndrome, fat metabolism is affected.

Fatty acids are either synthesized *de novo* or obtained from dietary sources. Dietary lipids that are not metabolized right away are converted into triglycerides, which are stored as an energy reserve (Figure 1.12.).

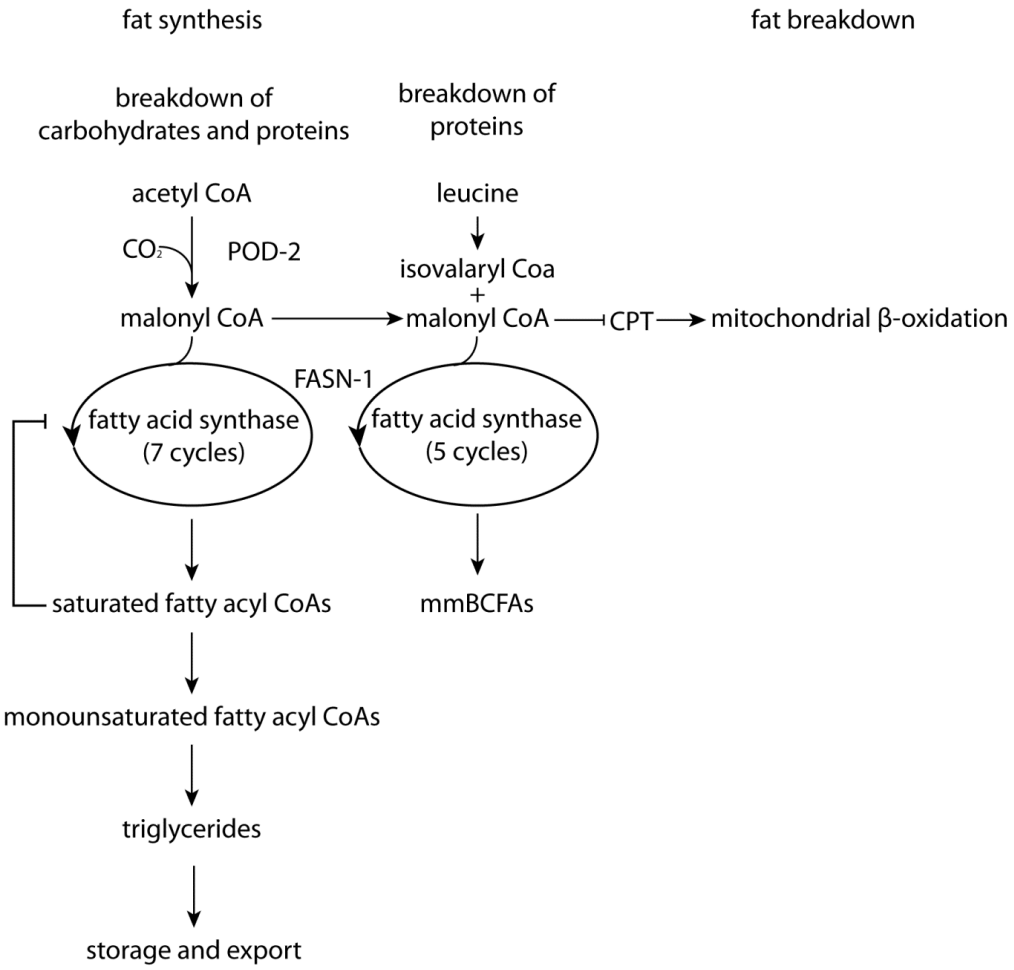

Figure 1.12. Simplified overview of lipid metabolism.

As the principal component of all biological membranes, it is crucial that fat levels of each specific lipid are tightly regulated, as they directly impact membrane fluidity. Membrane areas rich in lipids are called lipid rafts, and they serve as places of assembly of signalling molecules, regulating membrane protein and receptor trafficking, and important in the context of heat stress, they strongly influence membrane fluidity (Figure 1.13.). Lipid rafts can be distinguished from the surrounding membrane by the increased concentration of lipid species, predominantly cholesterol, as well as sphingolipids. All membrane lipids share amphipathic character, meaning that they have a

hydrophilic as well as a hydrophobic region. The lipid composition of the membrane directly influences its properties. For example, high levels of poly unsaturated fatty acids (PUFAs) is associated with increased sensitivity to oxidative stress as they are susceptible to peroxidation, while plasmalogens in the membrane act both as structural components as well as antioxidants, as they act as free radical traps through their vinyl ether function (Perluigi et al., 2012; Wallner & Schmitz, 2011).

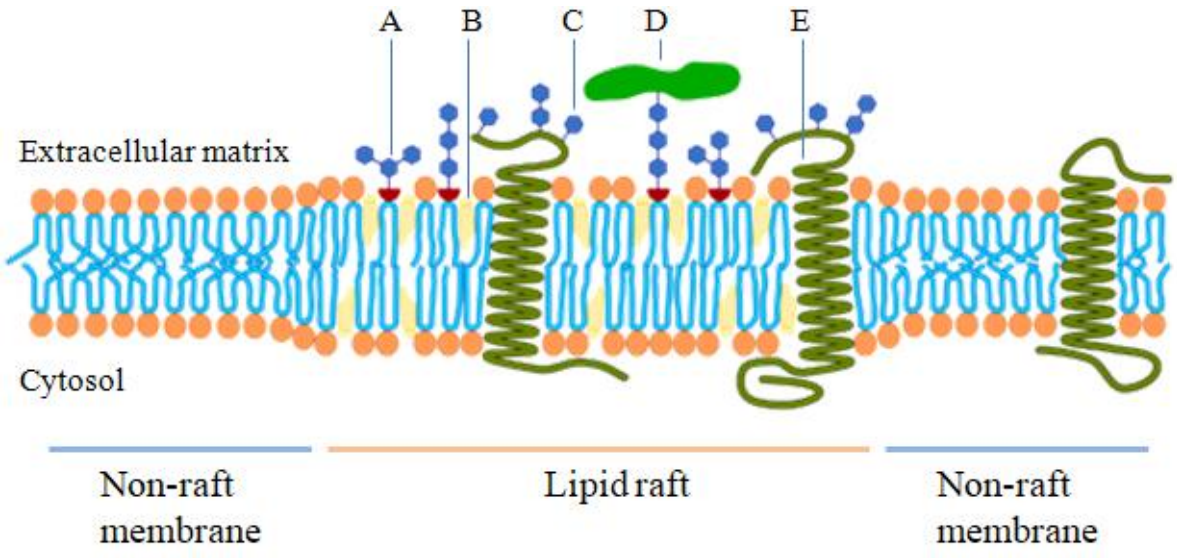

Figure 1.13. Membrane fluidity is modulated by lipids and lipid rafts. Cross section of a cell membrane illustrating the membrane phospholipid bilayer and the lipid raft regions. Lipid rafts can be differentiated from the surrounding membrane by the increased concentration of glycolipids (A) and cholesterol (B), as well as glycosylation modifications on either lipids or proteins, both transmembrane (C, E) and anchored (D).Image adapted from: (https://commons.wikimedia.org/wiki/File:Lipid_raft_organisation_scheme.svg).

Apart from energy storage and membrane structure, lipids also serve as signalling molecules. Disturbance in mitochondria has been shown to also activate cytosolic stress response, and the cross communication between the compartments requires lipid biosynthesis (Kim et al., 2016). Therefore, changes in lipid metabolism can have massive consequences on cellular homeostasis and fitness. For example, the amount of unsaturated bonds in a lipid molecule is correlated with its susceptibility to peroxidation (Papsdorf & Brunet, 2018).

1.9. Model organisms

1.9.1. Saccharomyces cerevisiae

S. cerevisiae or budding yeast is a unicellular eukaryote whose 6000 gene genome has been completely sequenced and mapped. Many of its genes have human orthologues, including genes whose perturbation leads to disease in humans. As multicellular organisms are more complex and difficult to study, budding yeast offers an alternative to look at cellular processes in a simpler context.

It has a short and simple life cycle, which makes it easy and cheap to work with in laboratory setting on simple medium (Figure 1.14.). We can distinguish two types of lifespan in budding yeast: replicative lifespan (RLS), defined as the number of daughter cells one mother cell produces i.e. number of generations, and chronological lifespan (CLS), time a cell survives after it stops dividing. Budding yeast can proliferate in both diploid and haploid state – diploid state is maintained during nutrient abundance, while depletion of nutrients and starvation trigger meiosis and spore formation, a haploid form that will continue to propagate once nutrients are reintroduced into the environment. Yeast cells are able to adapt to changes in the environmental conditions, including temperature and nutrient availability or absence, through changes in activity of RNA polymerases and degradation of mRNA. Unlike in multicellular organisms, including humans, stress response in yeast is cell autonomous i.e. each cell controls its own growth and development with little to no interaction with neighbouring yeast cells. Yeast cell to cell interaction is only crucial for different mating types attracting each other. Therefore, interaction with the environment is a lot simpler in yeast than it is higher metazoans, which is one of the drawbacks of yeast research. However, many of the pathways studied in yeast are conserved in humans or can otherwise be applied in learning more about human conditions (Janssens & Veenhoff, 2016) (Figure 1.15.).

Some of the key discoveries in the field of aging have been made observing *S. cerevisiae*. *S. cerevisiae* propagates through asymmetric division, with a “daughter” cell budding off the “mother” cell. Aging in yeast is thought to be driven through the unequal distribution of cellular contents during the asymmetrical division. During budding, transcription repressors are being contained to the bud (Gershon & Gershon, 2000), while the mother cell retains membrane proteins and protein aggregates (Baldi, Bolognesi, Meinema, & Barral, 2017). The asymmetric distribution of cellular components between the mother and the daughter cell is enabled by a so-called diffusion barrier.

The diffusion barrier anchors membrane bound proteins whose diffusion into the daughter cell has been shown to rejuvenate the mother but is detrimental for the daughter cell. Furthermore, nuclear diffusion barriers prevent the loss of extrachromosomal circles, whose accumulation increases exponentially with each division and contributes to cell death in yeast (Baldi et al., 2017; Saarikangas et al., 2017). These extrachromosomal circles, result of intra-chromosomal recombination, as well as plasma-membrane proteins and protein aggregate deposits are known as aging factors and are retained by the mother cell, driving its aging while the age of the daughter cell is 'reset' to zero (Aguilaniu, Gustafsson, Rigoulet, & Nyström, 2003; Eldakak et al., 2010; Hill, Hao, Liu, & Nyström, 2014; Saarikangas & Barral, 2015; Shcheprova, Baldi, Frei, Gonnet, & Barral, 2008; Sinclair & Guarente, 1997; Szostak & Wu, 1980). Disturbance of the diffusion barrier leads to the daughter cell inheriting the aging factors, conferring longevity to the mother (Baldi et al., 2017).

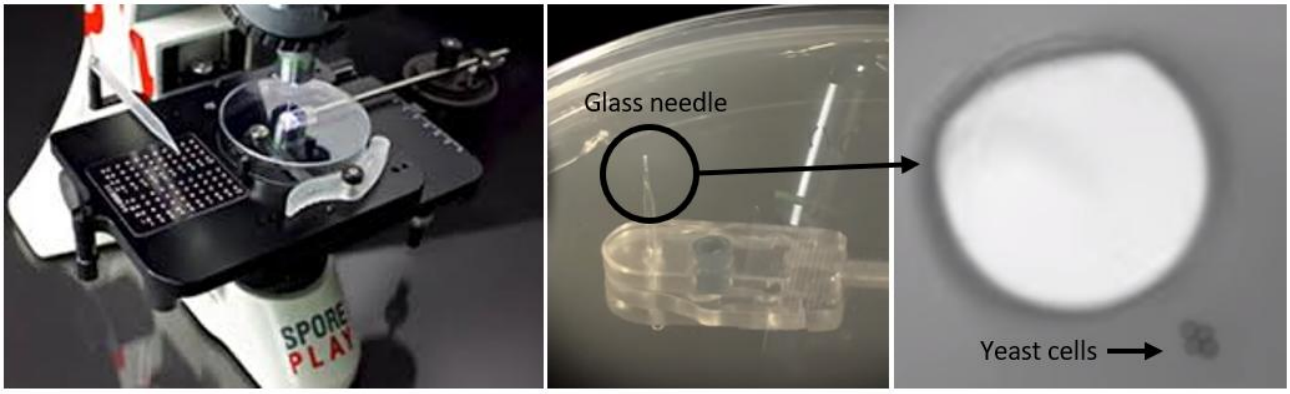

Figure 1.14. Yeast micromanipulator is used for RLS measurement. From left to right: yeast micromanipulator; micromanipulator needle setup with an agar plate containing individual yeast cells in designated fields; macro view of the needle and yeast cells.

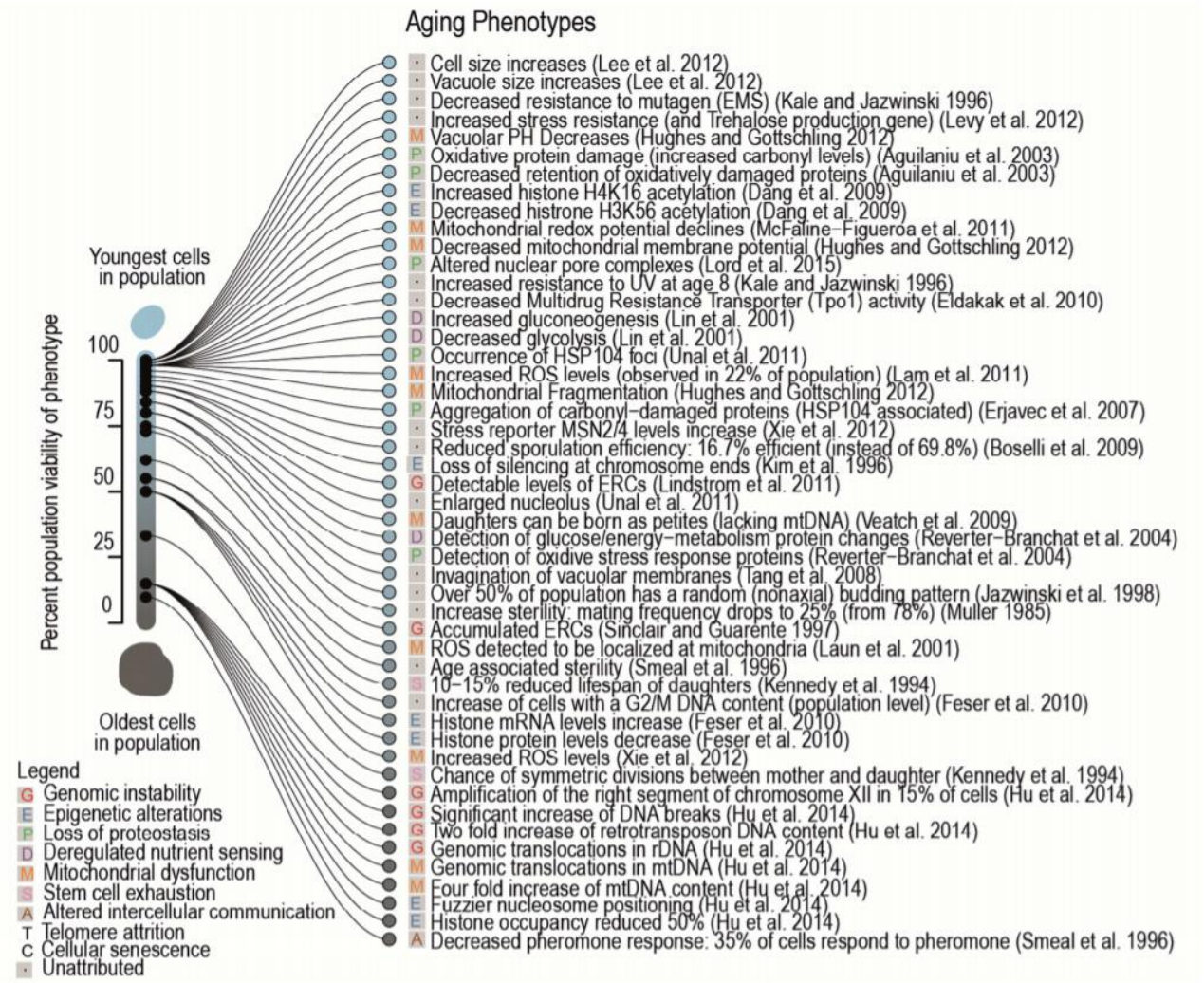

Figure 1.15. Aging phenotypes in budding yeast. Yeast lifespan is characterized by the same processes associated with ageing observed in higher eukaryotes. The aging process in yeast can be compared to stem cell exhaustion and senescence in mammals. Viability was either taken from the cited primary literature or estimated based on the timepoint of the measurement. From (Janssens & Veenhoff, 2016).

1.9.1.1. Nomenclature

S. cerevisiae genes are labelled with three italicized lower-case letters and an Arabic number (e.g. *ade5*). Recessive and dominant alleles can be marked with lower case italicized or uppercase italicized symbols, respectively (e.g. *ade5*, *CUP1*). Alleles are represented with a gene symbol and a hyphenated Arabic number (e.g. *his1-2*). Proteins are marked by the relevant gene symbol with the initial letter uppercase, non-italic and with a suffix 'p' if protein is not specified, to avoid confusion

with the phenotype (e.g. Ade5p or Ade5 protein). Phenotype designation is similar to the protein, without the suffix, and a '+' or '- 'superscript to designate WT or mutant phenotype (e.g. Arg^{-}) ("https://wiki.yeastgenome.org/," 2018).

1.9.2. Caenorhabditis elegans

C. elegans is a microscopic, free living nematode often found in rotting vegetable matter, where it feeds on bacteria. It has been proposed as a model organism in the 1960s by Sydney Brenner, who expressed concern that classical problems of molecular biology will soon all be solved and proposed that the future lies in expansion of molecular biology to development and the study of nervous system, for which he believed *C. elegans* is a suitable model.

In the laboratory, *C. elegans* is normally grown on agar plates known as nematode growth medium (NGM), though growth in liquid culture is also possible, and are fed bacterium Escherichia coli (Figure 1.16. A). C. elegans has a short life cycle with distinct growth stages (Figure 1.16. B, C), thus allowing tracking changes throughout its life, as well as across generations. It is a self-fertilizing hermaphrodite, although males do arise, albeit rarely (<0.2%), through random nondisjunction of the X chromosome; two X chromosomes give rise to hermaphrodites and embryos with one X chromosome will develop into males. Thus, it is also possible to study sex dimorphism and related phenomena as well.

Adult hermaphrodites are just about 1 mm long, making it easy to grow large numbers inside the laboratory. Further, the nematode is transparent, making their individual cells and subcellular details easily visualized by Nomarski optics. The number of somatic cells in *C. elegans* is invariable, and the fate of every cell has been tracked and cell lineage created (Sulston & Horvitz, 1977). Together with the fact that *C. elegans* neurons are most completely mapped out of all other model organisms *(White 1986, Jarrell 2012),* as well as having the first genome to be completely sequenced, led to identification of many genes important for development and biological processes.

gene homology/conserved genes

1.9.2.1. Life cycle

Life cycle of *C. elegans* is short, but interesting. After fertilization, embryo is protected by a virtually impenetrable eggshell, which enables it to develop independent of the mother. After hatching, the embryo becomes a first stage larva (L1) and it begins to eat and develop through stages

L1-L4. Each stage ends with a sleep-like state called lethargus during which a new collagenous cuticle is made, and the old one is shed. Approximately 12 hours (at 20°C) after the L4 lethargus ends, the worms start reproducing. The reproductive period is around 5 days long (majority of reproduction occurs in the first 3 days of adulthood), after which they can live several more weeks before dying.

There are also alternate cycles through which they can grow in conditions of low food availability or high population density. These are unfavourable conditions to which *C. elegans* has adapted through evolution of two main stress resistant forms in which it can survive until conditions are improved. When population density is high or food is limiting, L2 larvae can molt into an alternate L3 stage called dauer; the conditions are actually sensed by the L1 larvae but do not come in effect until the L2d stage, L2 equivalent which will develop into dauer (Figure 2). Dauer larvae grow a cuticle that completely covers their mouths thus preventing them from eating and therefore stopping them from further development. Dauer larvae can survive several months, and are the main dispersal form encountered in the wild. Once the conditions are sensed as favourable again by the dauer, they will shed their cuticle and molt into stage 4 larvae (L4). On the other hand, if the embryos hatch in absence of food, the L1 larvae will cease to develop until food is available again. This is called the L1 arrest. The arrested L1 larvae show no morphological changes as dauer larvae do, but are stress resistant and 'non-aging' (Baugh, 2013; T. E. Johnson, Mitchell, Kline, Kemal, & Foy, 1984), making it possible to freeze them for storage and synchronize the population (see Methods).

There are significant differences in the regulation of the L1 arrest and dauer formation. Dauer, unlike L1 arrest, can be considered a diapause: the arrest occurs at a specific stage in development, both arrest and recovery are triggered by specific external cues, and the metabolism is altered before the arrest in preparation (L2d). In contrast, starvation is not a specific cue, and animals starved at any stage will arrest development. *C. elegans* embryos complete embryogenesis on maternal stores and cease to grow beyond that, and postembryonic development is initiated by feeding. Therefore, L1s hatched without food are unable to continue with their development, but there is no evidence of any preparation for the arrest, as is the case with dauer. Therefore, it cannot be considered a diapause but rather starvation induced quiescence (Baugh, 2013; Kostál, 2006). These alternate cycles therefore raise a number of questions about how nutrient availability is sensed and how the responses are regulated, and provide a powerful model to study integrative organismal biology.

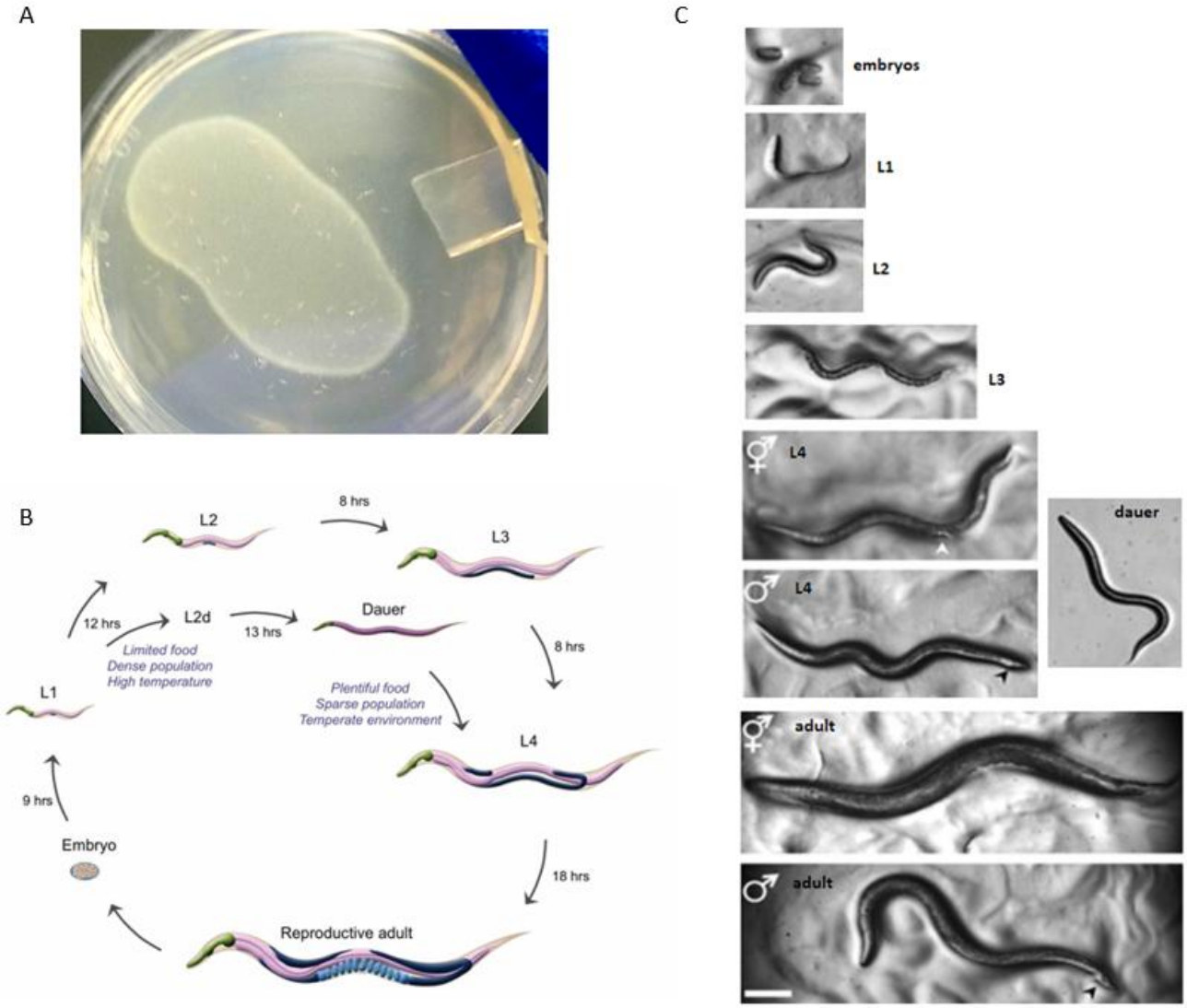

Figure 1.16. C. elegans lifecycle and maintenance. (A) *C. elegans* are grown on agar plates seeded with OP50 E. coli strain. Adults are roughly 1 mm long. (B) *C. elegans* has two alternative life-cycles. If food is abundant and conditions are favourable, after hatching the larva passes through 4 larval stages, L1-L4, after which it enters adulthood and becomes reproductively mature. If conditions are not favourable, newly hatched L1 enters an alternate development path, developing into a form called Dauer. A Dauer worm does not feed and can live for several months. When conditions are improved, Dauer develops directly into the L4 stage, and the development continues normally. Image taken from www.wormatlas.org. (C) Micrographs of worms in different stages of development. Males are distinguished by their distinctive tail morphology and are very rare in

nature. The white arrow points to the hermaphrodite vulva; the black arrows show the male tail. Images taken from www.wormbook.org.

1.9.2.2. Nomenclature

In *C. elegans*, genes listed in the WormBase are assigned identifiers such as 'WBGene00006415'. Alternatively, if the protein product can be classified as a member of a family, a name can be assigned consisting of three or four italicized lowercase letters and a hyphenated italicised Arabic number (e.g. *ctl-2*, *rsks-1*). Some genes will have additional numbers assigned, notifying equal similarity to a human homologue (e.g. *cln-3.1*, *cln-3.2*). Genes can also be referred to by their sequence name, which is derived from their position on a cosmid, fosmid, or YAC clone (e.g. F38H4.5). Protein can be referred to by the relevant gene name in non-italicized capital letters (e.g. CTL-2). For proteins whose names are distinct from the gene name, a combined name can be used (e.g. *let-60*/RAS or *let-60* RAS) (https://wormbase.org/).

2. METHODS

2.1. Part I

2.1.1. Strains and growth conditions

Wild type Y258 *Saccharomyces cerevisiae* strain was used. Y258 WT and the Sod2p overexpressing (oe *SOD2*) strains were purchased from Thermo Scientific (Dharmacon), and deletion mutants were constructed using a homologous recombination based procedure where the target gene was replaced by a hygromycin B resistance cassette (Goldstein & McCusker, 1999). Hygromycin B resistance cassette was amplified from pAG32 plasmid (Addgene). Oligonucleotides used for gene deletions are listed in the Table S2. Petite mutant strains were constructed following a standard protocol (Goldring, Grossman, & Marmur, 1971). Y258 and petite strains were grown on YPD medium with 2% (w/v) glucose, deletion mutants on YPD medium with 2% (w/v) glucose and 100 □g/mL hygromycin B (Sigma), and oe *SOD2* strain in uracil drop-out (-URA) medium with 2% (w/v) glucose, at 30^{o}C with shaking. Expression from the plasmid was induced by 2% galactose using the following procedure: overnight culture was diluted 100x and grown until mid-exponential phase. Then, the cells were pelleted by a 5-min centrifugation at 4000 g and resuspended in -URA

medium without glucose, supplemented with 2% galactose. HS was performed at 34°C for 3 hours with shaking starting at early exponential phase (OD 0.2-0.3). Control cells were kept at 30°C. For pharmacological treatments the following final concentrations were used: 220 nM rapamycin, 10 □M carbonyl cyanide m-chlorophenyl hydrazine (CCCP). The rapamycin treatment was performed for 90 minutes starting in the mid-exponential growth stage (OD 0.5-0.6). The cells were exposed to CCCP during HS, and at optimal growth temperature for control, starting in early exponential phase (OD 0.2-0.3) for 3 hours. Unless stated otherwise, the cells were harvested by 5-minute centrifugation at 3500 × g, washed and treated accordingly.

2.1.2. Replicative lifespan measurement

Replicative lifespan (RLS) for all strains was determined by micromanipulation. RLS measurement involves counting the number of daughters produced by individual mother cells. Briefly, using a microdissection apparatus equipped microscope suitable for yeast (SporePlay, Singer Instruments), cells were transferred to defined places on the agar plates and virgin daughter cells were collected. Each cell was monitored continuously over several days every 60-90 minutes until all mother cells stopped budding. A total number of daughter cells was noted for each mother cell. Control cells were incubated at 30°C on YPD plates for the duration of the experiment. HS was performed by placing the YPD plates at 34°C for 3 hours at the cell replicative age of 1-3 generations. For the RLS measurement of the oe *SOD2* strain, -URA plates were used.

2.1.3. Glutathione extraction and measurement

Cells were collected, washed and weighed. 10 mM PBS supplemented with zymolyase (0.06 U/µL) was used to lyse the cell wall, leaving behind spheroplasts. Spheroplast solution was centrifuged at 3500 x g, and the pellet was incubated with spheroplast lysis buffer (1mL buffer per 0.5 g of cell pellet; 0.6 M sorbitol, 10 mM Tris-HCl (pH 7.4), 1 mM PMSF) on ice for 30 minutes with occasional vortexing, and centrifuged at 14,000 x g. Supernatant was collected and the pellet was discarded. Proteins were precipitated using trichloracetic acid (TCA), where 1 volume of 100% TCA was mixed with 4 volumes of cellular extract followed by a 10-minute incubation at 4°C, in order to avoid the detection of thiol groups. Protein precipitate was pelleted at 10,000 x g for 5 minutes. The supernatant was collected and used for GSH measurement by the method of Ellman (ELLMAN, 1959). 2mM 5,5'-Dithio-bis(2-nitrobenzoic acid) (DTNB, Ellman's reagent, Sigma) stock solution was prepared and stored at 4°C. DTNB working solution was prepared by mixing 50

□L of the DTNB stock, 100 □L of 1M Tris pH 8.0 and 840 □L of water, which is then added to 10 □L of the sample, followed by a 5-minute incubation at room temperature. Absorbance was measured at 412 nm. Molarity of SH groups was then calculated by dividing the absorbance with the molar extinction coefficient, $13600 M^{-1}$ cm^{-1}.

2.1.4. Growth curves

Overnight cultures were diluted 50x in YPD medium with 2% glucose, and 200 µL were aliquoted in triplicate in sterile U-bottom transparent 96 well plates. Plates were incubated in a temperature controlled Tecan Infinite F200 instrument with shaking, and OD measurement was taken every 15 minutes to construct the growth curves. Generation times were extrapolated from the exponential growth phase of the curve using the following formula, where N_0 is the initial OD value, N_t is the final OD value, and t is the time between N_0 and N_t:

$$\frac{\log 10\left(\frac{Nt}{N0}\right)}{0.3} = g\,;\frac{t}{g} = \text{doubling time} \qquad (2.1.)$$

2.1.5. Respiration measurement

Oxygen uptake was monitored polarographically with a Clark-type electrode fitted oxygraphy (Oxygraph, Hansatech, Norfolk, UK). Cells were collected during the exponential growth phase, spun and resuspended in appropriate medium at the density of 30×10^6 cells/mL. 500 µl of density adjusted culture was transferred to an airtight 1.5 mL oxygraph chamber. Cells were assayed in conditions resembling to the ones in a flask culture (30°C and stirring). Oxygen content was monitored for at least 4 minutes. Complex III inhibitor antimycin (10 µg/mL final) was routinely added to the cultures and compared to the rate observed without antimycin, to ensure the oxygen consumption observed was due to the activity of the respiratory chain.

2.1.6. Flow cytometry – ROS level measurements

For the mitochondrial superoxide measurement, cells were incubated in the dark with 3 µM MitoSOX Red (Thermo Scientific) for 10 minutes at 37°C with shaking. For the total ROS level measurement, cells were incubated in the dark with 10 µg/µL 2',7'-dichlorofluorescein diacetate (H2DCFDA, Sigma) for 120 min at 37°C. Subsequently, all samples were analyzed on FACSCalibur flow cytometer. Fluorescence of both dyes was measured in 10,000 cells using excitation at 488 nm and monitoring emission at 635 nm. The collected data was analysed using

FlowJo software version 7.2.5 for Microsoft (TreeStar, San Carlos, CA, USA) to determine the mean green fluorescence intensity after each treatment. The results represent the mean fluorescence of the 10,000 cells. MitoSOX as well as H2DCFDA fluorescence of all strains is expressed as the percentage of the WT fluorescence at optimal growth temperature.

2.1.7. NADP+/NADPH ratio measurement

$NADP^+$/NADPH ratio was measured using the $NADP^+$/NADPH Quantification Kit from Sigma (MAK038) according to the manufacturer's instructions. Briefly, cells were harvested as previously described and washed using cold 10 mM PBS pH 7.4, followed by a 1-hour zymolyase treatment at 37^{o}C. Spheroplasts were harvested by centrifugation at 3000 rpm for 5 minutes and treated with $NADP^+$/NADPH extraction buffer supplied in the kit for 10 minutes on ice. Samples were then centrifuged at 10000 × g for 10 minutes and the supernatant was collected. Protein concentration was measured in the supernatant and used for normalization of $NADP^+$/NADPH ratios. Aliquots of the extracted samples were stored for measurement to give the levels of $NADP_{total}$. In the rest of the extracted samples, to detect NADPH, $NADP^+$ is decomposed by heating the extracted samples to 60°C for 30 minutes in a water bath, followed by cooling on ice. Under these conditions, all $NADP^+$ is decomposed leaving only NADPH. Standards and samples were distributed into a 96-well plate and exposed to a master reaction mix followed by a 5-minute incubation at room temperature and the addition of NADPH developer, supplied in the kit. The absorbance is then read at 450 nm. The $NADP^+$/NADPH ratio is calculated according to the following equation:

$$ratio = (NADP_{total} - NADPH)/NADPH$$

2.1.8. Vacuole staining

Yeast cultures were grown and treated as described. CellTracker Blue CMAC (4-amino-4-chloromethylcoumarin; Invitrogen) dye was added directly to the culture medium (0.1 mM final concentration) of the growing cultures and incubated for 30 minutes. Stain was added so that the ending of the 30-minute incubation coincided with the end of the HS or rapamycin co-incubation. Immediately following incubation cells were collected and imaged as described below.

2.1.9. Slide preparation

Microscope slides were prepared as follows: 200 µL of YPD media containing 2% agarose was placed on a preheated (30^{o}C for OGT and 34^{o}C for HS) microscope slide, covered with a cover slip,

and cooled before applying yeast cells directly onto the YPD-agarose pad to obtain a monolayer. Once dry, the cover slip was placed back and sealed. The slide was mounted on temperature-controlled Nikon Ti-E Eclipse inverted/UltraVIEW VoX (Perkin Elmer) spinning disc confocal setup, driven by Volocity software (version 6.3; Perkin Elmer). Images were recorded through 60xCFI PlanApo VC oil objective (NA 1.4) using coherent solid state 488 nm/50 mW diode laser with DPSS module, and 1000x1000 pixels 14 bit Hamamatsu (C9100-50) electron-multiplied, charge-coupled device (EMCCD). Unless specified otherwise, images were processed using Image J software.

2.1.10. Tor1p localization analysis

Untreated control strain with Tor1-GFP fusion (obtained as a gift from Prof. Tatsuya Maeda) as well as Tor1-GFP strains treated with 220 nM rapamycin or HS (described elsewhere) were centrifuged at 4000 × g for 3 minutes, resuspended in ≈50 μL YPD, and placed on agarose pads and imaged as described above. Images were analyzed using ImageJ software and manually scoring fractions of cells displaying distinct Tor1-GFP localization. Cells were scored as having completely vacuolar, completely cytosolic, or Tor1-GFP localization in both compartments.

2.1.11. Mitochondrial morphology

Mitochondrial morphology was monitored using the MitoLoc plasmid (obtained as a gift from Prof. Markus Ralser) (Vowinckel, Hartl, Butler, & Ralser, 2015). Each studied yeast strain was transformed according to the described protocol (Gietz & Schiestl, 2007) with the only difference that the cells were incubated with the plasmid overnight at room temperature. The exposure time was 100 ms for GFP and 5–10% laser intensity was used. Approximately 500 cells of each condition were examined. Images were analyzed using ImageJ software with the MitoLoc plugin.

2.1.12. RNA extraction

Total RNA was isolated from yeast cells following the procedure of the NucleoSpin RNA kit (Macherey & Nagel) for up to 3×10^8 yeast cells, which dictates incubation with 50-100 U of zymolyase for 1 hour at 30°C. The quality of resulting total mRNA was tested on 1% agarose gels.

2.1.13. Quantitative real-time PCR

cDNA was synthesized from 1000ng of total RNA using iScript™ cDNA Synthesis Kit (Biorad). The resulting cDNA was diluted 100×, mixed with primer pairs for each gene and SYBRgreen

(BioRad). All primer pairs were designed using Oligo Calc: Oligonucleotide Properties Calculator to have a melting temperature of 60°C. The qPCR reaction was run on a QuantFlexStudio 6 (Life Technologies) using 40 cycles, after which the melting curves for each well were determined. qPCR differential expression was estimated with EasyqpcR (https://bioconductor.org/packages/release/bioc/html/EasyqpcR.html) using the methods from (Hellemans, Mortier, De Paepe, Speleman, & Vandesompele, 2007). Final fold change values were estimated relative to the *UBC6* gene in the control strain replicates.

2.1.14. Quantitative real-time PCR primers

Table 2.1.1. **qPCR primer list for *S. cerevisiae*.**

YGR240C	PFK1 Fw	ATG CAA TCT CAA GAT TCA TGC TAC G
	PFK1 Rc	TCA ACC ATT TCA CAG ATT CTT TCC AAA
YHR174W	ENO2 Fw	ATG GCT GTC TCT AAA GTT TAC GCT AG
	ENO2 Rc	TTG GTC CCT AAC ATC TAG GTT GGC C
YBR196C	PGI1 Fw	ATG TCT GAA CCA GCT CAA AAG AAA CAA AA
	PGI1 Rc	ATG TCT GAA CCA GCT CAA AAG AAA CAA AA
YAL038W	PYK1 Fw	ATG TCT AGA TTA GAA AGA TTG ACC TCA TTA AA
	PYK1 Rc	TAC AAT TCT TCG GAC TTT CTG GCG TT
YNR001C	CIT1 Fw	ATG TCA GCG ATA TTA TCA ACA ACT AGC AA
	CIT1 Rc	GGT TTT ACC GTG TTC TTT CTT GAA TTT TTT A
YOR136W	IDH1 Fw	GCT TAA CAG AAC AAT TGC TAA GA
	IDH1 Rc	GTT GAT GAT TTC ATT CGT GAA GTC
YPL262W	FUM1 Fw	ATG TTG AGA TTT ACC AAT TGT AGT TGC AAG
	FUM1 Rc	AGG CAA TGG CAT TCT TTC ACG AGC
YKL085W	MDH1 Fw	ATG TTG TCA AGA GTA GCT AAA CGT GC
	MDH1 Rc	CTC TTC TGG AGT AAA CCC CTT GAC
YLR304C	ACO1 Fw	GCTAATAACTGGCCATTGGATGTCA
	ACO1 Rc	AAGGTTTCTAATTGGCCATCACGTT
Q0105	COB Fw	ATG GCA TTT AGA AAA TCA AAT GTG TAT TTA AGT T
	COB Rc	TAT GCA CAT CTC TTA TAA TAT GTT CAA CAG A
YOR065W	CYT1 Fw	ATG TTT TCA AAT CTA TCT AAA CGT TGG G
	CYT1 Rc	CTA CTT TCT TGG TTT TGG TGG ATT GA
Q0045	COX1 Fw	ATG GTA CAA AGA TGA TTA TAT TCA ACA AAT GC
	COX1 Rc	ATT AAA GCA GGC ATT ACT AAG AAG AAA ATC A

Q0250	COX2 Fw	ATG TTA GAT TTA TTA AGA TTA CAA TTA ACA ACA TTC AT
	COX2 Rc	GTC CAT GTT TAA TAT ATT TAT ATG CAA TAG GAT T
YGL187C	COX4 Fw	ATG CTT TCA CTA CGT CAA TCT ATA AGA TTT TT
	COX4 Rc	TCT AAC CTA GCT AAA CCA GTT TCT TGA T
YBL099W	ATP1 Fw	ATG TTG GCT CGT ACT GCT GCT ATT C
	ATP1 Rc	GCA ATA CCA TCA CCG ACT GCA AG
Q0085	ATP6 Fw	ATG TTT AAT TTA TTA AAT ACA TAT ATT ACA TCA CCA TTA
	ATP6 Rc	TAA ATA GCT TCT TGT GAA ATT AAT CAT CTT GAA C
YPR020W	ATP20 Fw	ATG CTA AGC AGG ATC CAA AAT TAT ACC A
	ATP20 Rc	TCT GTA GGC TTT AGA GCA AAG TTT AGG
YGL205W	POX1 Fw	GTTGGGTGATTATACTGAAATTTGG
	POX1 Rc	CCTTTGTAATTTCATCGGAAATATG
YIL160C	POT1 Fw	GGTAAGGGTGAATCGAAGAGGAAGA
	POT1 Rc	AGTTCAAATCAGCCCTCAAAGGTTC
YJR104C	SOD1 Fw	ATG GTT CAA GCA GTC GCA GTG TTA AA
	SOD1 Rc	TTG AAA GGA TTG AAG TGA GGA CCA G
YHR008C	SOD2 Fw	ATG TTC GCG AAA ACA GCA GCT GC
	SOD2 Rc	ATT GGT CAA CAG CAG TGT TGA ATC C
YER100W	UBC6 Fw	ATG GCT ACA AAG CAG GCT CAC AAG
	UBC6 Rc	GGT TTG TAT GGA TAA TCA GAC GGG AA
YBR072W	HSP26 Rc	ATG TCA TTT AAC AGT CCA TTT TTT G
	HSP26 Fw	TTA GTT ACC CCA CGA TTC TTG A
YDR171W	HSP42 Fw	ATG AGT TTT TAT CAA CCA TCC CTA TCT
	HSP42 Rc	CAA TTT TCT ACC GTA GGG TTG GG
YAL005C	SSA1 Fw	ATG TCA AAA GCT GTC GGT ATT GAT TTA
	SSA1 Rc	CTC TCA AGA CCT TTT CAA CTG GG
YLL026W	HSP104 Fw	ATG AAC GAC CAA ACG CAA TTT ACA G
	HSP104 Rc	ACA AGA AAT ATC AAC TAA ATC CAA AGC A
YGR088W	CTT1 Fw	ATG AAC GTG TTC GGT AAA AAA GAA GAA A
	CTT1 Rc	TTA ATT GGC ACT TGC AAT GGA CCA A
YDR256C	CTA1 Fw	ATG TCG AAA TTG GGA CAA GAA AAA AAT G
	CTA1 Rc	TCA AAA TTT GGA GTT ACT CGA AAG CTC
YPL091W	GLR1 Fw	ATG CTT TCT GCA ACC AAA CAA ACA TTT
	GLR1 Rc	TCA TCT CAT AGT AAC CAA TTC TTC TGC
YJL101C	GSH1 Fw	ATG GGA CTC TTA GCT TTG GGC A
	GSH1 Rc	TTA ACA TTT GCT TTC TAT TGA AGG CTT ATT
YNL241C	ZWF1 Fw	ATG AGT GAA GGC CCC GTC AAA TT
	ZWF1 Rc	CTA ATT ATC CTT CGT ATC TTC TGG CT
YPR035W	GLN1 Fw	GCT TGT TTG TAT GCC GGA TT
	GLN1 Rc	CGT TCC AGT CAC CCT TCA AT

YKR039W	GAP1 Fw	AGG GTT TGC CAA GTG TTG TC
	GAP1 Rc	AAC GCA ATA AGA CCG AAT GC
YNL142W	MEP2 Fw	TGT GGA TTA TGG TCC CAG GT
	MEP2 Rc	CGA AAC CCA AAG AAT TCC AA

2.1.15. Cloning primers

Table 2.1.2. *S. cerevisiae* cloning primer list.

Upstream flanking region of glr1	
FW1_glr1	GTT TGC GTT TGT TGG TCA ATT CTA
RC1_glr1	TAT GTC GAC AAA GTT CTG TAA ACT AAT
Downstream flanking region of glr1	
FW2_glr1	TAT GAG CTC AGC AAC GAA ACT AGA CGT
RC2_glr1	ACC AAA GAG CTT TGA AGG TCA GA
Upstream flanking region of hap4	
FW1_hap4	TCGATTTTGCAGATTGTTCTAAAAGTAAAT
RC1_hap4	TATCAGCTGAAAGTCTTTGCGGTCAT
Downstream flanking region of hap4	
FW2_hap4	TATGAGCTCAATAGGCATGTTGCAATA
RC2_hap4	TCTCTTGACGTGTTTCACCATACG
Hygromycin resistance cassette, amplified from pAG32	
FW_HygB	CGTACGCTGCAGGTCGAC
RC_HygB	ATCGATGAATTCGAGCTCG

2.1.16. Sequence mapping

Sequenced reads (Illumina 50bp single-end) were mapped to the SacCer3 reference genome (April 2001 revision, http://www.ncbi.nlm.nih.gov/assembly/285498/, genome obtained from the UCSC Genome Browser site http://genome.ucsc.edu/, (Rosenbloom et al., 2015)) using the STAR aligner (version 2.3.0e, (Dobin et al., 2013)). Reference transcripts were obtained from the Ensembl yeast genome resource in GTF format.

2.1.17. Read counting

Raw read counts were determined from the overlaps with the Ensembl yeast genes using the htseq-count version 0.6.0. from the HTSeq framework (Anders, Pyl, & Huber, 2015), with the following parameters: -a 10 –s no.

2.1.18. Differential expression analysis

Raw reads were analyzed for differential expression with the DeSeq2 package (Love, Huber, & Anders, 2014) within the Bioconductor framework (Huber et al., 2015) under R statistical package (R Core Team), by previously filtering out the outlier replicates with PCA analysis. Selected genes were visualized in a heatmap by using log2(FC) values. Conditions with adjusted p-value lower than 0.1 were crossed out as not significant (labeled with a gray X).

Experiments described in sections 2.1.17. through 2.1.19. were performed and analysed by dr. Kristian Vlahoviček from University of Zagreb.

2.2. Part II

2.2.1. Strains

Animals were passaged and maintained at 20 °C on NGM media seeded with OP50 bacteria. Strains were purchased from Caenorhabditis Genetics Center at the University of Minnesota (https://cgc.umn.edu/). To obtain *ctl-2* mutant with GFP reporters we crossed GFP-carrying strains (OG497 and VS15) as follows. Unsynchronized populations rich in L4 stage worms of GFP carrying strains were repeatedly heat shocked at 30°C or 37°C for multiple generations until male worms were observed on the plate. The males were then picked and placed on a separate 3 cm plate seeded with OP50 with 2 or 3 L4 hermaphrodites to obtain more males. GFP carrying males were then picked on a separate 0P50 seeded plates together with ctl-2 L4 hermaphrodites. Once resulting the progeny reached L4 stage, individual F2 worms were picked onto individual plates to lay eggs, after which they were collected for screening under fluorescent microscope. The eggs and the progeny of the worms who exhibited appropriate fluorescence were confirmed to be *Δctl-2* using PCR.

2.2.1.1. Genotyping primers

Table 2.2.1. *C. elegans* genotyping primer list.

ctl-2 Fw	TTAGATATGAGAGCGAGCCTGTTTC
ctl-2 Rc	CTAGTGGTACATCCATGCAAATGC

2.2.2. Synchronization

Mixed plates of worms were chunked onto fresh NGM plates seeded with OP50 and grown until they contained predominantly gravid adults. Gravid adults were washed from the plate with M9 buffer or water, and the plate was gently scraped with a spatula to collect the already laid eggs. The eggs and gravid worms were settled by gravity or brief centrifugation in 15 mL Falcon tubes. The worm and egg pellet was incubated in 20% hypochlorite solution (recipe) for 5 minutes with occasional vortexing, until most worms are broken. The eggs are then settled by centrifugation and washed with sterile M9 buffer two times. The pellet was then either incubated in a sterile 7 cm plate in 7 mL of sterile M9 buffer at RT with light shaking or seeded on a clean NGM plate where they can hatch without food. After hatching, the arrested L1 larvae are transferred to NGM plates seeded with appropriate food source to grow.

2.2.3. Lifespan measurement

10-15 L4 hermaphrodites from a synchronized population were transferred to 3 cm NGM plates seeded with OP50. They were counted and transferred to new plate every two days until they stopped responding to stimulation. Minimum of 100 worms was picked for each condition for every repetition to ensure sufficient number after censoring stragglers, bagged worms, and worms killed during transfer.

2.2.4. Heat shock

Heat shock was performed on plates in 30°C. Plates with synchronized and well fed L4 worms were incubated for 4 hours at 30°C, after which they were either collected for RNA isolation or staining without recovery, or returned to 20°C for lifespan analysis.

2.2.5. Thermotolerance assay

Plates with synchronized and well fed L4 worms were taken from 20°C and placed at 37°C. One plate was taken out each hour for 8 hours. Plates were left at RT to recover over night, and survival was scored the next day. Minimum of X worms were counted for each plate.

2.2.6. RNA isolation

RNA was isolated from worm pellets kept at -80°C. 250 µL of Trizol was added to the pellet, vortexed for 30 seconds and incubated at 4°C with shaking for 1 hour. Then 50 µL of chloroform was added, followed by 30 second centrifugation and 3 minutes at RT. The tubes were then

centrifuged for 15 minutes at 12000 rpm at 4°C. The top layer (app. 125 µL) was transferred to a fresh tube and the chloroform addition and centrifugation steps were repeated. 125 µL of 2-propanol was added, the tubes were mixed by inverting to avoid shearing the RNA and incubated at RT for 3 minutes. The tubes were centrifuged at 12000 rpm for 10 minutes and supernatant was carefully decanted without disturbing the RNA pellet. The pellet was washed with 250 µL of 70% ethanol and spun down at 14000 rpm for 5 minutes at 4°C. Supernatant was removed and the tubes air dried inside the hood. Pellets were dissolved in 10 µL RNAse-free water and heated at 65°C for 10 minutes. Concentration was determined using Nanodrop (Thermo Scientific) and the quality was checked on an agarose gel. Samples were stored and kept at -80°C.

2.2.7. List of primers (qPCR)

Table 2.2.2. qPCR primer list for *C. elegans.*

Act-1 Fw	AGGAGTCATGGTCGGTATGG
Act-1 Rc	GCTTCAGTGAGGAGGACTGG
gcs-1 Fw	GTGTCGTGCAAAGCTGAAGA
gcs-1 Rc	CTGTCTGCGCAATTTCATGT
nit-1 Fw	CACGAACTCCAGAAGGAAGG
nit-1 Rc	TCGGTGCTTTCCAAGGTAAC
raga-1 Fw	AGCTATTTTGGATGCCGATG
raga-1 Rc	TGAATGCGGAGAATTGACTG
skn-1 Fw	CTCCATTCGGTAGAGGACCA
skn-1 Rc	GGCGCTACTGTCGATTTCTC
daf-16 Fw	AATTGCTCCACCACCATCAT
daf-16 Rc	AATTCCAGGCAGTGGAGATG
mtl-1 Fw	ATGGCTTGCAAGTGTGACTG
mtl-1 Rc	GTCTTGTCTCCGCACTGCTT
gst-10 Fw	ATTCGAAGACATTCGGTTCG
gst-10 Rc	AACATGTCGAGGAAGGTTGC
sdz-8 Fw	GAGCTACGGAACGAATACGG
sdz-8 Rc	CAGTGATGGAACCAAGTCCA
pod-2 Fw	CTTGAATGGTCATGGCACAG
pod-2 Rc	ATAGTCGCGGAGCAGTTGAT
fasn-1 Fw	TCCATTTGCAACTGATTCCA
fasn-1 Rc	ATCCAATTTGATTGGCTTGG
FAT-5 Fw	GAGGATCCGGTGCTGATG
FAT-5 Rc	AGCAGAAGATTCCGACCAAG
fat-6 Fw	CTCGTTCAAACATCGCAAAA

fat-6 Rc	GAGCTGGTAGAGTCCGATGG
Pdi-6 Fw	GAACCTTTGGGGATGGATTT
Pdi-6 Rc	GAAGTGCGTCCCTTTCCATA
Hsp-60 Fw	GTCGGAACCACTGGAGTCAT
Hsp-60 Rc	CCGGCACAATATCCTGAACT
Clpp-1 Fw	GGTGAAAAAGGAATGCGAAG
Clpp-1 Rc	TCACGGTCAAGGGTTTTCTC
Hsp-6 Fw	GAGCTCCAGCCAAAAGACAG
Hsp-6 Rc	AATGCTCCAACCTGAGATGG
ND1 Fw	CCATCCGTGCTAGAAGACAA
ND1 Rc	TCCCTTTCACCTTCAGAAAAA
Sdhd-1 Fw	TGGAATGCTCCCAATTCTTC
Sdhd-1 Rc	CGAGCAGAAGACCAGTGATG
CYTB Fw	AATGGGGCCAGGTTATTTTT
CYTB Rc	TGGCCCTCAAATTGGAATAA
Cyc-1 Fw	TGGAGTGAAGGTTGATGACG
Cyc-1 Rc	GAGCCCACTTCTTTCTGGTG
Cox-1 Fw	TCGGTGGTTTTGGTAACTGA
Cox-1 Rc	TGCCCCATTGTTCTTAAAGG
Cox-2 Fw	TGTTATTCATGCTTGGGCATT
Cox-2 Rc	TGCTCCACAAATCTCTGAACAT
Cox-3 Fw	TTGGCAGCTTATTTTACAGGAA
Cox-3 Rc	TCCAACCCCAGATGATGATT
Cox-4 Fw	GGATACGGAGCAAATGGAGA
Cox-4 Rc	GAATTCGGACAGCGTTTGAC
Atp-2 Fw	GAACCTTCCACCAATCCTCA
Atp-2 Rc	TACGGCCAAGAGTTTCTGGT
Atp-6 Fw	TGTCCTTGTGGAATGGTTGA
Atp-6 Rc	CGCACTGTTAAAGCAAGTGG
Sod-1 Fw	ATCCGAGATCCGTCACGTAG
Sod-1 Rc	GCGTTTCCAGTCTTCTTGGA
Sod-2 Fw	TTGTTCAACCGATCACAGGA
Sod-2 Rc	TGACGTTTCCTTTGGAGACC
Sod-3 Fw	CTTGGCTAAGGATGGTGGAG
Sod-3 Rc	TTCCAAAGGATCCTGGTTTG
Sod-5 Fw	GGAACTGCTGTCTTCGGAAC
Sod-5 Rc	CGGAATCTCTTCCTCCATGA
Prx-5 Fw	GCAAACCCTTTCACAACCAT
Prx-5 Rc	AACATTTTTGGAACGCTTGC
Prx-11 Fw	GGAATTCCTCACAGGAGCAG
Prx-11 Rc	TGCGATTTTTCGATTCCTTT

Tomm-40 Fw	GCGACACCAACAGAAAGTGA
Tomm-40 Rc	AAATCGGTATCCGGTGTTCA
Tin-44 Fw	CCATGAAAGGGCCTACACAC
Tin-44 Rc	CAACTTTTCCATCGGCATTT
Gspd-1 Fw	CCAGCAAGTTTGAATGCTGA
Gspd-1 Rc	CAGCAAGAGCATACGTTGGA
daf-22 Fw	AGGTGATCAATGCCCGTAAG
daf-22 Rc	TTGAATTCTCAGCGAACACG
maoc-1 Fw	GGGCTGGAAATGATTCTGAC
maoc-1 Rc	ACTGTTGGAAGTTCGGAAGC
acox-1 Fw	AGCGATCTCCTCCATCTTCA
acox-1 Rc	CGGCCTAGGACAGATCTCAG
hsp-16.1 fw	CGCAGTTCAAGCCAGAAGAT
hsp-16.1 rc	AATCGCTTCCTTCTTTGGTG
hsp-16.2 fw	CAGCTCAACGTTCCGTTTTT
hsp-16.2 rc	GATAGCGTACGACCATCCAAA

2.2.8. GSH measurement

Glutathione was measured as described in (Caito & Aschner, 2015). In short, L4 worms were washed from the plates and pelleted with sterile water. The pellets were resuspended in 110 µL extraction buffer (0.4 mM KH_2PO_4, 11 mM K_2HPO_4, 1 mM EDTA, 1% Triton X-100, 27.5 mM sulfosalicylic acid, and protease inhibitor), flash frozen in liquid nitrogen and thawed at 37ºC three times, followed with 20 second sonication. Samples were then pelleted for 10 minutes at 9200 ×g, 4ºC. 20 µL supernatant was used for GSH measurement. DTNB solution is added (0.8 mM 5,5 - Dithiobis(2-nitrobenzoic acid), 10 U glutathione reductase, 0.4 mM KH_2PO_4, 11 mM K_2HPO_4) and GSH in the sample reacts directly with the DTNP to create a chromophore GSH-3-thio-6 nitrobenzoate or GSH-TNB. The rate of GSH-TNB formation is proportional to the amount of GSH in the sample. When NADPH is added, GSH is recycled back into the pool both from GSH-TNB and GSSH, and the reaction with the DTNB is continued until DTNB is exhausted from the mixture, thus the entire GSH pool is measured. The rate of change in absorbance is linear and the GSH concentration is determined by linear regression from a standard curve of known GSH concentrations (Figure 2.2.1.).

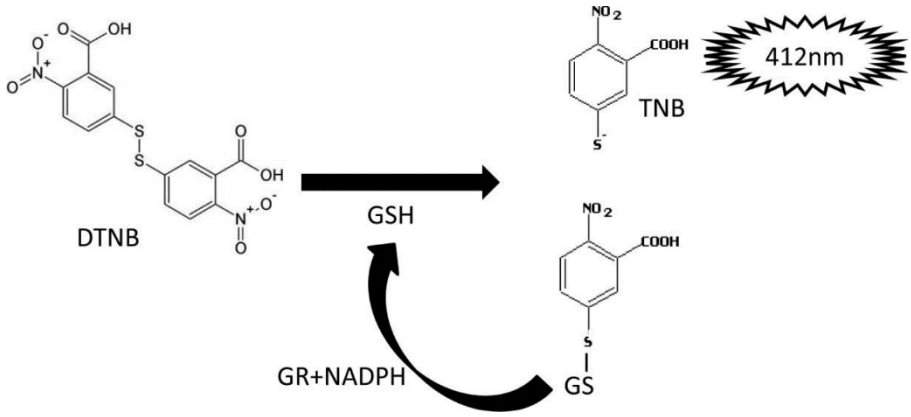

Figure 2.2.1. Schematic of the DTNB reaction with the glutathione in the sample. Image taken from (Caito & Aschner, 2015).

2.2.9. Live imaging

Synchronized worms were washed off the plates and washed from bacteria. Slides with 2% agarose in M9 pads were prepared fresh before each imaging. Washed worms were immobilized using imidazole, placed on the agarose pad, and covered with a cover slip. The cover slip was secured with nail polish. Imaging was done on temperature-controlled Nikon Ti-E Eclipse inverted/UltraVIEW VoX (Perkin Elmer) spinning disc confocal setup, driven by Volocity software (version 6.3; Perkin Elmer). Unless otherwise specified, images were analysed using ImageJ.

2.2.10. MitoTracker staining and imaging

Worms were grown on NGM plates containing 2 µM Mitotracker Deep Red until L4 stage. After washing, worms were immobilized with imidazole and imaged on a temperature-controlled Nikon Ti-E Eclipse inverted/UltraVIEW VoX (Perkin Elmer) spinning disc confocal setup, driven by Volocity software (version 6.3; Perkin Elmer). Unless otherwise specified, images were analysed using ImageJ.

2.2.10.1. Mitochondrial morphology analysis

Mitochondrial morphology was analysed using ImageJ as described in (Valente, Maddalena, Robb, Moradi, & Stuart, 2017). In short, images were thresholded and skeletonized for the network analysis. Individual mitochondria were analysed manually from raw images with removed background (Figure 2.2.2.). Statistical difference between groups was determined using t-test.

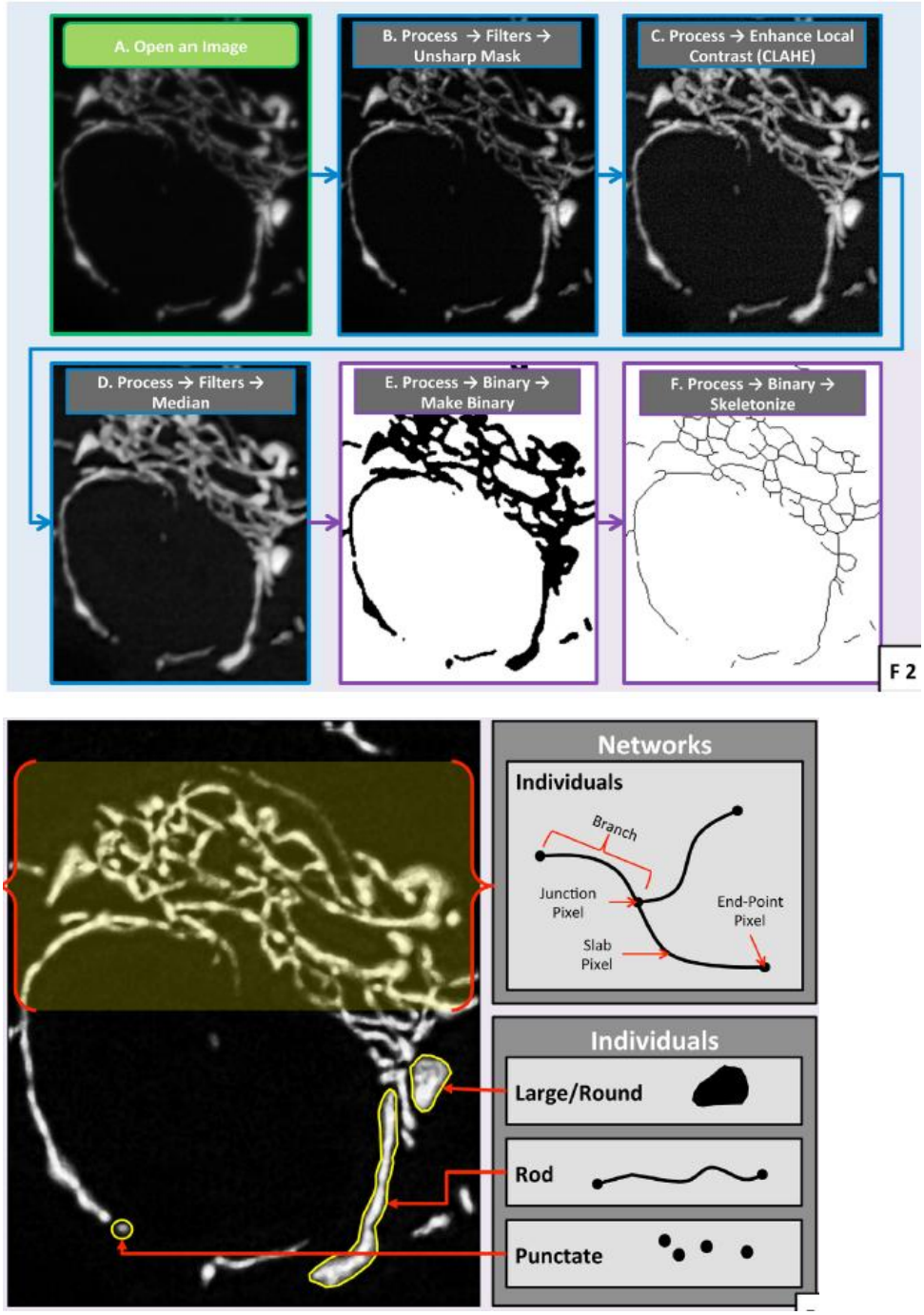

Figure 2.2.2. Mitochondrial morphology analysis. For the analysis of mitochondrial network, images are first processed as described above, then ImageJ ″analyze skeleton″ function is used (top). The explanation of different morphological categories of networked and individual mitochondria (bottom). Images taken from (Valente et al., 2017).

2.2.11. Nile red staining

Nile red stock solution was prepared as a 5 mg/mL solution in acetone. The stock solution was stirred in dark for 2 hours before being used. Working solution was made by diluting 6 µL of the stock solution in 1 mL of 40% isopropanol. Worms were washed from the plates and bacteria were removed by washing in PBST. Pellet of washed worms was incubated for 3 minutes at RT with gentle rocking in 40% isopropanol. After incubation worms were pelleted and the supernatant removed. Worm pellet was incubated in 600 µL of working solution for 2 hours in the dark. After incubation, Nile red solution was removed and the worm pellet was washed in PBST for 30 minutes. Worms were imaged on a 2% agarose pad on a Nikon Ti-E Eclipse inverted/UltraVIEW VoX (Perkin Elmer) spinning disc confocal setup, driven by Volocity software (version 6.3; Perkin Elmer). Green fluorescence was recorded. Unstained control imaged under the same conditions gave no signal.

2.2.12. Oil red O staining

Oil Red O stock solution was prepared as a 5mg/mL solution in 100% isopropanol. To make the working solution, the solution is diluted 3:2 in water (60% isopropanol final concentration). The working solution is filtered through a 0.2 µm filter and allowed to mix for 2 hours before use. Worms were washed from the plates and bacteria were removed by washing in PBST. Pellet of washed worms was incubated for 3 minutes at RT with gentle rocking in 40% isopropanol. After incubation, worms are pelleted and the supernatant is removed. The worm pellet is incubated for 2 hours in 600 µL of ORO working solution with gentle mixing. After staining, the pellet is washed for 30 minutes in PBST. Imaging is done with a colour capable camera.

2.2.13. CellROX staining

Worms were washed from the bacteria until the supernatant is clear. Washed worms were fixed in 3.7% formaldehyde for 15 minutes. Fixed worms were pelleted and washed in M9. The worm pellet was stained with 5 µM Cell ROX Deep Red for 1 hour. Imaging was done within 2 hours of staining. Images were analysed with ImageJ. Statistical difference was determined using multiple t-tests.

2.2.14. Respiration measurement

Oxygen uptake was monitored polarographically with a Clark-type electrode fitted oxygraphy (Oxygraph, Hansatech, Norfolk, UK). Worms were washed until bacteria was removed, then left for

around 15 minutes in clear M9 to allow digestion of the remaining bacteria. Oxygen consumption was recorded for at least 4 minutes. The rate of respiration was normalized to protein content from the sample.

2.3 Statistical analysis

Unless otherwise stated, data in graphs are mean ± SEM from three biological and three technical replicates. Survival experiments were tested with log-rank (Mantel-Cox) test. ANOVA and t-test were used for all other measurements, as indicated for individual graphs. Graphing and statistical analysis was done using GraphPad Prism 7 software. Data in Figure 3.2.12 was visualized using Minitab 19 statistical software. ****P <0.0001; ***P < 0.001; **P < 0.01; *P < 0.05.

3. RESULTS

3.1. Part I: heat stress induced lifespan extension in *Saccharomyces cerevisiae*

This part of the here described research has been published in Aging (Musa, M.*, Peric, M.*, Bou Dib, P., Sobočanec, S., Šarić, A., Nikolić, A., Milošević, I., Vlahoviček, K., Raimundo, N., Kriško, A. (2018). Heat-induced longevity in budding yeast requires respiratory metabolism and glutathione recycling. Aging, 10;9, 2407-2427. *equal contribution)

3.1.1. Mild transient heat stress induces lifespan extension and metabolic changes

It was previously reported that mild transient heat stress is able to induce replicative lifespan extension in yeast (Baldi et al., 2017; Shama, Lai, Antoniazzi, Jiang, & Jazwinski, 1998). RLS was measured as a number of daughter cells produced by one mother cell. For our experiments, the control cells were kept at 30°C for the duration of the experiment i.e. until the mother stopped producing daughter cells. For the heat shock experiment, mother cells were allowed to grow at 30°C until they produced at least one and up to 3 daughter cells, to ensure they are alive and able to reproduce. They were then shifted to 34°C for 3 hours, after which they were placed back to 30°C until the end of the RLS measurement. Number of buds produced is monitored throughout the experiment.

We saw an increase in the number of generations in the heat-treated yeast cells; the median RLS increased from ≈12 generations to ≈18, an approximately 50% increase (Figure 3.1.1.). These results are concurrent with the previously published literature. To understand the underlying changes in the organism that brought about the RLS extension, we looked at the expression levels of key metabolic enzymes and members of the proteostasis network next.

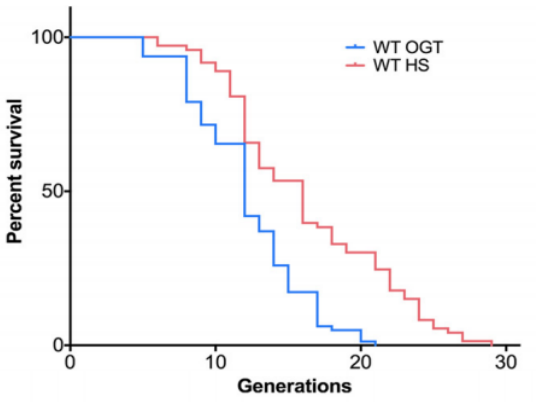

Figure 3.1.1. Mild transient HS leads to RLS extension. Mean and maximum lifespan is extended in yeast that underwent a 3-hour HS at 34ºC. Number of curated cells was 81 for control and 73 for HS-treated cells. Significance of the results was tested with log-rank (Mantel–Cox) test. *P* value is <0.0001.

RNA-Seq results from exponentially growing yeast culture collected directly after heat show that glycolysis is repressed, although glucose is still present in the medium (Figure 3.1.2.). This is interesting because normally in the presence of glucose, glucose metabolism is favoured over respiratory as it produces more molecules of ATP and enables faster growth. Furthermore, maintenance of homeostasis during stress requires energy. However, glucose deprivation has also been shown to extend RLS; therefore, as glycolysis is repressed during mild HS, the mechanisms of HS meadiated and CR mediated lifespan extension might be similar in this case. Further, respiratory chain subunits are upregulated, as well as peroxisomal beta oxidation enzymes, indicating increased energy production.

qPCR measurement confirmed the results of RNA-Seq, and showed upregulation of HSPs, indicative of HSR activation (Figure 3.1.2.). Further, *ZWF1*, encoding glucose-6-phosphate dehydrogenase (G6PD), a rate limiting enzyme of PPP, was upregulated following HS. As only the oxidative branch of PPP was upregulated (TAL1 enzyme, part of the non-oxidative branch, is downregulated), and gene transctipts of ROS scavenging enzymes (*SOD1, SOD2, CTT1, CTA1*), as well as glutathione reductase (*GLR1*) were also upregulated, suggested that cells were undergoing oxidative stress. Lastly, components of the HSR were upregulated, confirming that the mild HS was enough to activate HSR.

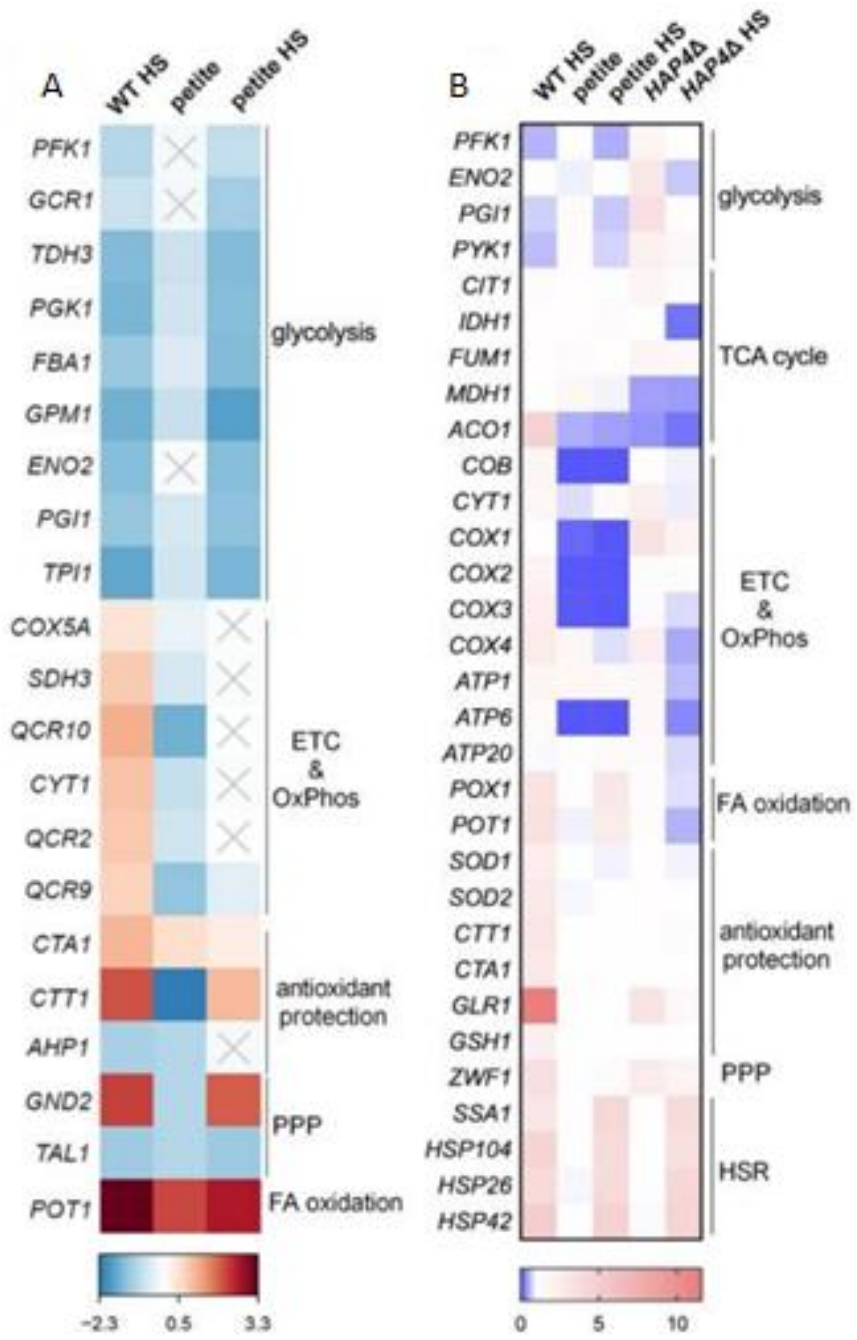

Figure 3.1.2. Differential gene expression reveals changes in metabolic activity. (A) RNA sequencing (RNA-Seq) results reveal changes in metabolic activity during 3 hour HS at 34°C, most prominent being repression of glycolysis and activation of respiration in WT strain; glycolysis is repressed in respiration deficient petite strain as well. Grey X indicates statistically insignificant change. (B) qPCR measurements confirm repression of glycolysis and activation of respiration, and reveal activation of the pentose phosphate pathway and glutathione recycling in WT but not in respiration deficient petite and *HAP4*Δ strains. Individual transcript levels are normalized to *UBC6*.

3.1.2. Heat stress induced replicative lifespan extension relies on increased respiratory activity

The upregulation of respiratory chain subunits revealed by RNA-Seq and RT qPCR indicated increased respiratory capacity. Respiration measurement using a Clark electrode-based setup showed that respiration indeed was increased during HS exposure in WT (Figure 3.1.3A).

To test if increase in respiration is related to the extension of RLS after HS, we measured RLS of the respiration deficient petite strain upon HS exposure. Petite strain showed only background levels of steady state O_2 consumption (Figure 3.1.3A), which did not increase during HS. Further, RLS was unchanged after HS (Figure 3.1.3B). Metabolic response of the petite strain was similar to that of WT in regard to HSR, repression of glycolysis, and peroxisomal beta oxidation, but differed in few key aspects. Unsurprisingly, transcript levels of mitochondrially encoded respiratory chain subunits were very low. Oxidative stress response was also absent in petite strain, evidenced by lack of upregulation of ROS scavenger enzymes and G6PD (Figure 3.1.2.).

The switch from glycolysis t respiration is usually characteristic of the diauxic shift in yeast. Diauxic shift is the switch from fermentative growth in the presence of a carbon source to slower exponential growth by aerobic respiration after carbon source exhaustion. Thus, diauxic shift is accompanied by increased generation time. Although glucose was present in the medium, the downregulation of glycolysis indicated that HS caused the cells to undergo diauxic shift. To exclude this possibility, we measured the growth curves during HS conditions to extrapolate the generation time (Figure 3.1.3C). We determined that the generation time was actually shorter in the heat-treated cells (72 ±4 minutes compared with 120 ± 6 minutes at OGT), which rules out the possibility that the cells underwent diauxic shift during the experiment and caused the observed increase in respiration.

To further support the idea that increased respiration during HS is required for HS induced RLS extension, we repeated the same experiment with *HAP4*Δ strain. *HAP4* is a transcription factor regulating the expression of nuclearly encoded respiratory chain components. *HAP4*Δ yeast can respire, albeit less than WT, but is unable to increase its respiration rate (Figure 3.1.3A). Following HS, *HAP4*Δ strain did not show increase in RLS (Figure 3.1.3D). RT qPCR analysis showed that glycolysis was downregulated, as were peroxisomal beta oxidation enzymes compared with WT. Further, respiratory chain subunits were either downregulated or unaffected, while PPP was not

activated (Figure 3.1.2.). Thus, we believe that the RLS extension is a result of oxidative stress induced by the increase in respiratory activity.

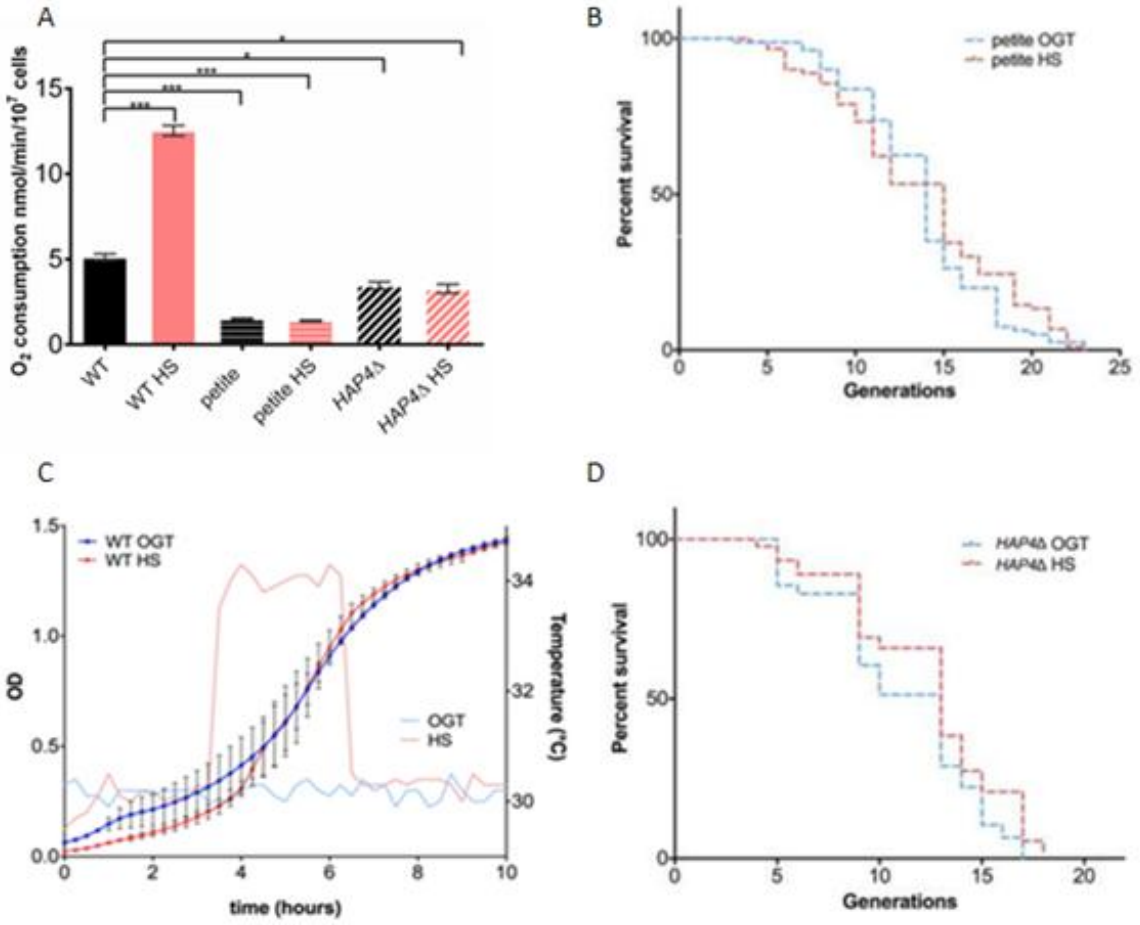

Figure 3.1.3. HS-induced RLS extension is triggered by increased respiratory activity. (A) Oxygen consumption is increased in HS-treated WT. Petite yeast has negligible respiration rate which is unaffected by HS, while *HAP4*Δ strain is unable to upregulate its respiration rate. Data on the graph are mean ± SEM from three biological and three technical replicates. *P* values were calculated using ANOVA plus post hoc. ***$P < 0.001$; **$P < 0.01$; *$P < 0.05$. (B) Growth curves of WT control and WT HS show that generation time is decreased during HS. Respiration deficient petite strain (C) and *HAP4*Δ strain (D) do not have increased RLS following HS treatment. *P* value is >0.05 (Mantel-Cox).

3.1.3. ROS increase is necessary for HS induced RLS extension

Increased respiration was accompanied by increased levels of ROS. Mitochondrial superoxide levels were increased by approximately 50%, while intracellular ROS as measured by 2',7'-dichlorodihydrofluorescin (H2DCF) was increased about 75% in WT but not in petite or *HAP4*Δ strains (Figure 3.1.4A,B). This is concurrent with the results of RNA-Seq and qPCR, which indicate that petite and *HAP4*Δ did not undergo oxidative stress during HS as WT did (Figure 3.1.2.). These results also suggest that the PPP activation in WT is a result of oxidative stress.

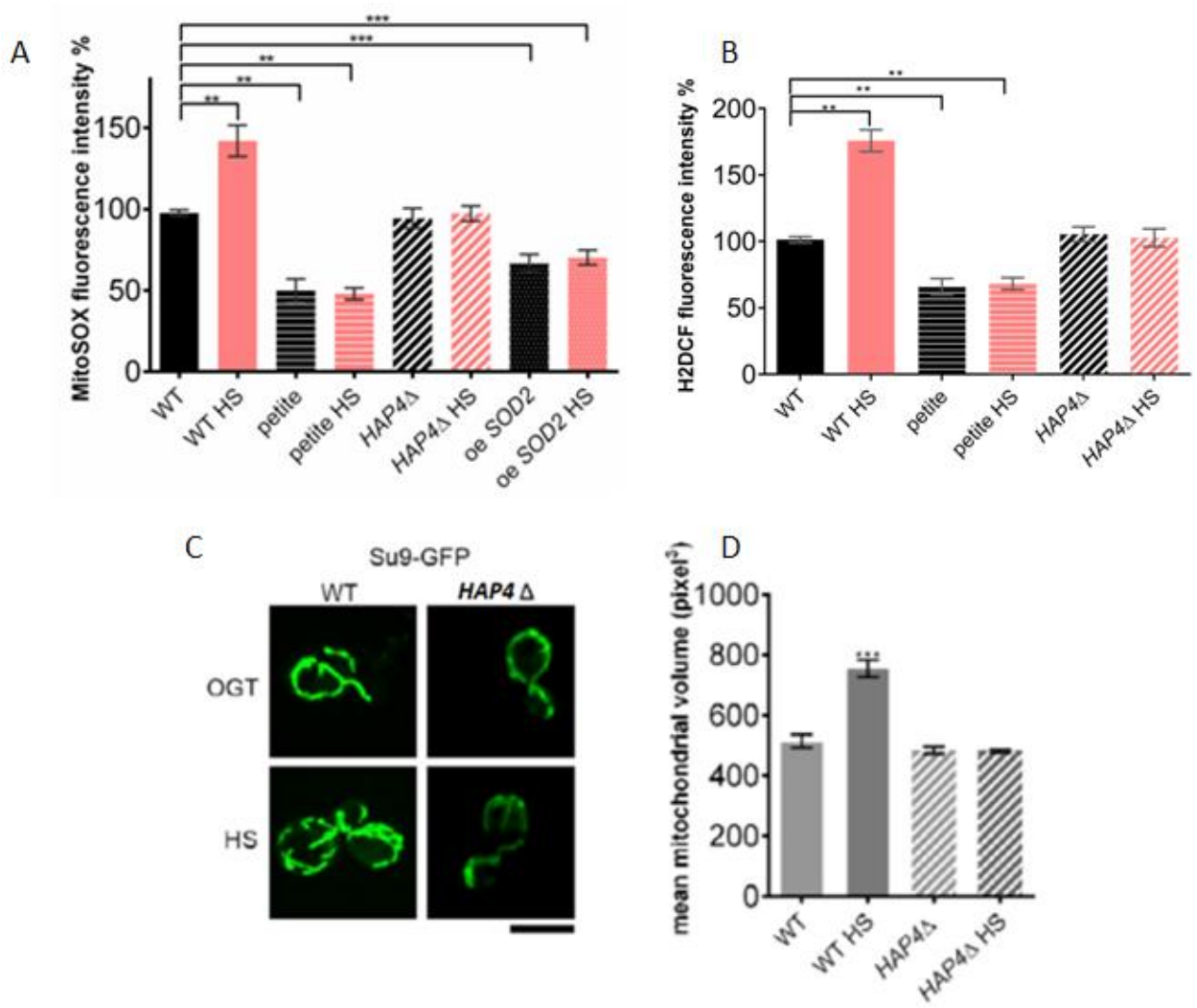

Figure 3.1.4. Mitochondrial superoxide levels and mitochondrial volume are increased during HS. (A) Mitochondrial superoxide levels as measured by MitoSOX fluorescent dye are increased during HS in WT, but not in respiration deficient petite and *HAP4*Δ strains, nor in oe*SOD2* strain. Superoxide was measured by FACS as MitoSOX fluorescence in 10000 cells. (B) Intercellular ROS levels measured by H2DCF fluorescence are similar to MitoSOX measurements and show increased

ROS in WT, but not in respiration deficient petite and *HAP4*Δ strains. (C)Increase in mitochondrial superoxide is accompanied by increased mitochondrial volume. (D) Quantification shows that mitochondrial volume is roughly 30% increased during HS in WT but remains unchanged in *HAP4*Δ strain. *P* values were calculated using ANOVA plus post hoc. ***$P < 0.001$; **$P < 0.01$; *$P < 0.05$.

The ROS levels are also reflected in the increased mitochondrial volume in the WT but not in *HAP4*Δ strain (Figure 3.1.4C,D). As they lack functional mitochondria, mitochondrial volume could not be measured in petite strain. In CCCP treated cells there was no increase in O_2 uptake after HS, as well as no mitochondrial superoxide increase (Figure 3.1.5A,B). In agreement with these results, there was no activation of PPP or antioxidant protection, while the HSR was activated (Figure 3.1.5C). Together, these results indicate that the observed RLS extension is a consequence of increased mitochondrial ROS. Therefore, we sought out to further test this hypothesis by modifying ROS levels in mitochondria.

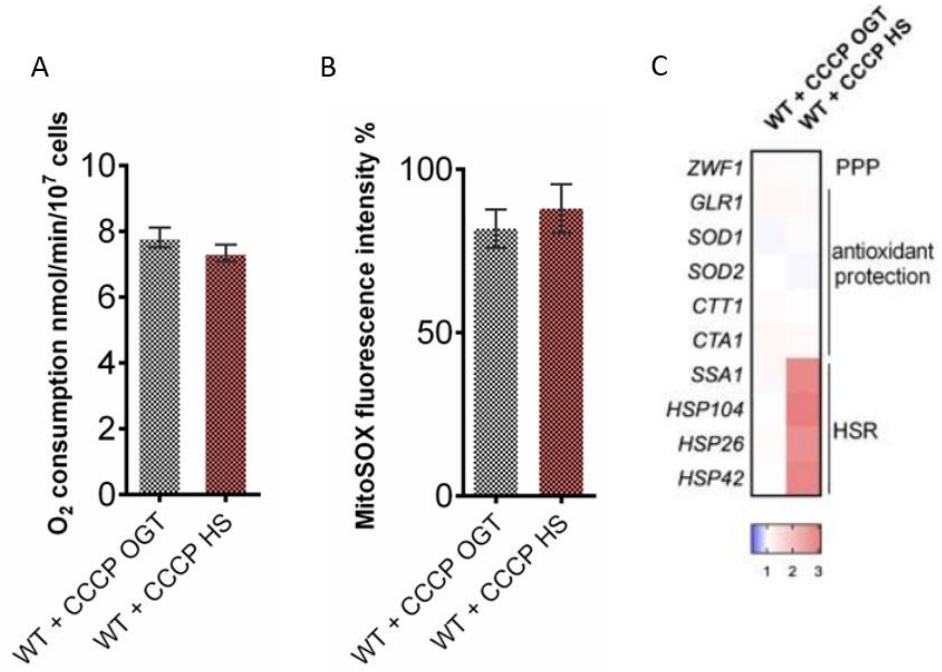

Figure 3.1.5. Respiration is required for activation of pentose phosphate pathway and redox maintenance during HS. (A) In the presence of mitochondrial uncoupler CCCP (10μM) respiration is increased compared to WT untreated control and is not affected by HS. (B) Mitochondiral superoxide levels are decreased in the presence of 10 μM CCCP at OGT and was unaffected by HS.

Superoxide was measured by FACS as MitoSOX fluorescence in 10000 cells. Results are represented as percentage of MitoSOX fluorescence measured in WT at OGT. (C) qPCR measurements in the presence of CCCP show that respiration activity is required for pentose phosphate pathway activation, as well as maintenance of redox status. Individual transcript levels are normalized to *UBC6*.

To test if the mitochondrial ROS plays a role in the HS induced RLS extension, the experiments were repeated using a yeast strain overexpressing *SOD2*, the mitochondrial manganese superoxide dismutase. While O_2 consumption rate has been increased in the *oeSOD2* strain (Figure 3.1.6A), the mitochondrial superoxide levels were markedly lower compared with WT and were unchanged after HS (Figure 3.1.4A). Further, the PPP was not activated, while the glycolytic enzymes and the peroxisomal beta oxidation were downregulated (Figure 3.1.6B). Finally, the RLS of the *oeSOD2* strain was unchanged after the HS treatment, maximum lifespan being 25 generations for both conditions, and median being 12 generations for OGT and 13 generations for the HS (Figure 3.1.6C).

This supports the idea that increase in respiration and resulting increase in produced ROS are necessary for the HS induced RLS extension.

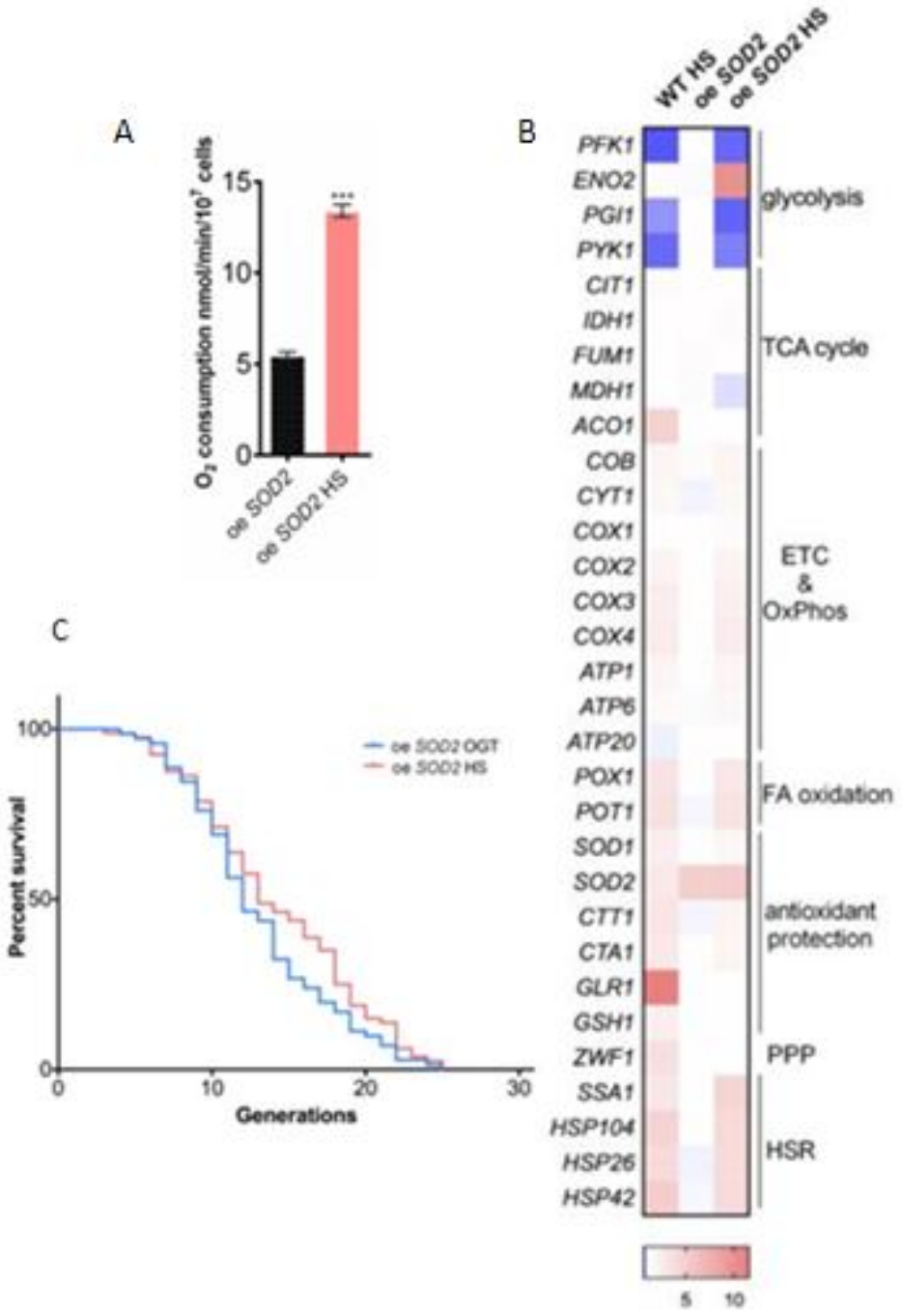

Figure 3.1.6. Neutralization of mitochondrial superoxide abolishes RLS extension. (A) oe*SOD2* strain had increased respiratory activity at HS. (B) qPCR analysis of the oe*SOD2* strain shows no activation of oxidative stress response enzymes, including G6PD (ZWF1) following HS. Individual transcript levels are normalized to*UBC6*. ***$P < 0.001$; **$P < 0.01$; *$P < 0.05$ (ANOVA plus post hoc). (C) Mean and maximum replicative lifespan (RLS) remain unchanged in oe*SOD2* strain

following HS. Control cells were kept at 30°C. The number of curated cells is 71 for oe*SOD2* and 80 for oe*SOD2* HS. *P* value is >0.05 (Mantel-Cox).

3.1.4. Glutathione increase is necessary for HS induced RLS extension

As PPP was activated during HS, we hypothesized that the purpose of PPP activation was NADPH production for glutathione recycling. Glutathione or GSH is oxidized to GSSH, which can be reduced back to GSH by glutathione reductase Glr1p, which requires NADPH.

Therefore, we measured $NADP^+$/NADPH ratio in the studied strains. In WT strain there was a decrease in the $NADP^+$/NADPH ratio while the total NADP level was unchanged, suggesting an increase in NADPH level. Petite, *HAP4*Δ, CCCP treated WT, and the *oeSOD2* strains, on the other hand, showed no such trend i.e no change in the $NADP^+$/NADPH ratio. Furthermore, the trend was absent in the *ZWF1*Δ strain, which cannot activate PPP, thus highlighting the central role of PPP in NADPH production (Figure 3.1.7).

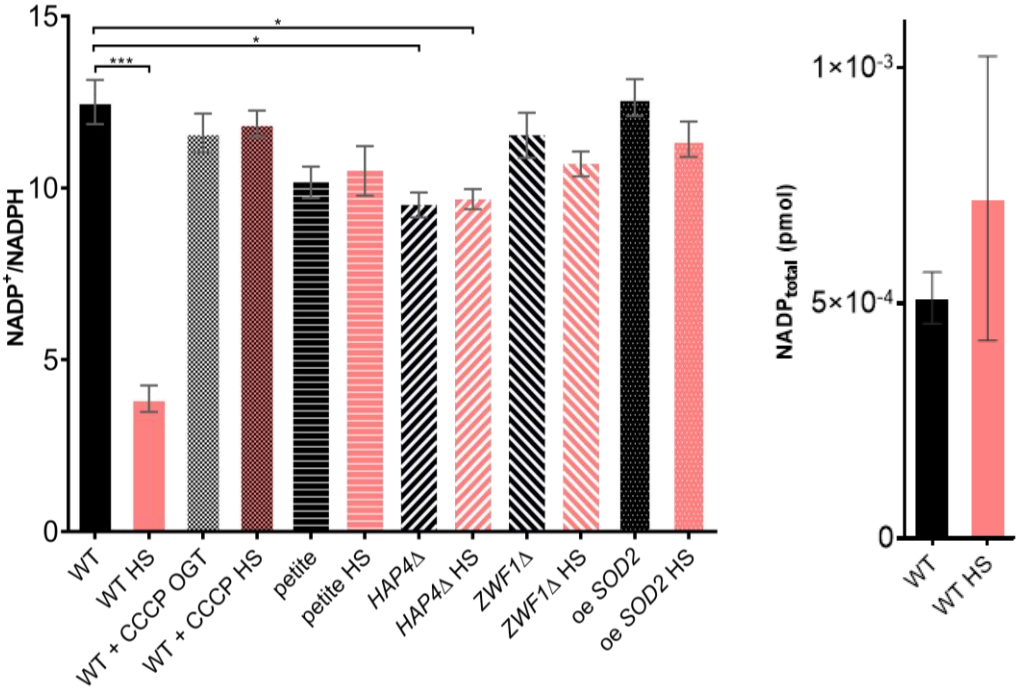

Figure 3.1.7. $NADP^+$/NADPH ratio is decreased during HS in WT. $NADP^+$/NADPH ratio was decreased during 3 hour HS at 34°C in WT strain, while total NADP levels were unchanged,

suggesting increased NADPH levels. In the presence of CCCP, however, as well as in respiration deficient petite and *HAP4*Δ, G6PD deficient *ZWF1*Δ strain and the oe *SOD2* strain, the ratio was unchanged. ***$P < 0.001$; **$P < 0.01$; *$P < 0.05$ (ANOVA plus post hoc).

GSH levels mirrored the trends observed in the $NADP^+$/NADPH ratio changes; the GSH level was increased following HS in WT but not in other studied strains. In *ZWF1*Δ strain, lacking the PPP rate limiting enzyme G6PD, the GSH levels dropped after HS, implying its depletion, thus confirming that NADPH is required for GSH recycling. Further, GSH levels were unaffected in the *oeSOD2* background, suggesting that superoxide was sufficiently neutralized in the presence of extraneous *SOD2* (Figure 3.1.8.).

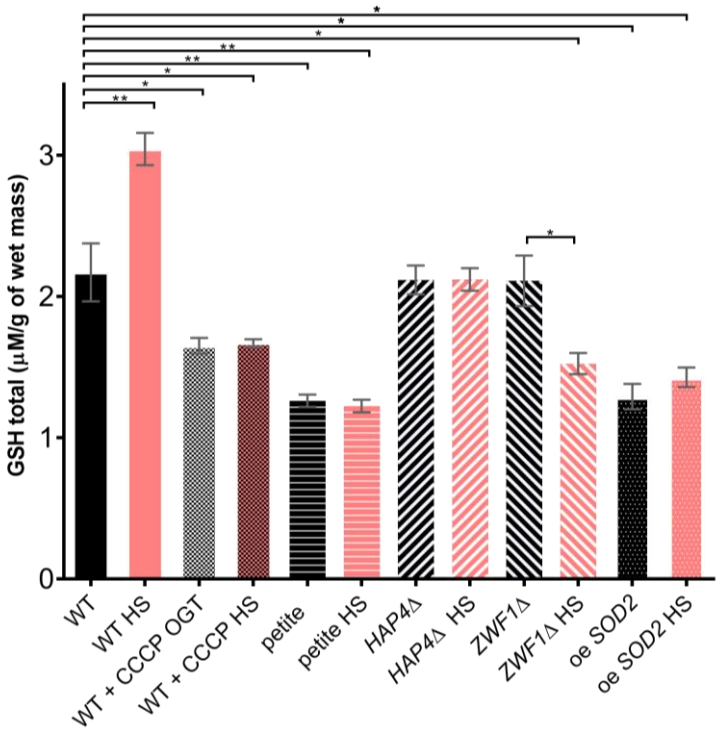

Figure 3.1.8. GSH levels increased during HS in the WT strain. Heat shock did not induce the GSH levels in the petite, *HAP4*Δ strain, WT in the presence of CCCP, in the strain deficient in G6PD (*ZWF1* Δ), or in the strain carrying overexpression of *SOD2*. ***$P < 0.001$; **$P < 0.01$; *$P < 0.05$ (ANOVA plus post hoc).

In order to corroborate the importance of glutathione recycling, we looked at a *GLR1*Δ strain, which lacks the glutathione reductase and therefore is unable to recycle glutathione. *GLR1*Δ strain exhibited increased respiration after HS comparable to WT, followed by an increase in mitochondrial superoxide levels (figure 3.1.9A,B). Further, *GLR1*Δ strain had a similar metabolic response to WT, characterized by glycolysis repression, upregulation of respiratory chain subunits, HSR and PPP activation (Figure 3.1.9C). However, there was no change in the $NADP^+$/NADPH ratio while $NADP^+$ was increased (Figure 3.1.9D, E). GSH levels were unchanged due to lack of *GLR1*, despite increased $NADP^+$ (Figure 3.1.9F).

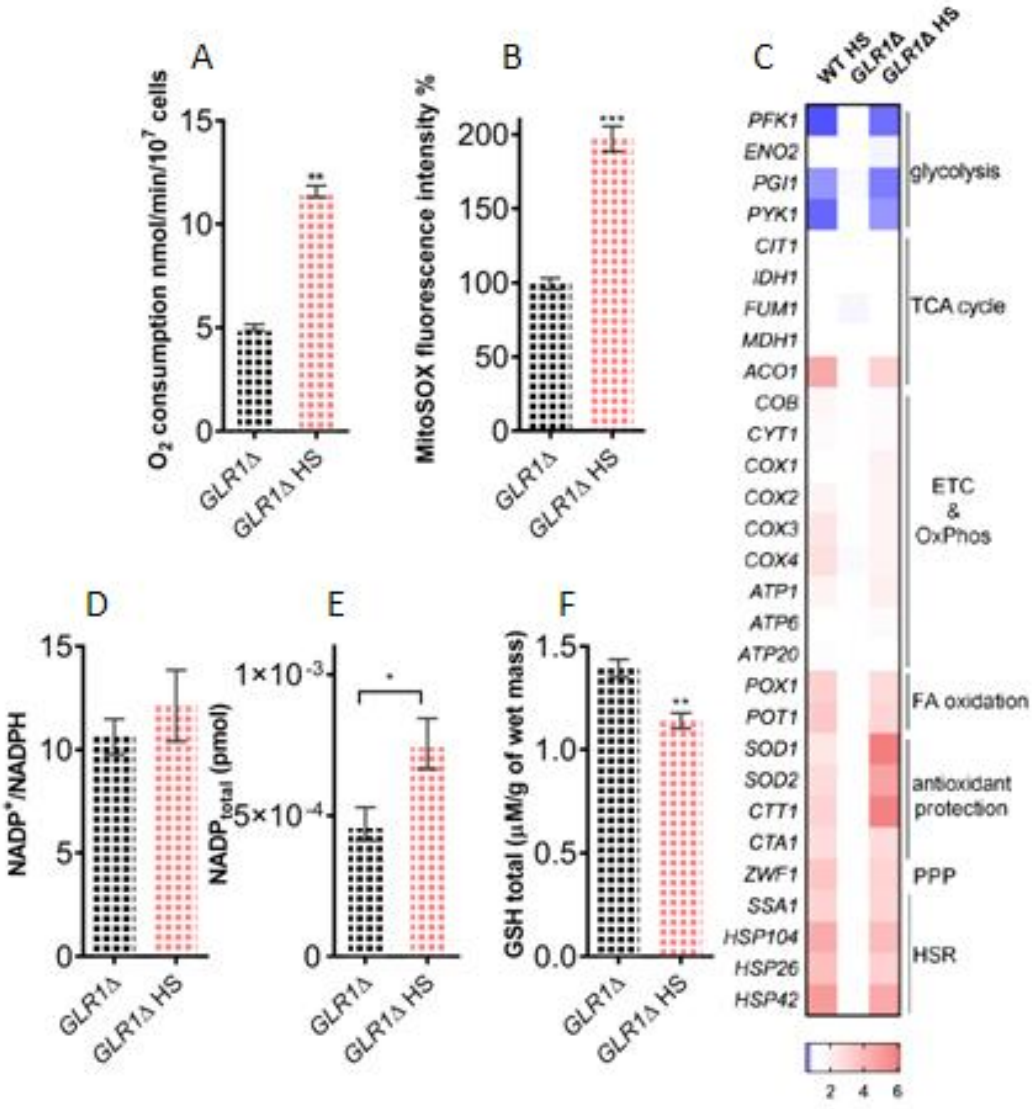

Figure 3.1.9. *GLR1*Δ strain at HS displays similar metabolic changes as WT but no change in the $NADP^+$/NADPH ratio. (A) Oxygen consumption was increased in the *GLR1*Δ strain during

HS. Oxygen consumption was measuring polarographically using an oxygraph equipped with a Clark electrode. (B) Mitochondrial superoxide was increased in *GLR1*Δ strain during HS. Mitochondrial superoxide was measured by FACS as MitoSOX fluorescence in 10000 cells. The results are represented as percentage of MitoSOX fluorescence detected in WT at OGT. (C) *GLR1*Δ strain displays similar metabolic changes as WT at HS, as measured by qPCR. Colour of the squares on the heat map corresponds to the mean value of the log fold change. Individual transcript levels are normalized to *UBC6*. (D) NADP+/NADPH ratio was unaffected by HS, despite increased $NADP^+$ levels (E). (F) GSH levels decreased during HS in *GLR1*Δ strain. ***$P < 0.001$; **$P < 0.01$; *$P < 0.05$ (ANOVA plus post hoc).

Lastly, the RLS was unchanged after HS in the *GLR1*Δ strain (Figure 3.1.10.).

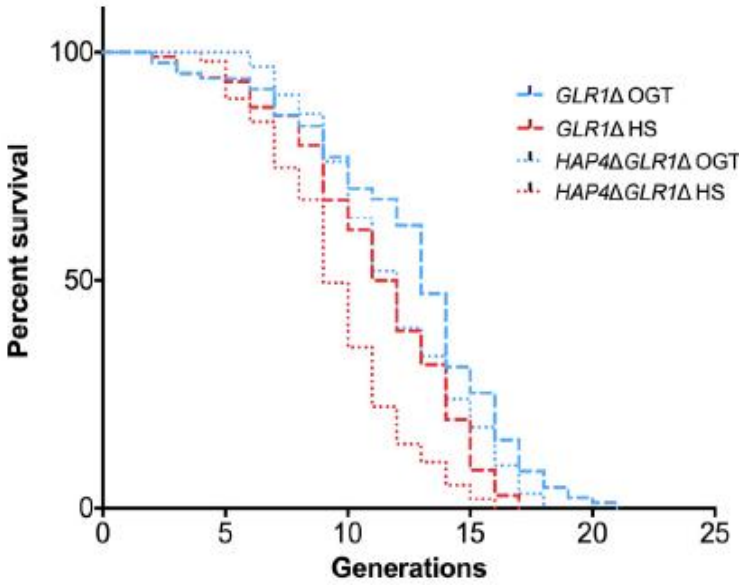

Figure 3.1.10. Glutathione recycling is necessary for the HS induced RLS extension and *GLR1* is epistatic to *HAP4*. Mean and maximum RLS were decreased in *GLR1*Δ following HS. RLS of the double mutant *HAP4*Δ*GLR1*Δ reveals that *GLR1* is epistatic to *HAP4* under the conditions of mild heat shock. The number of curated cells if 87 for *GLR1*Δ, 107 for *GLR1*Δ HS, 96 for *HAP4*Δ*GLR1*Δ and 99 for *HAP4*Δ*GLR1*Δ HS. *P* value is <0.0001 (Mantel-Cox).

3.1.5. Glr1 is epistatic to Hap4

Epistasis refers to the dependence of one genes effect to its genetic background. As inhibition of both respiration upregulation and glutathione recycling by deleting *HAP4* and *GLR1*, respectively, annulled the HS induced RLS extension, we tested if these two genes are epistatic. Therefore, we measured the RLS of a strain lacking both *HAP4* and *GLR1*, and found that, while at OGT the RLS of the *HAP4*Δ*GLR1*Δ strain is unchanged compared to *GLR1*Δ, the HS induced RLS extension is absent; mean RLS is 11 and maximum RLS is 17 , compared to 14 and 21, respectively, in *GLR1*Δ (Figure 3.1.10.). This suggests that *GLR1* is indeed epistatic to *HAP4*, acting downstream of the changes induced by the *HAP4* activity.

3.1.6. Glutathione replenishment requires YAP1

Further, we tested strain lacking Yap1p (*YAP1*) transcription factor, responsible for the activation of the oxidative stress response. *YAP1*Δ strain exhibited both increase in respiration rate and production of mitochondrial superoxide during HS (Figure 3.1.11A, B). The changes at the transcript level were comparable to those observed in WT, including repression of glycolysis, upregulation of genes coding for respiratory chain subunits, PPP, and enzymes responsible for oxidation of fatty acids (Figure 3.1.11C). Importantly, HSR was activated along with upregulation of superoxide dismutases and catalases, but there were no changes observed in the levels of either *GLR1* or *GSH1*, suggesting glutathione is not recycled despite the cell experiencing stress. In line with this data, NADP+/NADPH ratio decreased during HS, while the level of GSH remained constant (Figure 3.1.11D, E). Finally, the RLS of the *YAP1*Δ strain was decreased at OGT compared with WT and underwent further decrease following HS; at OGT the median RLS was 11 generations, compared with 9 generations after HS (Figure 3.1.11F). These results corroborate the importance of GSH recycling in the HS induced RLS extension, and underscore GSH recycling as one of the most distal contributing events.

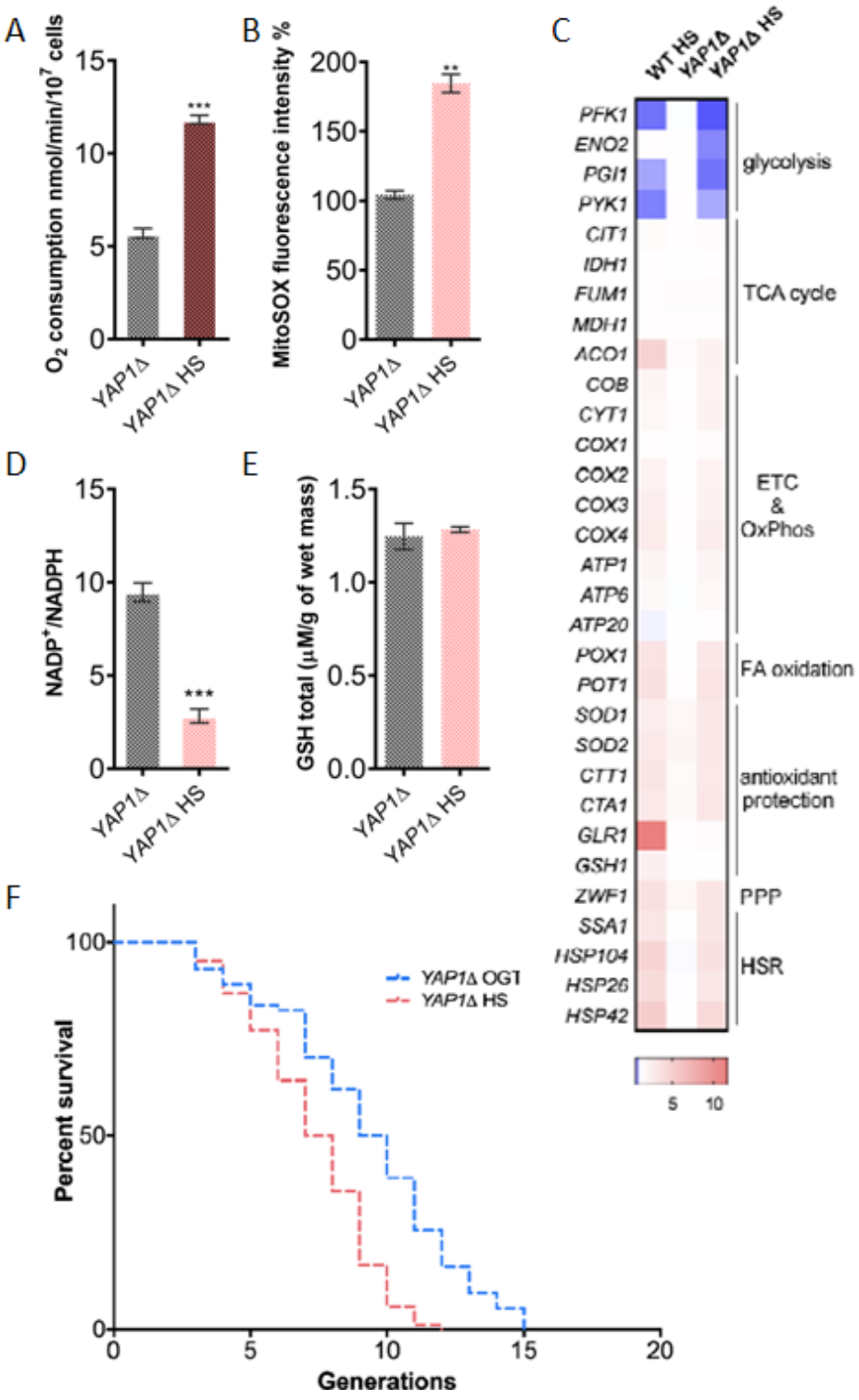

Figure 3.1.11. YAP1 is required for the HS induced RLS extension. (A) Oxygen consumption was increased during HS in the *YAP1*Δ strain. Oxygen consumption was measuring polarographically using an oxygraph equipped with a Clark electrode. (B) Mitochondrially produced

superoxide was increased in the *YAP1*Δ strain during HS. Mitochondrial superoxide was measured by FACS as MitoSOX fluorescence in 10000 cells. Results are expressed as percentage of MitoSOX fluorescence measured in WT at OGT. (C) qPCR measurement showed that *YAP1* absence did not affect the HS induced metabolic changes observed in WT. Individual transcript levels are normalized to *UBC6*. (D) NADP+/NADPH ratio was decreased during HS in the *YAP1*Δ strain, while GSH levels remained unchanged (E). (F) Both mean and maximal RLS were decreased in *YAP1*Δ at OGT compared to WT, and further decreased after HS. The number of curated cells is 74 for *YAP1*Δ and 84 for *YAP1*Δ HS. *P* value is <0.0001 (Mantel-Cox).

3.1.7. TORC1 inactivation is crucial for HS induced RLS extension

How respiration is activated during HS remained to be elucidated. As TORC1 has been shown to modulate respiratory activity in yeast (Bonawitz et al., 2007; Pan, Schroeder, Ocampo, Barrientos, & Shadel, 2011; Perić et al., 2017), we next tested TORC1 complex involvement in the observed HS induced RLS extension. To measure TORC1 activity, as phospho-TORC1 antibodies are not commercially available, we measured transcript levels of TORC1 downstream targets. These genes are transcribed when TORC1 is inactivated. Increased transcript levels of *GLN1*, *MEP2*, and *GAP1* following HS suggest that TORC1 was inhibited in these conditions. Similar upregulation was observed in control cells treated with Rapamycin, inhibitor of TORC1 (Figure 3.1.12A).

The result was also supported by live cell imaging of cells bearing GFP tagged Tor1p kinase (Tor1-GFP). The images show that at OGT Tor1-GFP localized to the vacuole, stained with CellTracker Blue. This is consistent with active TORC1. During HS, the signal is relocated from the vacuolar membrane, forming either cytosolic foci or diffusely colouring the cytosol (Figure 3.1.12B, C).

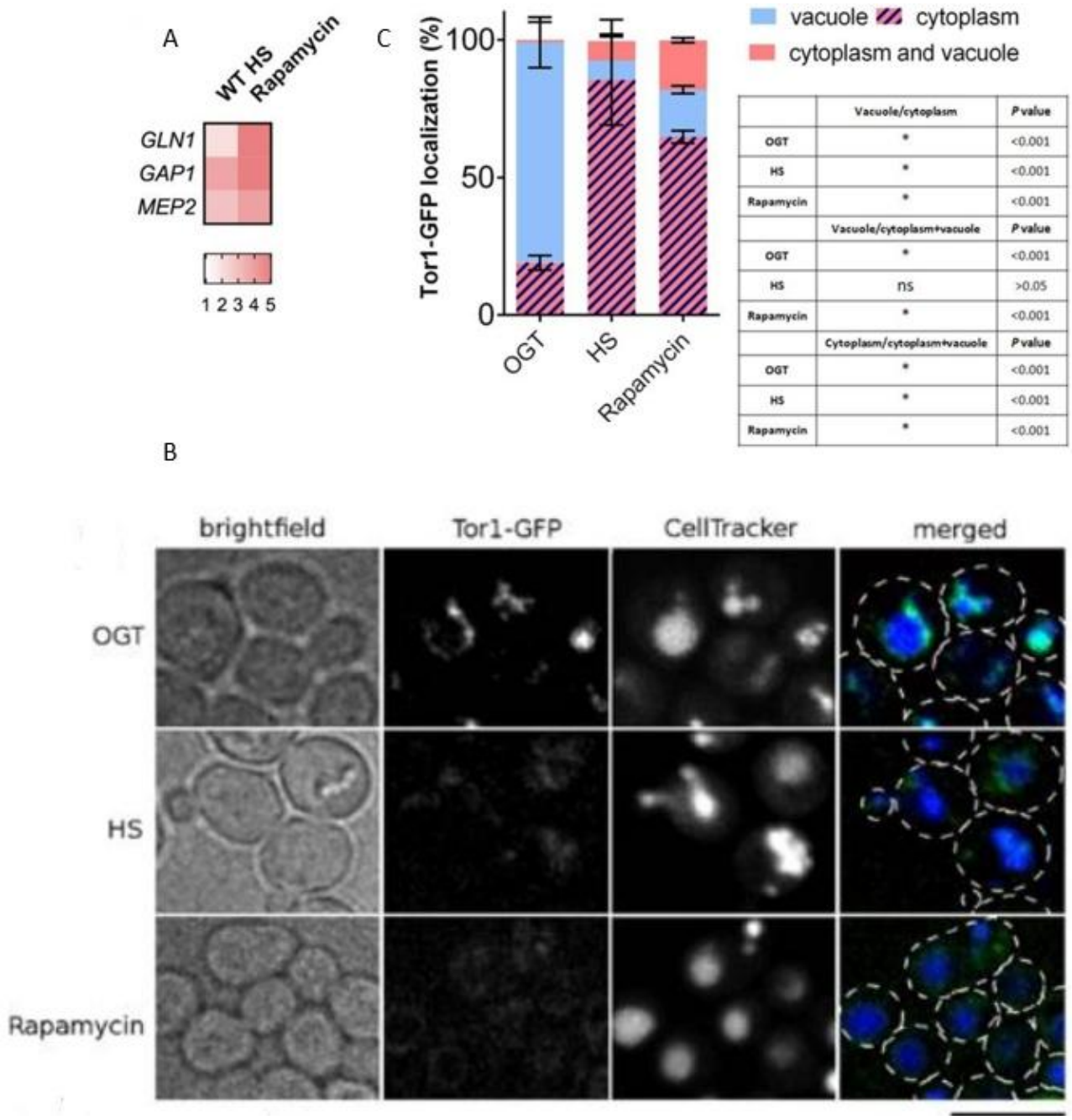

	Vacuole/cytoplasm	*P* value
OGT	*	<0.001
HS	*	<0.001
Rapamycin	*	<0.001
	Vacuole/cytoplasm+vacuole	*P* value
OGT	*	<0.001
HS	ns	>0.05
Rapamycin	*	<0.001
	Cytoplasm/cytoplasm+vacuole	*P* value
OGT	*	<0.001
HS	*	<0.001
Rapamycin	*	<0.001

Figure 3.1.12. TORC1 is inactivated by mild transient HS. (A) Transcipt levels of TORC1 transcriptional targets shows they are upregulated during HS, consistent to their upregulation during TORC1 inhibiton with rapamycin. Color of the squares on the heat map corresponds to the mean value of the log fold change. Individual transcript levels are normalized to *UBC6*. (B) Imaging shows that TORC1 is displaced from the vacuole during HS and rapamying treatment, consistent with its inactivation. The black bar represents 5µm. (C) Quantification of cell fractions with

different Tor1-GFP localization. A minimum of 200 cells were quantified per condition. Data on the graph are mean ± SD from three independent cultures. ***$P < 0.001$; **$P < 0.01$; *$P < 0.05$ (ANOVA).

To test if TORC1 inactivation is necessary for the HS induced RLS extension or simply a downstream event, we tested a strain with constitutively active TORC1. This strain has A1957V substitution in the Rapamycin binding domain of the Tor1p kinase, resulting in constitutive activity (caTor1). In this strain, HS did not lead to an increase in respiration rate (Figure 3.1.13A). At transcript level, there were no recorded changes in the respiratory chain components, TCA cycle, glycolysis enzymes, or antioxidant protection genes. However, HSR was activated, as well as peroxisomal beta oxidation enzymes (Figure 3.1.13B). $NADP^+$/NADPH ratio and mitochondrial superoxide levels were unchanged by HS in the caTor1 strain (Figure 3.1.13C, D), while GSH levels were reduced by roughly 25% (Figure 3.1.13E). Lastly, the RLS of the caTor1 strain was unaffected by HS; median RLS was 13 generations for both OGT and HS, and maximum lifespan was 21 generations (Figure 3.1.13F).

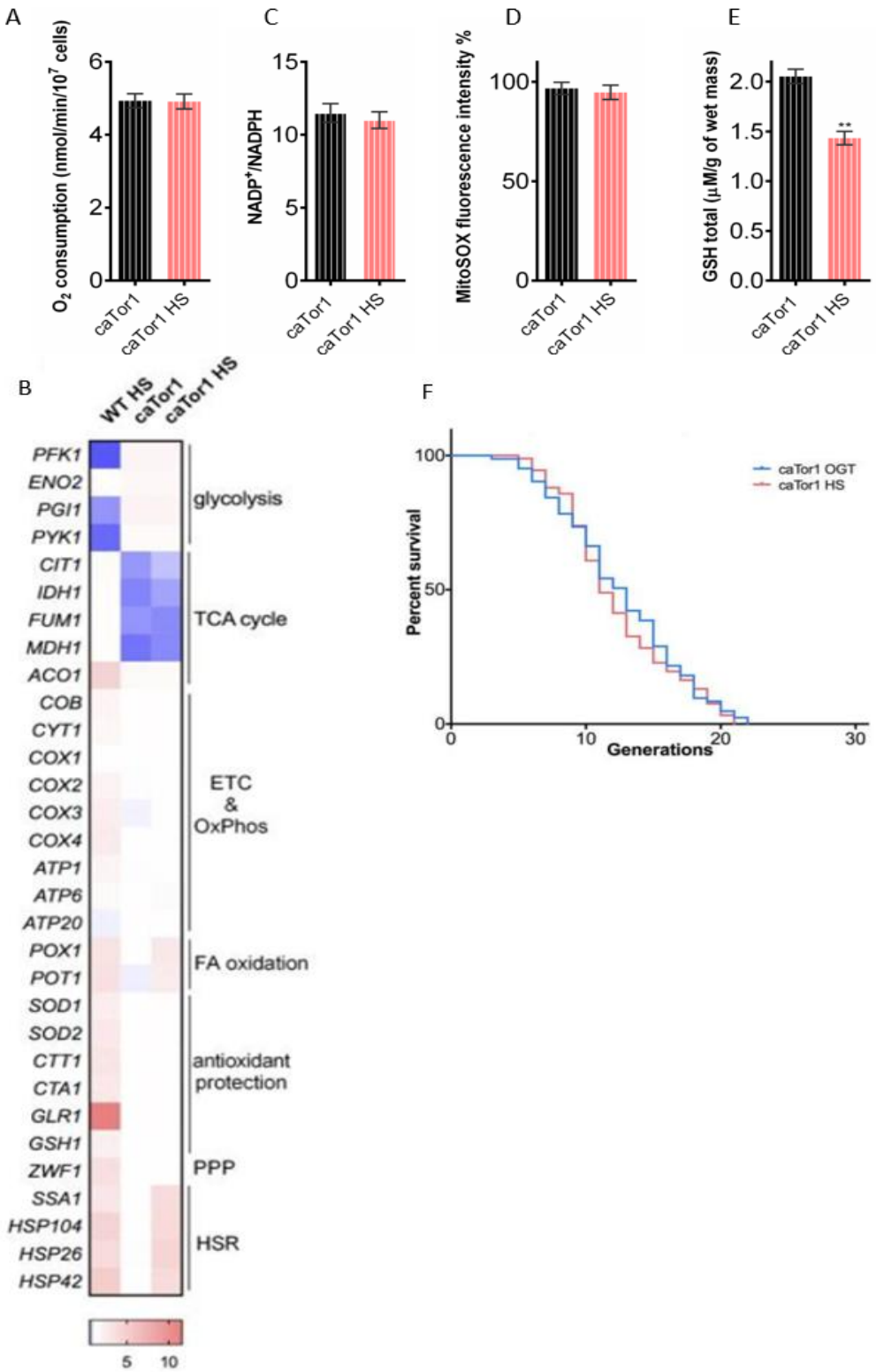

Figure 3.1.13. TORC1 inactivation is necessary for HS-induced activation of respiration. (A) In caTor1 background HS does not affect the respiration rate, while there is a slight upregulation of

glycolytic activity and downregulation of TCA cycle compared with WT as shown by qPCR Individual transcript levels are normalized to *UBC6*. (B). Neither $NADP^+$/NADPH ratio (C) or mitochondrial superoxide levels were affected by HS in caTor1 strain (D), while GSH levels were decreased (E). ***$P < 0.001$; **$P < 0.01$; *$P < 0.05$ (ANOVA plus post hoc). (F) Both mean and maximum lifespan were unchanged by HS in caTor1 background. Control cells were kept at 30°C. The number of curated cells is 83 for caTor1 and 92 for caTor1 HS. *P* value is >0.05 (Mantel-Cox).

3.2. Part II: heat stress induced lifespan extension in *Caenorhabditis elegans*

This part further explores the nature of HS-induced lifespan extension by investigating HSR in nematode C. elegans. By employing a multicellular model organism, we aim to get a better perspective on the differences of the HS-induced lifespan extension between unicellular and multicellular organisms.

3.2.1. Peroxisomal catalase mutant has attenuated/weakened/constricted HSR

We sought to investigate the mechanisms of cellular response to HS in nematode *C. elegans* and see if the metabolic response is similar to the one observed in yeast. It should be noted, that what we refer to as response to HS is not equivalent to HSR: while HSR refers to HSF1 regulated components of the stress response, we are interested in seeing a broader cellular response during heat stress, which includes elements of the HSR such as chaperone upregulation but also metabolic changes not normally observed in the context of HSR alone, such as changes in respiration rates.

In this context, we looked at the response to HS in WT and in peroxisomal catalase, *ctl-2*, deficient worms (*Δctl-2*). At optimal temperature, this strain exhibits shortened lifespan and smaller brood size (Petriv & Rachubinski, 2004). Now, we were interested to characterize the effects of HS on this short-lived organism.

In WT, 4-hour exposure to 30°C at L4 stage, after which the worms were returned to OGT of 20°C, resulted in life span extension; median and maximum life span after HS were 14 and 20 days, respectively, compared to 12 days for median and 17 days for maximum lifespan at 20°C (Figure 3.2.1A). In *Δctl-2* worms, however, the life span extension was absent; median life span for both control and HS was 11 days, while maximum lifespan was 13 days for HS and 15 days for control. The change was not statistically significant (Figure 3.2.1B).

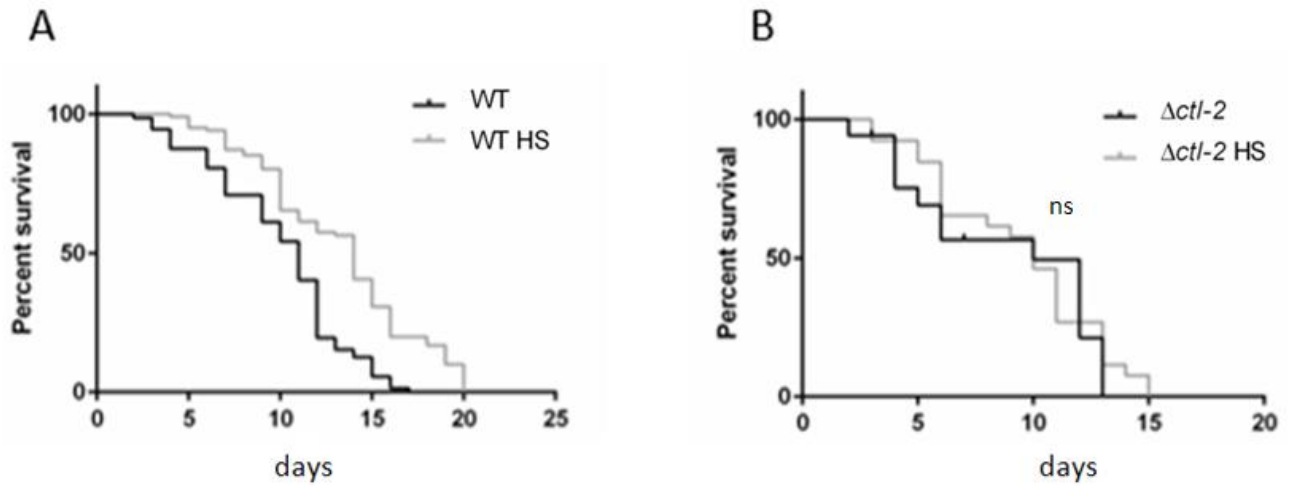

Figure 3.2.1. WT worms display HS-induced lifespan extension, but not the peroxisomal *Δctl-2* mutant. (A) Mild transient HS at L4 stage extends WT lifespan, median lifespan following HS was 14 days compared to 11 days at OGT, and maximum lifepan was extended from 17 days to 20 days after HS. *P* value is <0.05 (Mantel-Cox). (B) In *Δctl-2* background lifespan was not affected by HS; median lifespan was 10 days for both conditions, and maximum lifespan was 13 days at OGT and 15 days following HS treatment. P value is >0.05 (Mantel-Cox).

To investigate the absence of life span extension in *Δctl-2* strain following HS, we studied the HSR of both WT and *Δctl-2* strain in more depth. We found that both strains had activated HSR, evidenced by the increased transcript levels of HSR hallmark proteins *hsp-16.1*, *hsp-16.2*, and *hsp-70.* However, both small heat shock proteins *hsp-16.1* and *hsp-16.2* were upregulated to a lesser extent in the *Δctl-2* compared to WT: while WT during HS upregulated *hsp-16.1* and *hsp-16.2* genes roughly 400 and 2000 times, respectively, in the *Δctl-2* these genes were upregulated only 17 and 100 times, respectively. *Hsp-70* transcript level in *Δctl-2* strain, on the other hand, was almost twice the one measured in WT after HS (Figure 3.2.2.). We do not presently understand the reason behind this or its possible consequences, but it implies possible compensation between the different HSPs. Furthermore, we do not know if the differential chaperone expression is tissue specific or uniform among tissues, which would affect their capability to manage the consequences of HS.

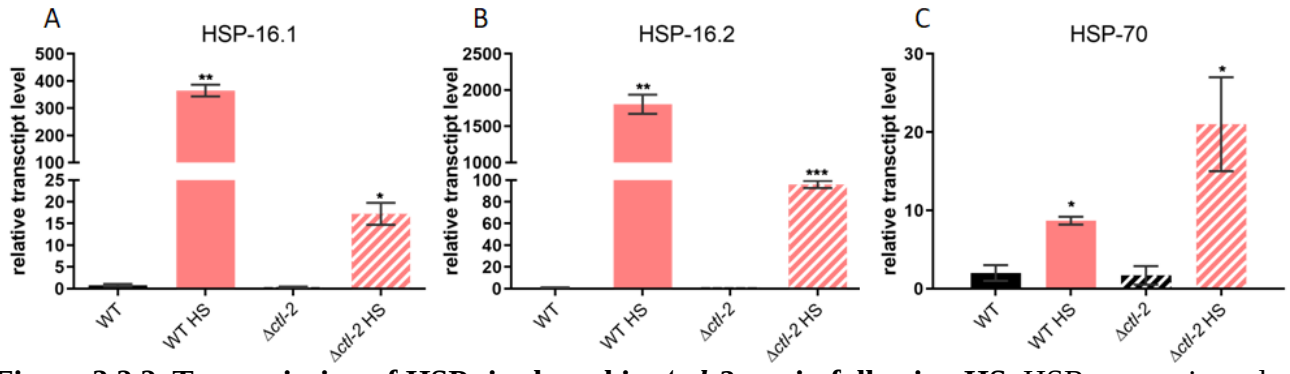

Figure 3.2.2. Transcription of HSPs is altered in *Δctl-2* strain following HS. HSR was activated in both strains after 4-hour HS, however, transcript levels of *hsp16.1* (A) and *hsp16.2* (B) were lower in ctl-2 compared to WT. (C) *hsp-70* expression was higher in *Δctl-2* mutant compared to WT following HS. Gene expression normalized to *act-1*. Error bars are mean ± SD. ****P<0.0001; ***P < 0.001; **P < 0.01; *P < 0.05 (t-test).

In order to gain more insight into why heat shock proteins would be differentially expressed between WT and *Δctl-2*, we turned our attention to HSF-1 and looked at HSF-1::GFP puncta creation in the nucleus. As HSF-1 is released from its accompanying chaperones and trimerized (Figure 1.6.), its binding to HSEs can be visualized using a HSF-1::GFP fusion protein as a transition from a diffuse GFP signal to bright puncta in the nucleus. We were interested in seeing if there were any changes in the binding of HSF to the DNA between WT and *Δctl-2* mutant.

The lessened HSR of the *Δctl-2* strain was mirrored in reduced formation of HSF-1::GFP puncta in the nucleus. We observed that HSF-1 in the WT has a higher tendency to create puncta compared with the one in *Δctl-2*: nuclei with multiple puncta were nearly three times as common in WT compared to *Δctl-2* (Figure 3.2.3A, B). As inactive HSF-1 is bound to *hsp-70* and *hsp-90*, higher availability of *hsp-70* in the *Δctl-2* mutant during HS (Figure 3.2.2C), might prevent the HSF-1 trimerization, but this remains unclear.

To further support the claim that HSR is affected in the *Δctl-2* mutant, we tested the survival of both WT and *Δctl-2* at the restrictive temperature of 37°C. We hypothesized that attenuated HSR would result in increased mortality at a restrictive temperature. At 37°C, all WT worms were dead after 8 hours (n=160), with median survival being at 5 hours, while all *Δctl-2* mutants were dead already at 5 hours (n=100), median survival being at 4 hours (Figure 3.2.3C). This demonstrates that are *Δctl-2*

worms indeed have decreased thermo tolerance, and that this may in fact be due to the attenuated HSR.

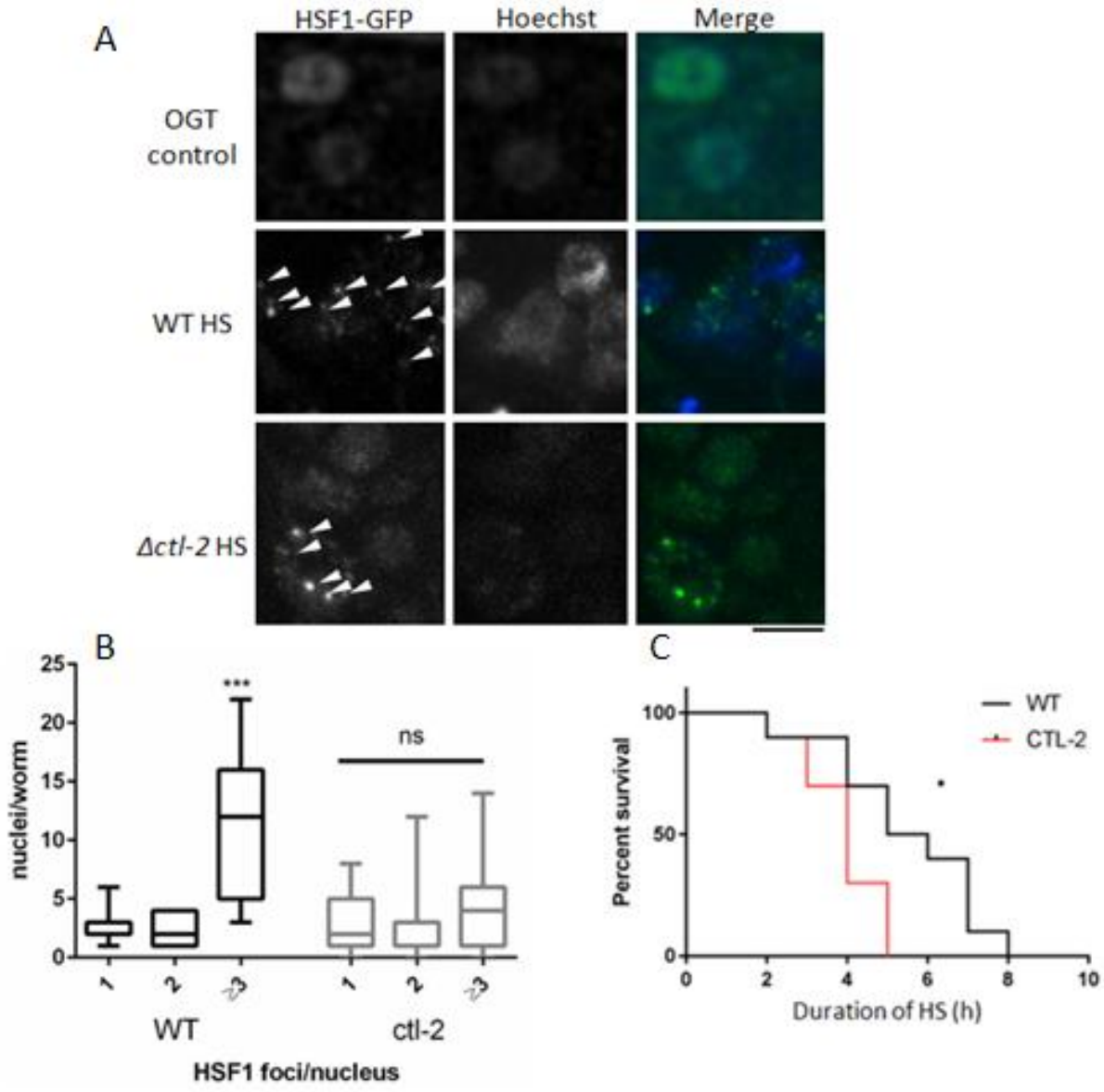

Figure 3.2.3. HSR is attenuated in *Δctl-2*. (A) HSF-1::GFP forms foci in the nucleus during HS in the WT. (B) HSF-1::GFP foci formation is more robust in WT than in *Δctl-2* mutant. The black bar represents 5 µm. (C) Quantification of images displayed in (A) and (B) shows that *Δctl-2* mutants have a significantly lower proportion of nuclei with more than 3 foci: WT averages 15 nuclei with 3 or more HSF1 puncta after 4 hours of HS, compared to only 4 nuclei in *Δctl-2*. ***$P < 0.001$; **$P < 0.01$; *$P < 0.05$ (ANOVA). (D) *Δctl-2* mutant shows decreased ability to withstand heat stress. ***$P < 0.001$; **$P < 0.01$; *$P < 0.05$ (Mantel-Cox).

3.2.2. *Δctl-2* stress response is attenuated

To further investigate the potential of the *Δctl-2* strain to respond to stress, we turned to stress responses other than HSR. Outside of causing upregulation of heat shock proteins, stressors such as heat will often lead to other types of proteotoxic effects, such as protein oxidation, and organelle specific stress responses. As *Δctl-2* strain has diminished capacity to deal with peroxisomal peroxide due to the missing catalase, we wanted to see if other antioxidant protection was upregulated. Therefore, we measured the transcript levels of both cytosolic and mitochondrial SOD enzymes, as they are upregulated in oxidizing conditions. Furthermore, the results from HS experiments in *S. cerevisiae* suggest that mitochondrial superoxide was crucial for the HS-induced RLS extension. Surprisingly, following HS, SOD genes were not upregulated in the *Δctl-2* background, compared with significant upregulation on the WT strain. Furthermore, transcript levels coding the cytosolic copper/zinc superoxide dismutase SOD-5 were significantly upregulated already at OGT in the *Δctl-2* strain and remained unchanged following HS (Figure 3.2.4.). This may be due to the compensation between the cytosolic superoxidases SOD-1 and SOD-5 (Yanase, Onodera, Tedesco, Johnson, & Ishii, 2009). Lack of upregulation of antioxidative enzymes also suggests that the *Δctl-2* strain has either adapted to increased oxidative load in a yet undetermined way, or the HS administered was too low for it to pass the threshold needed to activate these mechanisms in this strain. Given that we do see upregulation of HSPs during HS in the *Δctl-2* strain, it suggests that the administered stress is indeed sufficient to illicit a response but the *Δctl-2* mutant is most likely adapted to the increased oxidative stress. Moreover, the PPP is not activated in the *Δctl-2* mutant, as indicated by the transcription levels of PPP rate limiting enzyme G6PD (*gspd-1*), suggesting that this strain does not fully perceive the oxidative stress, possibly as a consequence of the catalase deficiency (Figure 3.2.4.). As prolonged activation of any stress response pathway is toxic to the cell, it is likely that *Δctl-2* strain adapted by having a higher threshold for stress response activation.

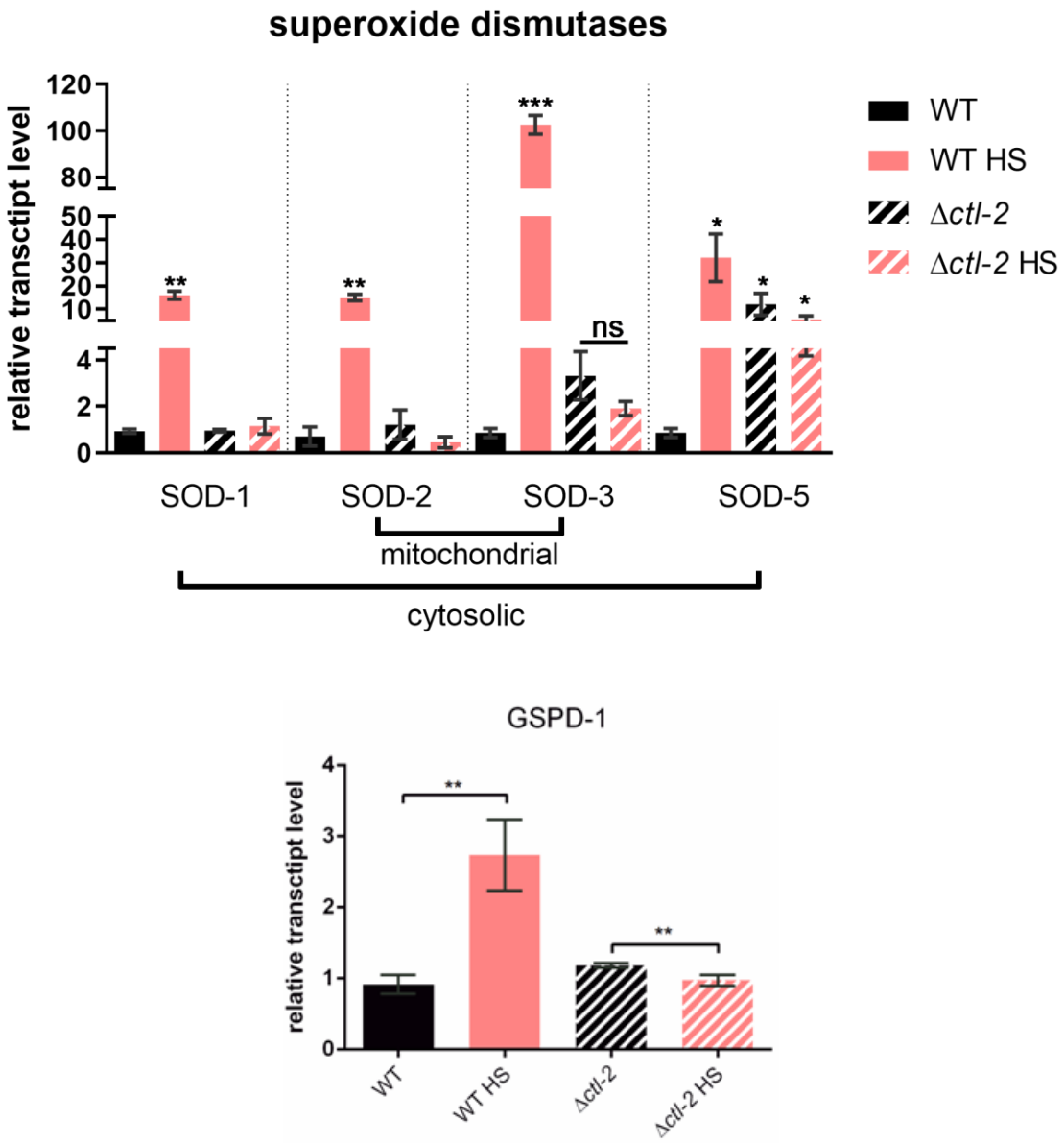

Figure 3.2.4. ***Δctl-2*** **strain has diminished oxidative stress response.** (A) Both cytosolic and mitochondrial superoxide dismutases were upregulated after HS in WT but not in *Δctl-2* strain. (B) PPP rate limiting enzyme G6PD was not upregulated in *Δctl-2* suggesting that PPP was not activated during HS in this strain. Graphs represent data from biological and technical duplicates. Transcript levels were normalized to *act-1*. Error bars are mean ± SD. ****P<0.0001; ***P < 0.001; **P < 0.01; *P < 0.05 (ANOVA).

Furthermore, the unfolded protein response (ER UPR) was activated (figure 3.2.5A). ER UPR is a stress response related to accumulation of unfolded proteins in the ER. Similar to HSR, it involves halting the cellular processes and increasing expression of chaperones in order to refold or eliminate non-native proteins. However, the ER UPR activation in the *Δctl-2* was modest compared to the one in WT (Figure 3.2.5A). As was observed before by Ben Zvi et al.(Ben-Zvi et al., 2009), the ability to activate HSR and ER UPR is constrained in older animals, meaning that the *Δctl-2* mutants exhibit some features of older animals despite being the same chronological age as the control. Further, mitochondrial UPR was not activated following HS in *Δctl-2* strain, while in WT it was modest and evidenced only by 2-fold upregulation of *clpp-1* peptidase in the mitochondrial matrix (Figure 3.2.5B). As peroxisomes in a way stand between the two organelles –they bud from the ER and provide metabolites for mitochondria – this may be interpreted as a certain level of dysregulation of the cross-organelle signalling.

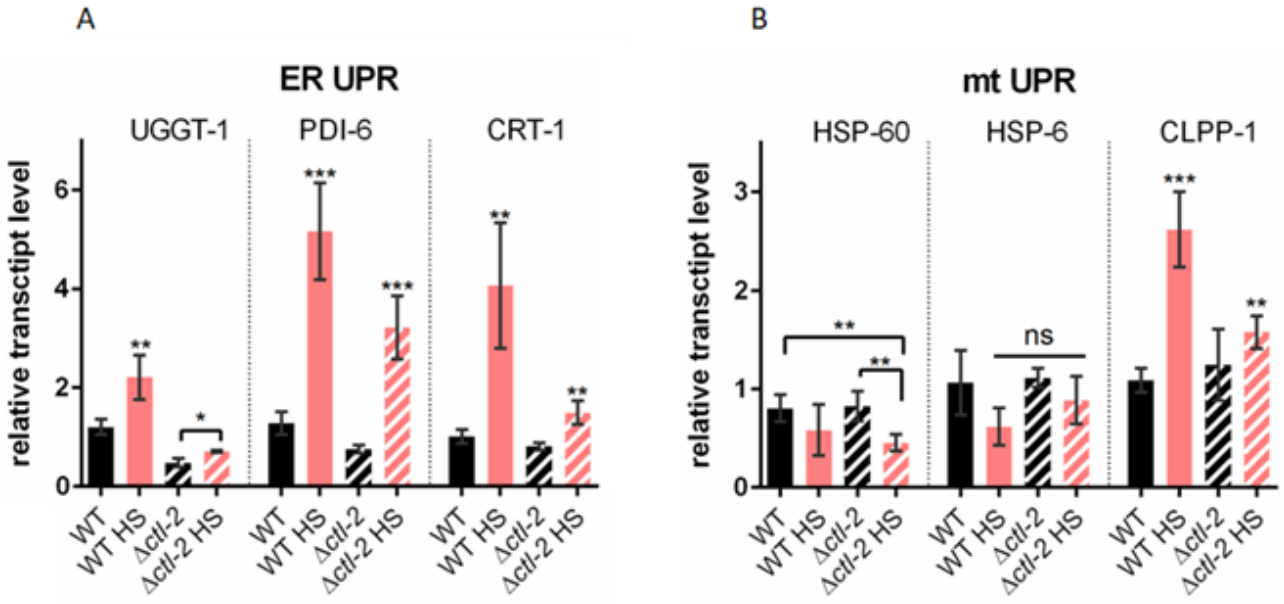

Figure 3.2.5. ER UPR but not mitochondrial UPR are activated in *Δctl-2* worms. Graphs represent data from biological and technical duplicates. Transcript levels were normalized to *act-1*. Error bars are mean ± SD. ****P<0.0001; ***P < 0.001; **P < 0.01; *P < 0.05 (ANOVA).

3.2.3. ROS

Due to the lack of the peroxisomal catalase, we would expect the *Δctl-2* strain to be under increased oxidative stress compared with WT. While we do not have evidence of strong oxidative stress response activation during HS in *Δctl-2*, we see that transcript levels at OGT for SOD-3 and SOD-5 are higher in *Δctl-2* than in WT (Figure 3.2.6). This may be indicative of increased ROS levels at OGT in *Δctl-2* strain. Interestingly, measurement of ROS levels with CellROX shows that *Δctl-2* strain has ROS levels comparable to WT at OGT, and at HS they are increased to levels surpassing those in heat treated WT.

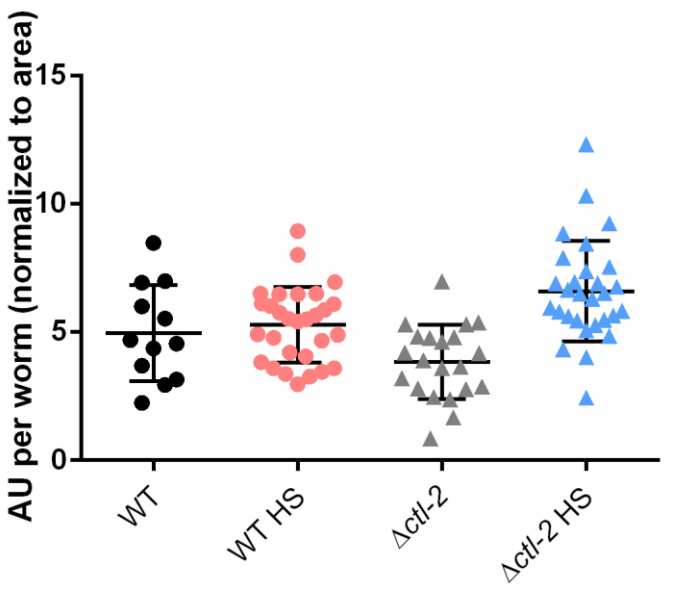

WT vs. WT HS	ns
WT vs. *Δctl-2*	ns
WT vs. *Δctl-2* HS	*
WT HS vs. *Δctl-2*	*
WT HS vs. *Δctl-2* HS	*
Δctl-2 vs. *Δctl-2* HS	****

Figure 3.2.6. ROS levels are comparable between WT and *Δctl-2* mutant but are increased in *Δctl-2* during HS. ****P<0.0001; ***P < 0.001; **P < 0.01; *P < 0.05 (ANOVA).

Thus, it is possible that the initially high levels of SOD present in this strain are efficiently containing the ROS levels, while increasing ROS levels during HS may be too much for the already strained system. Unlike the *Δctl-2* strain, WT ROS levels remain constant, concurrent with massive upregulation of antioxidant enzymes. This may be another example of prolonged stress response activation being detrimental to the organism.

3.2.4. *Δctl-2* peroxisome function is compromised

As the *Δctl-2* strain had different expression patterns of metabolic enzymes and chaperones (figure), compared to the WT during HS, we looked at several parameters indicative of peroxisomal function to try to discern if peroxisomal function plays a role in the HSR. More specifically, we looked at peroxisomal import, morphology, and FA β-oxidation. As peroxisomes provide metabolites to mitochondria, changes in peroxisomal metabolism can affect mitochondria, as well as other downstream targets.

First, we checked if the import into peroxisomes works properly. The import machinery is important both for peroxisome biogenesis so that all components can be present, and later for mature peroxisomes in order to deliver all the substrates. There were no observed differences in the expression of transport proteins, PRX-5 and PRX-11, responsible for import of peroxisomal constituents between WT and *Δctl-2*, either at OGT or HS temperatures (Figure 3.2.7). This indicates that their morphogenesis is not impacted, and, except for *Δctl-2*, all proteins needed for their proper formation and function should be present.

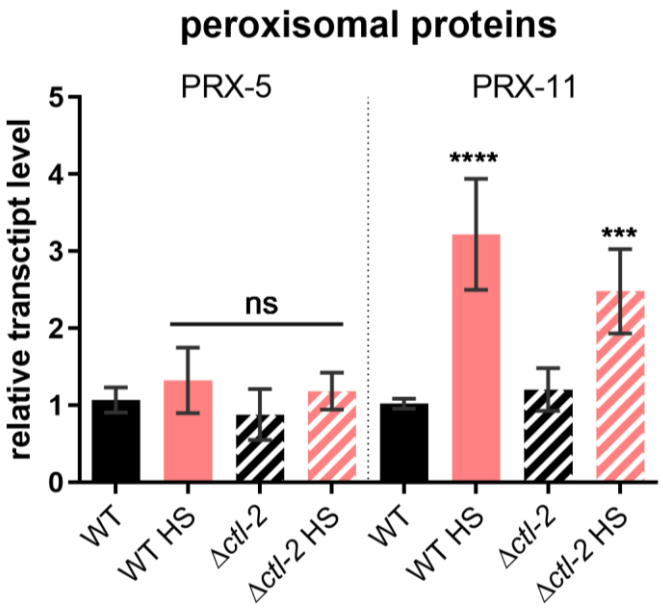

Figure 3.2.7. Peroxisomal biogenesis machinery is intact in the *Δctl-2* mutant. Transcript levels of main biogensis proteins in peroxisomes responsible for transporting its contents is similar in WT and *Δctl-2* both in control and HS-treated samples, suggesting there is no significant change in peroxisomal import in *Δctl-2* strain compared to WT. Graphs represent data from biological and

technical duplicates. Gene expression normalized to *act-1*. Error bars are mean ± SD. ****$P<0.0001$; ***$P < 0.001$; **$P < 0.01$; *$P < 0.05$ (ANOVA).

New peroxisomes are created either by budding from the ER or fission of already existing peroxisomes, while peroxisomal fusion has not been recorded thus far. Peroxisomes are known to change in shape, size and abundance depending on the environmental conditions and the status of the cell. Therefore, we looked at their morphology in the conditions of interest. Peroxisomes were visualized by a peroxisomal import signal tagged with GFP (PTS::GFP) (Figure 3.2.8A). Quantification of images reveals that the peroxisomes number decreases following HS in both WT and Δctl-2 strain, while Δctl-2 has less abundant peroxisomes compared to WT at OGT (Figure 3.2.8B). Interestigly, the peroxisomes also become bigger during HS in WT, but decrease in size in Δctl-2 strain. At OGT, the peroxisomes imaged in Δctl-2 strain are larger than those observed in WT, consistent with previous reports (Petriv & Rachubinski, 2004). We also observe that WT peroxisomes tend to become more rod like during HS, most likely in preparation of fission, while more of the *Δctl-2* peroxisomes retain their spherical shape following HS (Figure 3.2.8D).

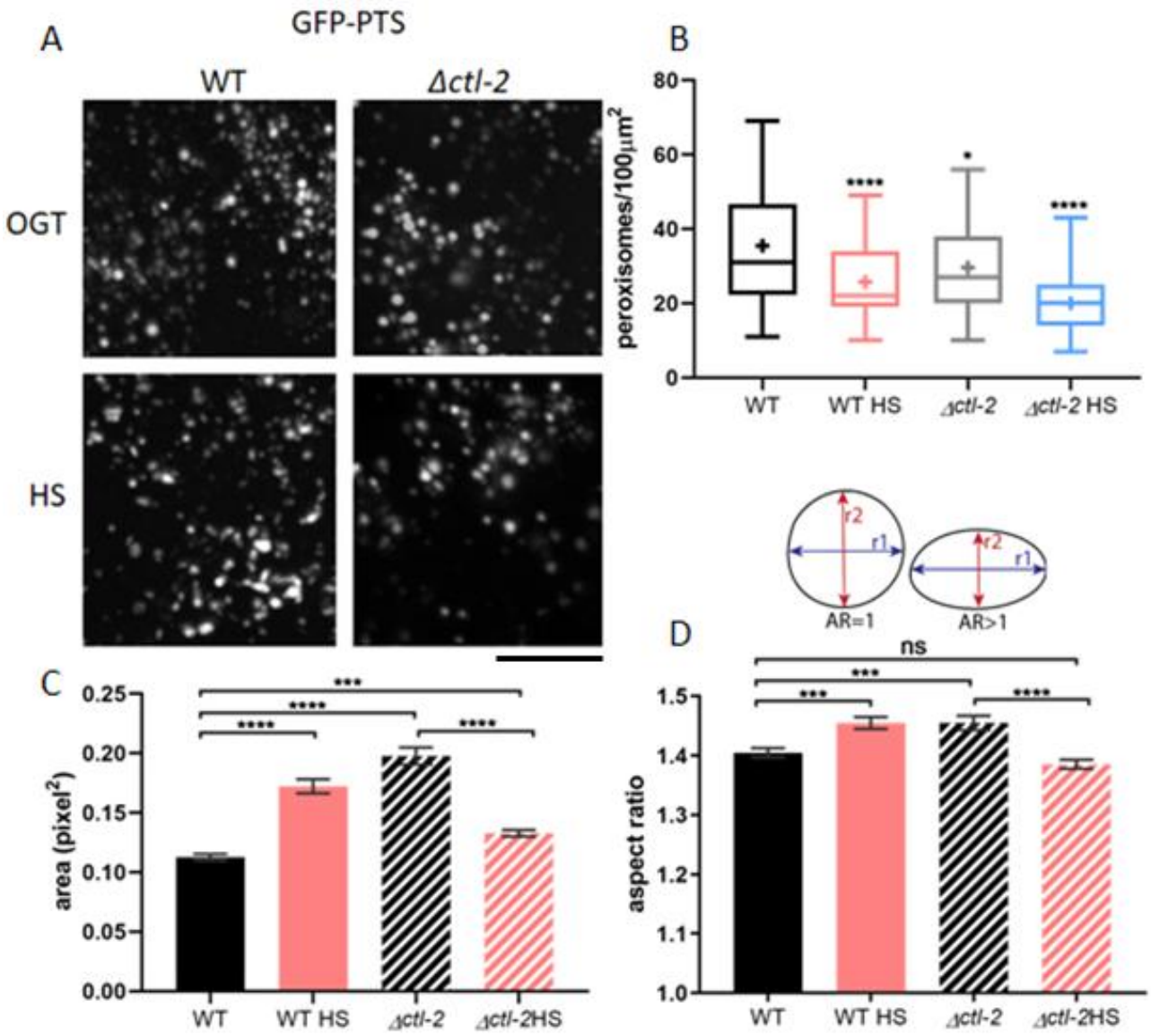

Figure 3.2.8. Peroxisome morphology and number are affected by mild transient HS. (A) Peroxisomes were visualized with a GFP-PTS fusion protein. The black bar represents 5 μm. (B) Quantification of the images represented in (A) shows that, on average, WT worms have more peroxisomes than *Δctl-2* strain. Their number is further reduced during HS. The plus signifies the mean. (C) *Δctl-2* peroxisomes are on average larger than those in WT; during HS WT peroxisomes increase in size while *Δctl-2* peroxisomes become smaller. (D) Aspect ratio of the imaged peroxisomes shows that WT peroxisomes become more elongated during HS, while in *Δctl-2* the trend is opposite. The graphs represent mean ± SEM. ****P<0.0001; ***P < 0.001; **P < 0.01; *P < 0.05 (ANOVA).

One of the most important functions carried out in the peroxisomes is β-oxidation of fatty acids, as its products are shuttled out to mitochondria as fuel. While mitochondria are able to perform oxidation of FAs themselves, very long FAs or VLCFAs can only be oxidized in peroxisomes, after which their shortened versions can be shuttled to mitochondria.

We see that, during HS, β-oxidation is suppressed in both WT and *Δctl-2*, as evidenced by downregulation of gene coding for ACOX-1, the rate limiting enzyme in this reaction: following HS both WT and *Δctl-2* display approximately a quarter of the transcript levels measured at OGT (Figure 3.2.9.). A similar trend is observed in the second step, catalysed by MAOC-1: following HS, *maoc-1* expression levels are halved, while the *Δctl-2* mutant shows roughly 2-fold upregulation of *maoc-1* at OGT, but only half of the WT level at HS (Figure 3.2.9.). However, the last step, thiolytic cleavage of 3-ketoacyl-CoA, is unaffected in WT, probably as it is unnecessary, indicated by unchanged transcript levels of *daf-22* (Figure 3.2.9.). In *Δctl-2* however, *daf-22* is upregulated 2-fold at OGT and severely suppressed at HS (Figure 3.2.9.), which may indicate that β-oxidation is overactive in the *Δctl-2* mutant. As ACOX-1 catalysis step is the main source of peroxide in the peroxisome, this may be one the main reasons behind the shortened lifespan of the *Δctl-2* strain. Further, as β-oxidation enzyme levels are notably higher in *Δctl-2* strain, it is possible that the levels of β-oxidation intermediates and final products are changed, thus affecting mitochondrial function.

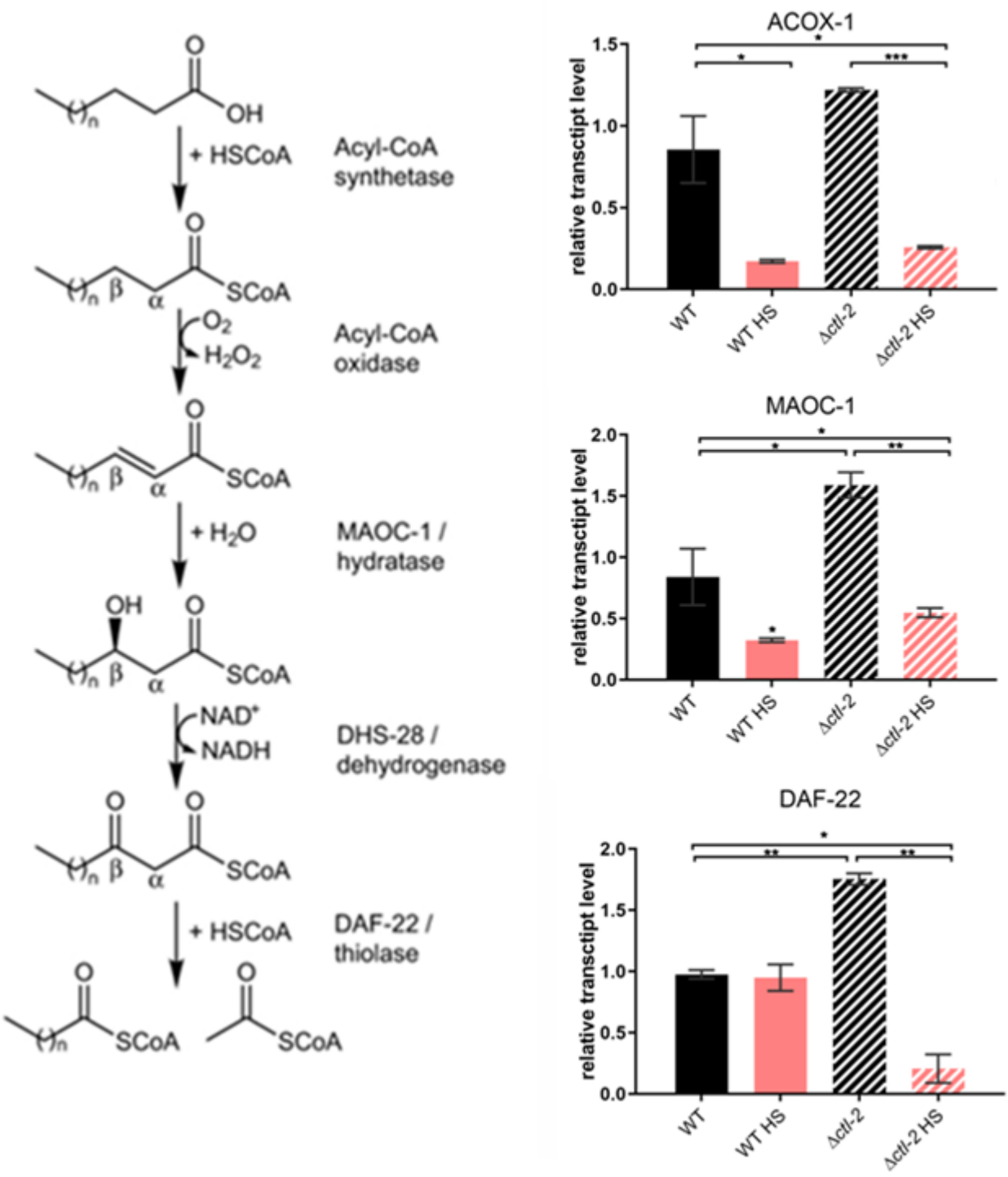

Figure 3.2.9. Fatty acid β-oxidation in peroxisomes is affected in the *Δctl-2* mutant. Major peroxisomal FA β-oxidation enzymes expression levels are increased in the *Δctl-2* mutant. Gene expression normalized to *act-1*. Error bars are mean ± SD. ****P<0.0001; ***P < 0.001; **P < 0.01; *P < 0.05 (ANOVA).

3.2.5. FA synthesis is affected in Δ*ctl-2* mutant

FAs are obtained by *C. elegans* either as nutritional FAs (through food) or through *de novo* synthesis. FAs are either broken down by mitochondria or stored as triglycerides. As we have evidence that β-oxidation is affected in the *Δctl-2* mutant, we also wanted to see if any changes occurred at the level of FA synthesis. The FA metabolism in extremely important, as lipids are major components of cellular membranes, which change their lipid composition in order to deal with different stressors, especially changes in temperature. To that end, we looked at transcript levels of major enzymes involved in FA synthesis, as well as visualized FA stores in fixed worms.

Again, we see a clear difference in the rate limiting step of FA synthesis; *pod-2* (acetyl-CoA carboxylase) transcript levels are very low at OGT and are upregulated at HS, but only to about a third of the WT level in same conditions (Figure 3.2.10.). This suggests that FA synthesis is impeded in the *Δctl-2* worms. Further, even though there are no changes in transcript levels of *fasn-1* (fatty acid synthase), Δ9 desaturases, *fat-5* and *fat-6* transcript levels are differently regulated, implying that the FA acid composition of the *Δctl-2* mutant may differ from the one of WT. More specifically, the *fat-5* expression is roughly 2-fold increased in WT following HS, while in the *Δctl-2* mutant after HS it is halved. Further, the *fat-6* expression is unchanged by HS in the WT, while in the *Δctl-2* mutant it increases by about 25% (Figure 3.2.10.). Although both *fat-5* and *fat-6* are Δ9 desaturases, they have different substrate specificities, with *fat-5* readily desaturating palmitic acid (16:0), but not common Δ9 substrate stearic acid (18:0), which is desaturated by *fat-6* (Watts & Browse, 2000), suggesting that their differential expression would impact the proportion of different FA species. As lipid composition is crucial, especially in conditions of changing temperature, these changes could have major impact on these worms survival at elevated temperatures. Therefore, we turned to microscopy and visualizing FA storage.

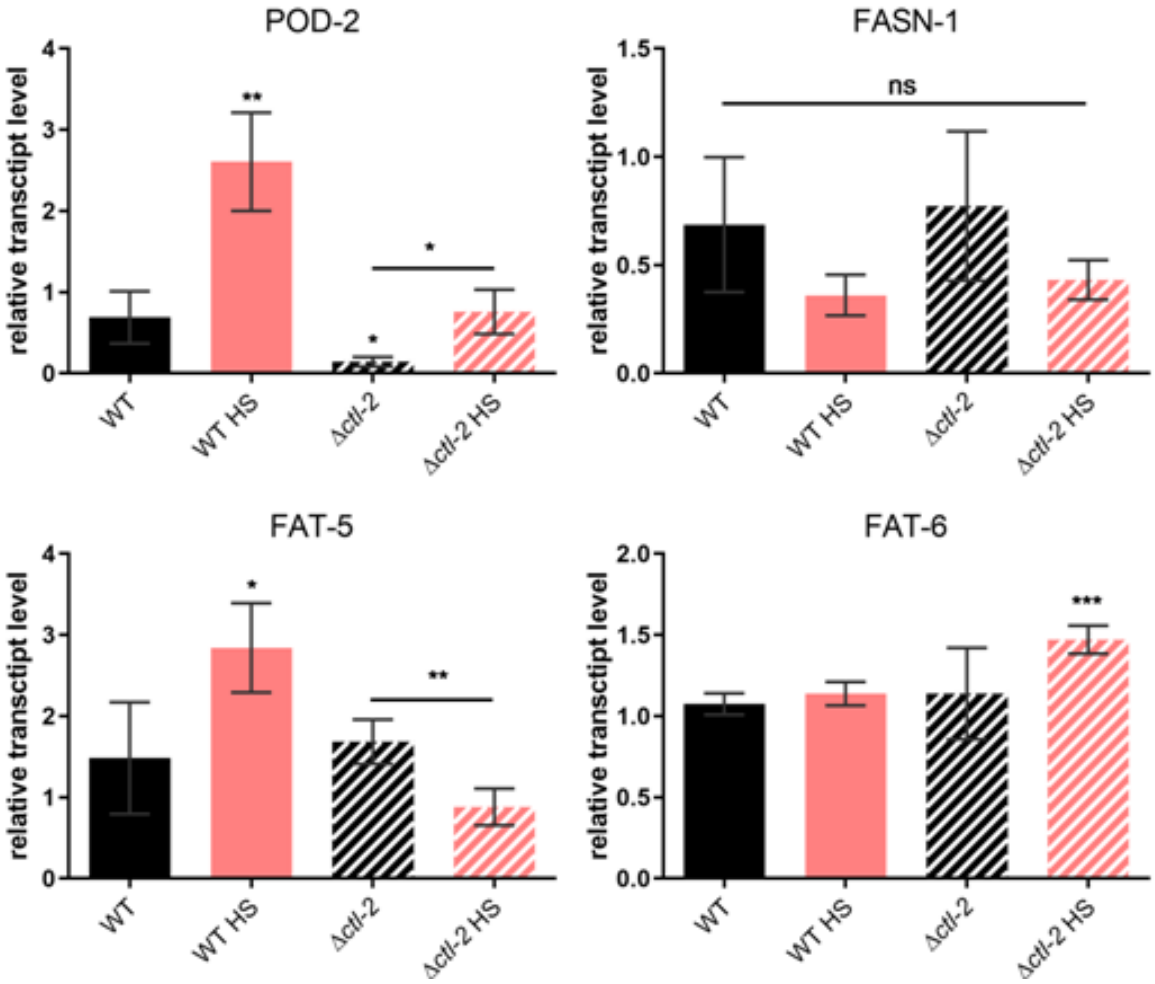

Figure 3.2.10. Fatty acid synthesis is affected by HS and *Δctl-2* mutation. *Δctl-2* mutant displays different regulation of genes involved in fatty acid synthesis during HS compared to WT. Gene expression normalized to *act-1*. Error bars are mean ± SD. ****P<0.0001; ***P < 0.001; **P < 0.01; *P < 0.05 (ANOVA).

FAs are stored in lipid droplets, mainly in the *C. elegans* intestine. The lipid droplets can be visualized using Nile Red dye, which stains neutral lipids. Nile Red staining, however, does not differentiate between different lipid species; therefore, it is a measure of total lipids stored by the worm. Nile Red revealed a slight increase in lipid droplet size following HS in WT but not in *Δctl-2* strain. Furthermore, at OGT, there was no significant difference between WT and *Δctl-2* strains in this aspect (Figure 3.2.11.). In the context of the observed transcript levels of FA oxidation and synthesis genes, we see that rate limiting enzymes were decreased and increased, respectively,

which is mirrored by the Nile Red staining. However, as the difference in lipid droplet size, as revealed by Nile Red staining, in WT is very slight, though statistically significant, it is unclear if it is biologically relevant.

Furthermore, as Nile Red is not specific to any FA species, we do not know if the FA composition in *Δctl-2* is also changed while the net amount remained the same. Therefore, we specifically stained triglycerides using Oil Red O stain. Oil Red O staining showed a difference, albeit not drastic, between the two strains, which suggests that triglyceride production and/or storage is affected in *Δctl-2* worms, as they retained less of the Oil Red O dye (Figure 3.2.12.). This is consistent with the qPCR results revealing differences in FA synthesis (Figure 3.2.10.), as decreased transcription of *pod-2* is usually associated with decreased triglyceride levels (Kim et al., 2016). In other words, *Δctl-2* mutant lipid storage is different than the one of WT.

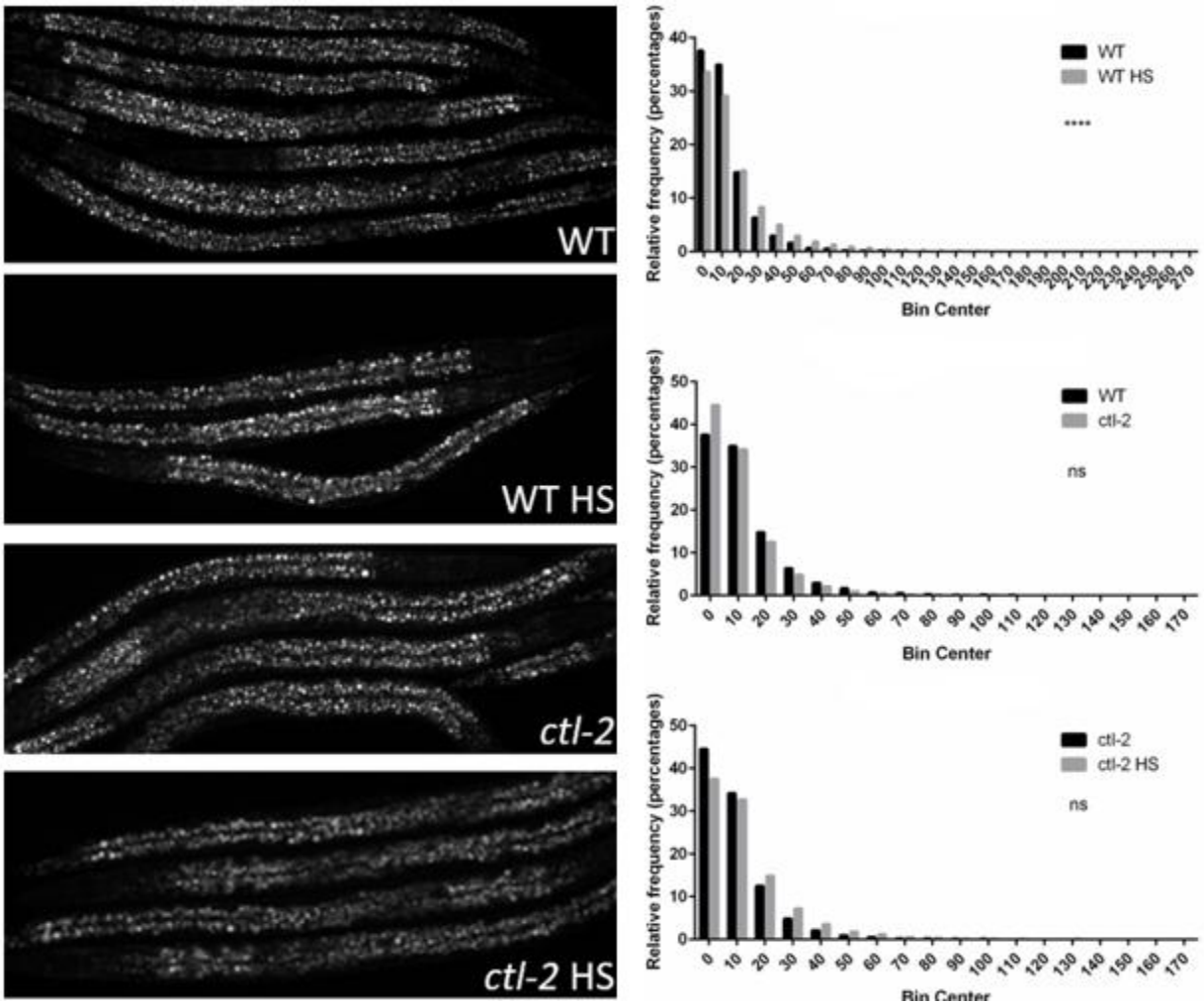

Figure 3.2.11. Lipid storage is not affected by HS in *Δctl-2* mutant. The size of lipid droplets, visualized by Nile Red staining, was not significantly affected by HS in *Δctl-2* strain, while the in WT the lipid droplets slightly increased, mirroring the decreased FA oxidation. Bin center represents lipid droplet area measured in pixels. ****P<0.0001; ***P < 0.001; **P < 0.01; *P < 0.05 (Mann-Whitney).

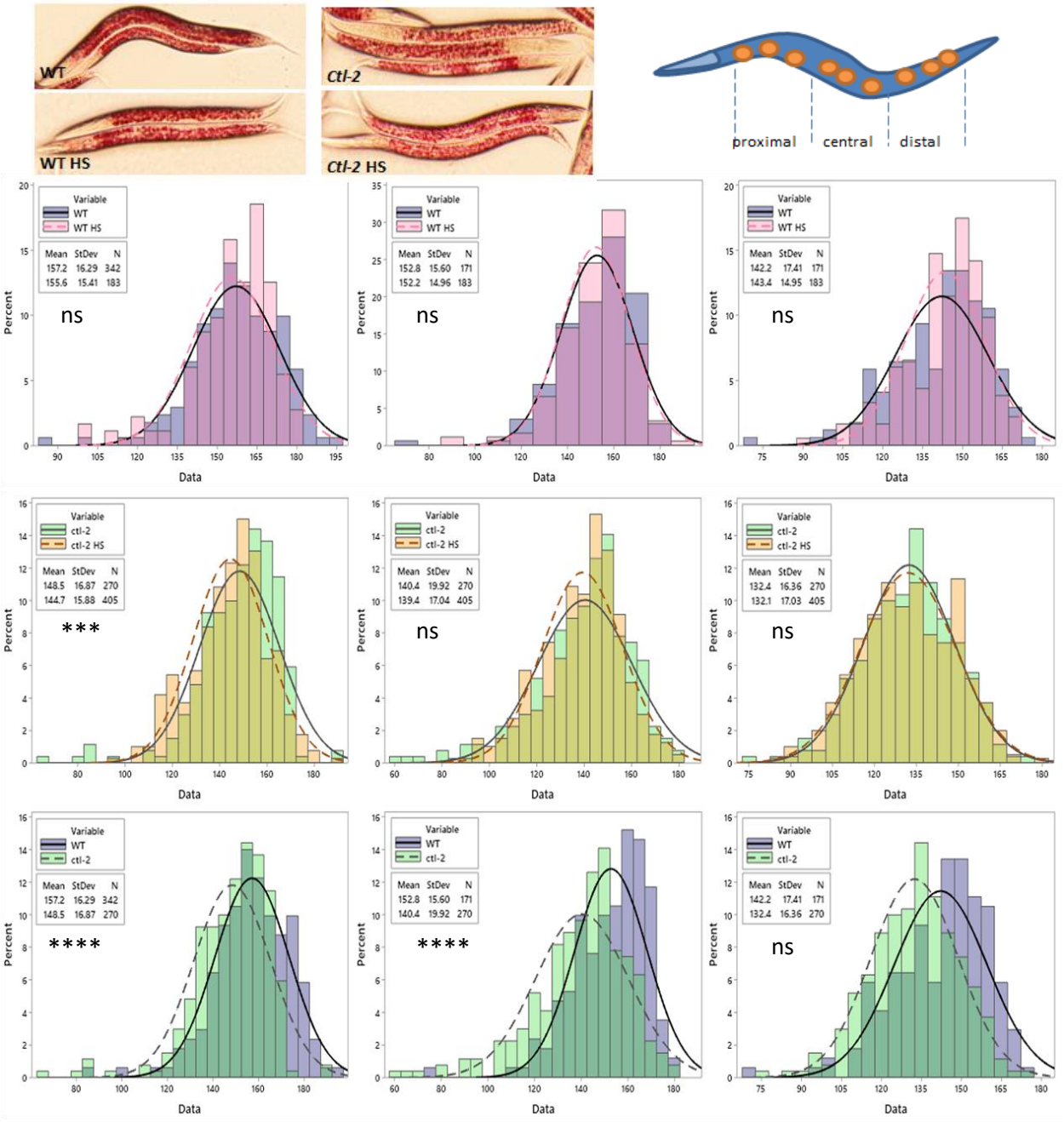

Figure 3.2.12. Triglyceride levels are altered in *Δctl-2* strain. *Δctl-2* worms show lower intensity Oil Red O staining compared to WT, indicating lower triglyceride content. Staining intensity was measured separately in the area between the pharynx and the vulva (anterior), area around the vulva (central), and the tail section (distal), avoiding the darker edge of the worm and the vulva, as integrated density i.e. sum of values of pixels normalized to area. Three measurements of each

section were averaged for each worm. ****P<0.0001; ***P < 0.001; **P < 0.01; *P < 0.05 (Mann-Whitney).

3.2.6. Mitochondrial morphology is affected during HS in the *Δctl-2* mutant

Mitochondria are known as the main energy source in the cell and their proper function is imperative for the cell's wellbeing, even more so because mitochondria are not simply passive cellular batteries, but active modulators of the cell metabolism, in constant communication with the nucleus. Similar to peroxisomes, their morphology changes and is indicative of both their status and the status of the cell. Cessation of fission results in a more interconnected, networked structures, while fission will result in increased proportion of small, round mitochondria.

Mitochondria were stained with MitoTracker Deep Red dye and imaged in live worms using spinning disc confocal microscope (Figure 3.2.13.). Analyses of MitoTracker Deep Red stained mitochondria indicate that WT and *Δctl-2* mitochondria display some differences in morphology, based on the number of branches, number of branch junctions, and their average length. These parameters are used to describe networked mitochondria, while individual mitochondria are separated based on their shape (rod, punctuate or large, round mitochondria). Analysis of mitochondrial networks is done on thresholded and skeletonised images of mitochondria, from which the software can recognize the number of mitochondrial "branches". A single, straight mitochondrion, for example, would be registered as a single branch, while increasing the number of branches would describe increasingly more complex, net-like mitochondria. The branch length is simply their length in pixels, while the number of "junctions" represents the number of pixels at the intersection of two branches, and as such correlates with the number of branches (see Methods, ref).

The analysis of the mitochondrial network shows that, on average, *Δctl-2* worms have less branched mitochondrial networks, with fewer and shorter branches. In both WT and *Δctl-2* mitochondria appear less branched following HS compared to OGT. More specifically, WT mitochondrial branches seem to be around 25% longer compared to *Δctl-2* mitochondria. Furthermore, after HS, there is a 50% decrease of mitochondrial branches length in the WT, while *Δctl-2* mitochondria become approximately 20% longer. At the same time the number of junctions is lowered during HS in both strains, concurrent with decrease in number of branches (Figure 3.2.14.).

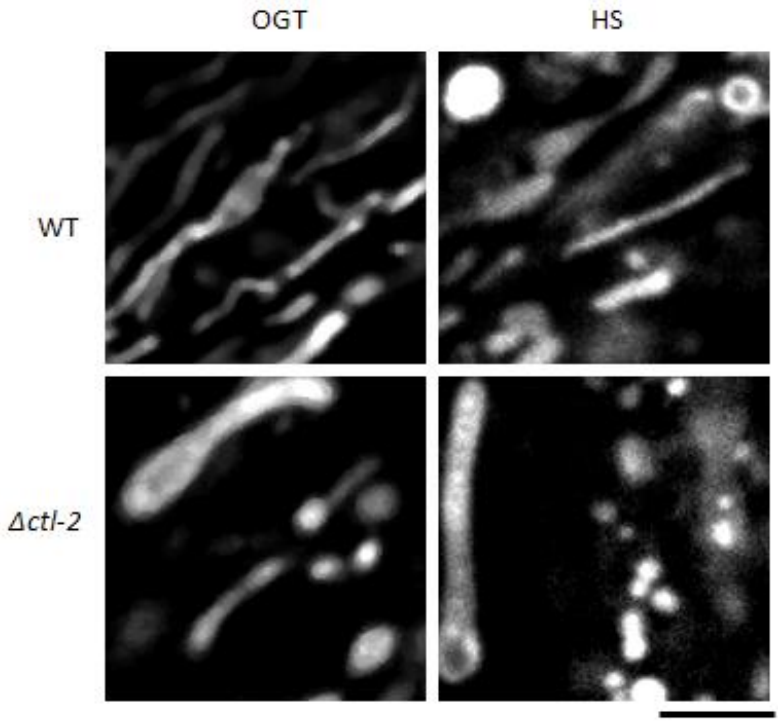

Figure 3.2.13. Mitochondrial morphology is altered by *Δctl-2* mutation and HS. Spinning disc confocal microscopy representative images of MitoTracker Deep Red stained live worms show morphological differences between WT mitochondria and those observed in the *Δctl-2* mutant at OGT and 4 hours at 30°C HS. The black bar represents 5 µm.

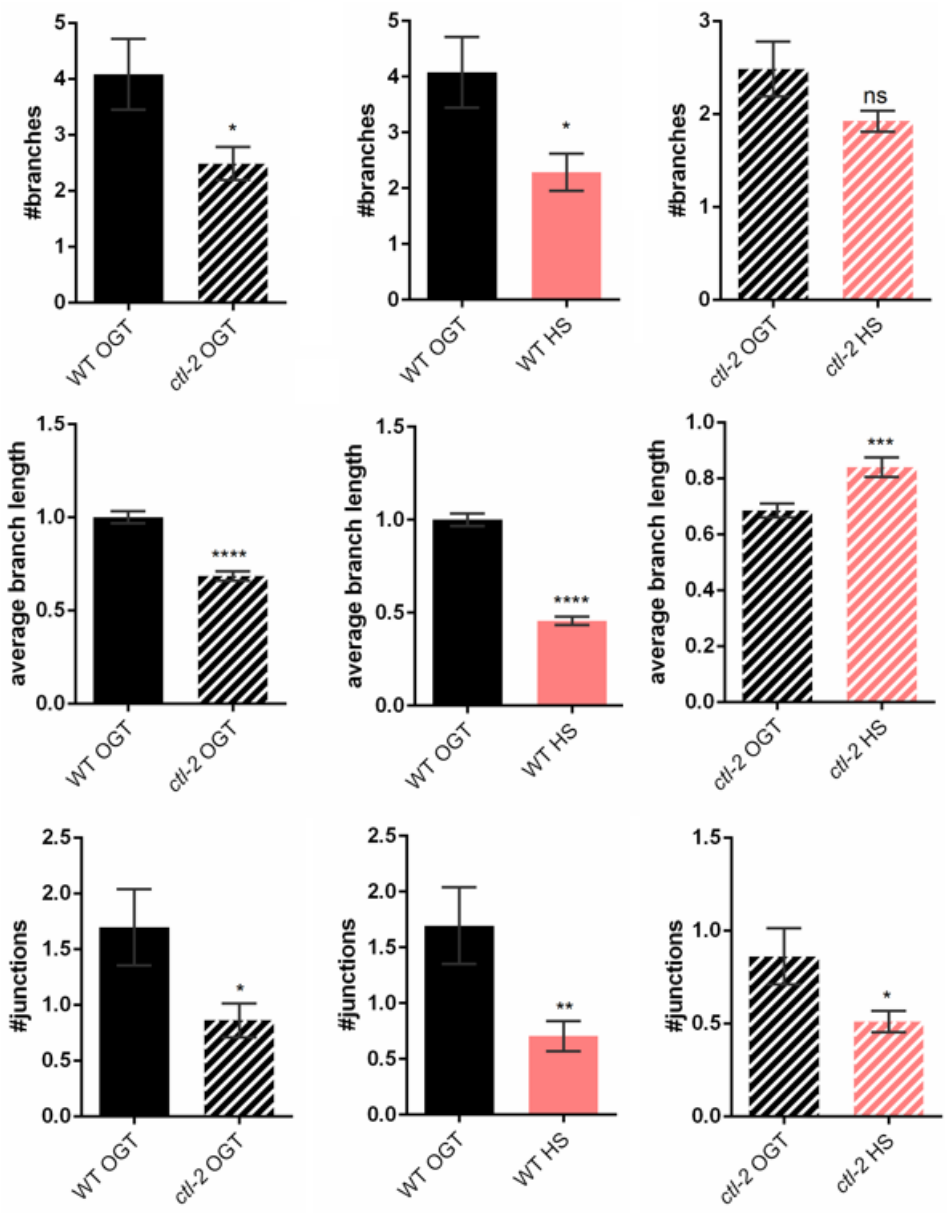

Figure 3.2.14. Quantification of mitochondrial networks in WT and *Δctl-2 C. elegans*. Network analysis reveals that 4 hour HS at 30°C causes general loss of interconnectedness of the networked mitochondria, evidenced through decrease number of mitochondrial branches, average branch length, and number of junctions. *Δctl-2* mutants display shorter and less branched out mitochondria. ****P<0.0001; ***P < 0.001; **P < 0.01; *P < 0.05 (t-test).

Analysis at single mitochondrion level reveals further differences (Figure 3.2.15.). At OGT, long, rod like mitochondria are the most commonly observed. However, at HS, WT has a greater proportion of large and round mitochondria, while *Δctl-2* accumulates both the large round mitochondria as well as small, punctuate mitochondria, indicative of increased fission. This result is also concurrent with the previous analysis showing the *Δctl-2* mitochondria are less networked than those observed in WT; instead they are either individual long mitochondria or form clusters, observed as large and round mitochondria. While the shape distributions/proportions of differently shaped mitochondria at OGT are relatively similar, their behaviour is markedly different during stress. Therefore, we also looked at transcription levels of the respiratory chain subunits and oxygen consumption as a functional parameter.

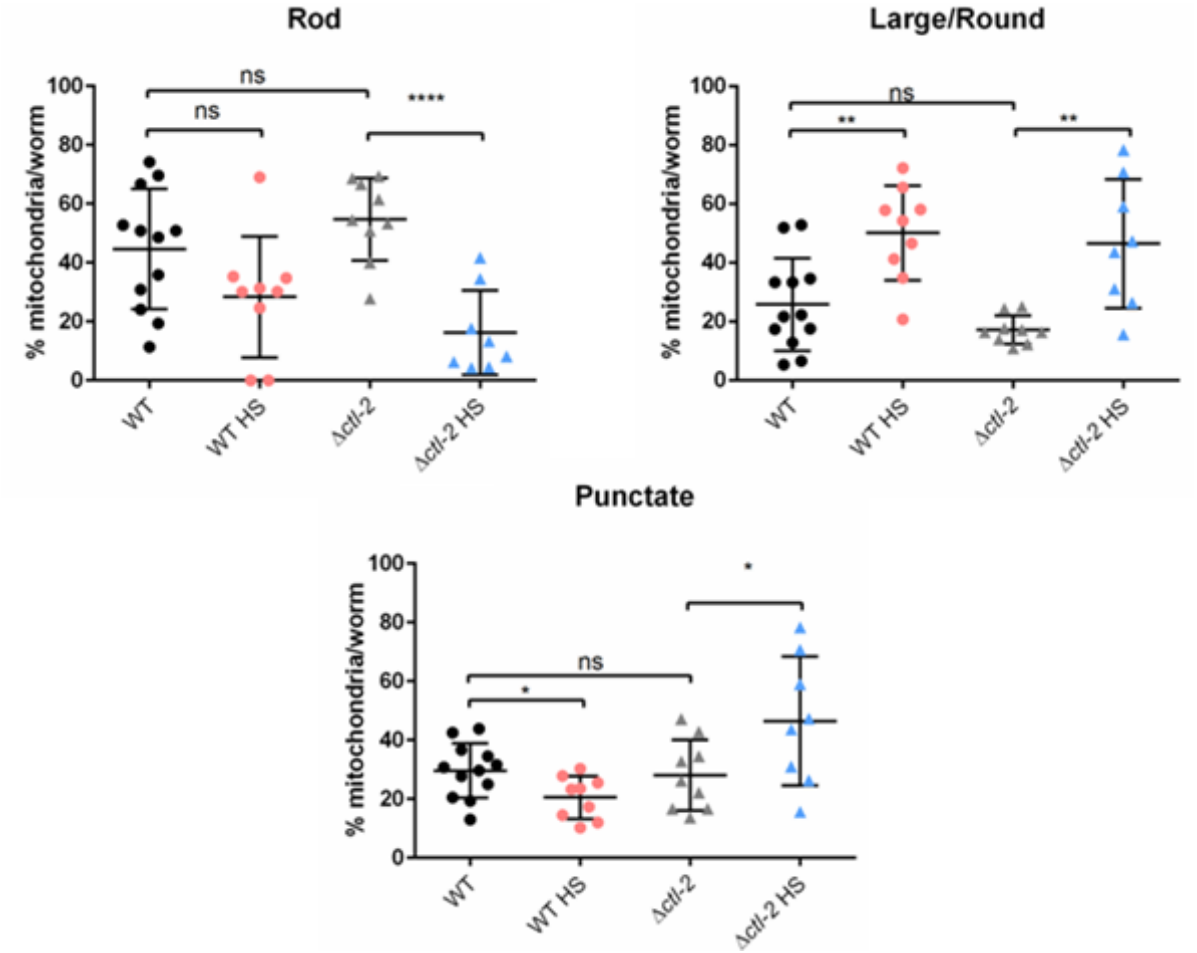

Figure 3.2.15. Comparison of individual mitochondria in WT and *Δctl-2*. At OGT both strains display similar mitochondrial morphology with predominantly single rod shaped mitochondria, but at HS *Δctl-2* mutant displays a more marked decrease in rod shaped mitochondria and accumulation

of both large and punctuate mitochondria. ****P<0.0001; ***P < 0.001; **P < 0.01; *P < 0.05 (ANOVA).

3.2.7. Subunits of the respiratory chain are upregulated during HS

In yeast, transcript levels of genes coding for respiratory chain subunits were upregulated during HS (Figure 3.1.3A). Therefore, we used qPCR to look at expression of genes coding for complex subunits in C. elegans. Similar to the results observed in yeast, respiratory chain subunits were largely upregulated, with a few exceptions. Notably, CTB-1 subunit of complex III was not upregulated during HS in *Δctl-2* mutant, while complex IV COX-1 (CTC-1) subunit was upregulated only in the *Δctl-2* strain, approximately 3-fold (Figure). Furthermore, complex IV COX-3 (CTC-3) subunit was approximately 6 times higher in WT during HS, level comparable to the one measured in *Δctl-2* mutant at OGT and HS (Figure 3.2.16.). As complex IV contributes to the membrane potential by removing protons from the mitochondrial matrix, increased expression of its subunits may cause electron leakage, thus contributing to ROS formation.

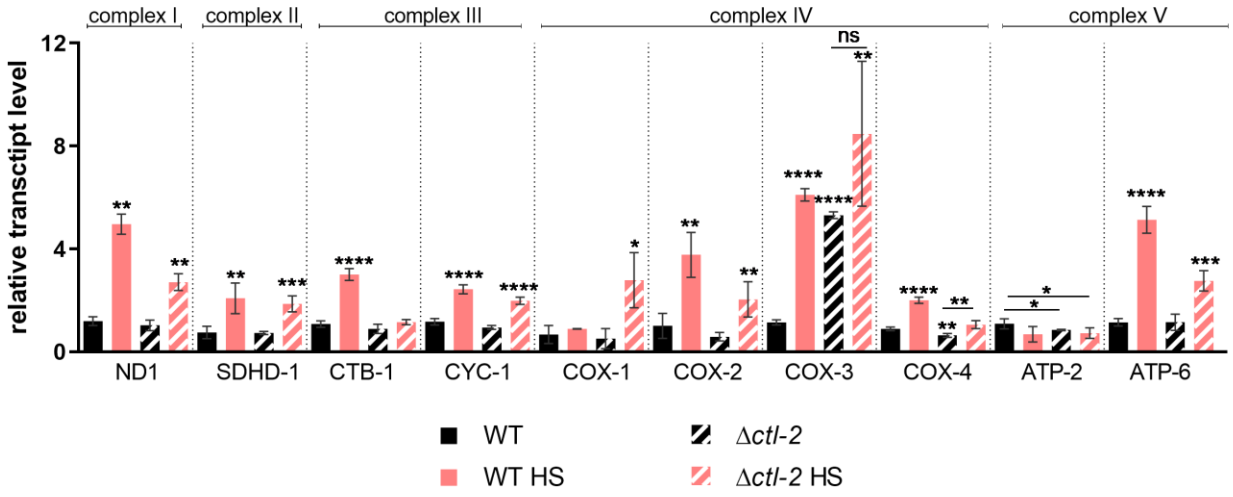

Figure 3.2.16. Respiratory chain subunits are upregulated during HS. Individual transcript levels are normalized to *act-1*. Error bars are mean ± SD. ****P<0.0001; ***P < 0.001; **P < 0.01; *P < 0.05 (ANOVA).

3.2.8. Respiration is not affected during HS

In budding yeast, we have shown that increased respiration was required for the HS induced lifespan extension. Furthermore, we have shown that mitochondrial dynamics during HS were impacted by the peroxisomal catalase absence. Therefore, we looked at the respiration rates in *C. elegans* immediately following HS treatment. Surprisingly, we found no significant difference in the oxygen consumption of the two strains (Figure 3.2.17.), suggesting that the life-extending properties of HS are activated through different pathways in the budding yeast and *C. elegans*.

Although we do not know the exact mechanisms of HS induced lifespan extension, we know that the HSR is not cell autonomous in *C. elegans*, unlike in yeast, and is therefore subject to more regulation. HS in *C. elegans* is perceived by the AFD thermosensory neuron, which signals distal tissues during heat stress (Prahlad et al., 2008). While increase in respiration and the resulting increase in ROS generation is necessary to prolong lifespan in yeast, in *C. elegans* this upregulation may not be necessary, as it is possible that the role of the respiration increase in yeast is played at least in part by the AFD neuron signalling.

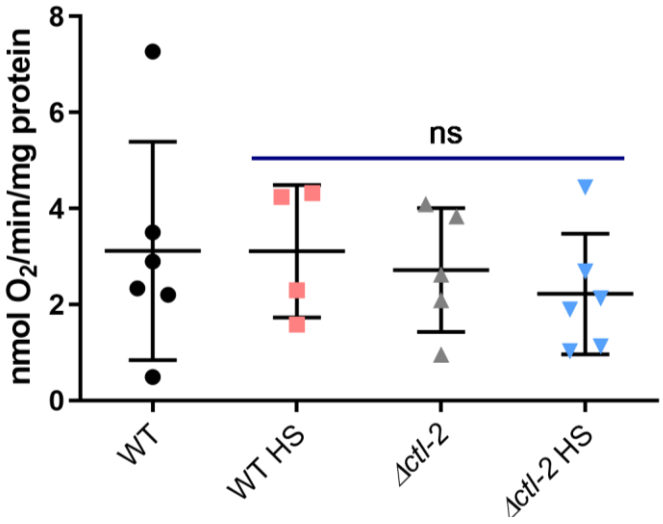

Figure 3.2.17. Respiration rate is not changed during HS in *C. elegans*. The graph represents rate of O_2 consumption of whole worms suspended in M9 medium. from at least four biological replicates. Measurements were performed using a Clarke electrode equipped oxygraph and then normalized to total protein concentration of the measured sample. The error bars represent mean ± SD. $P>0.05$ (ANOVA).

3.2.9. Glutathione

We previously established that glutathione recycling is the most downstream event in the heat shock-induced lifespan extension in yeast. Therefore, to further compare the cellular response to mild heat shock between yeast and nematodes, we quantified glutathione levels in *C. elegans* immediately after HS. Surprisingly, we observed no significant change in glutathione levels in C. elegans: both WT and *Δctl-2* strain averaged around 23 nM GSH at OGT, while at HS we measured around 19 nM and 16 nM GSH respectively (Figure 3.2.18.). Interestingly, while the difference is not statistically significant, in *C. elegans* the GSH levels tended to lower following HS, while in yeast we observed a significant increase. Together with the absence of increase of respiratory activity (Figure), these results suggest that oxidative stress in not a major contributing factor in the mild HS-induced lifespan extension in C. elegans. However, GSH was quantified in complete worm extracts, and if a possibility existed to measure it in a tissue specific manner, we would have been able to search for tissue-specific increases in GSH levels.

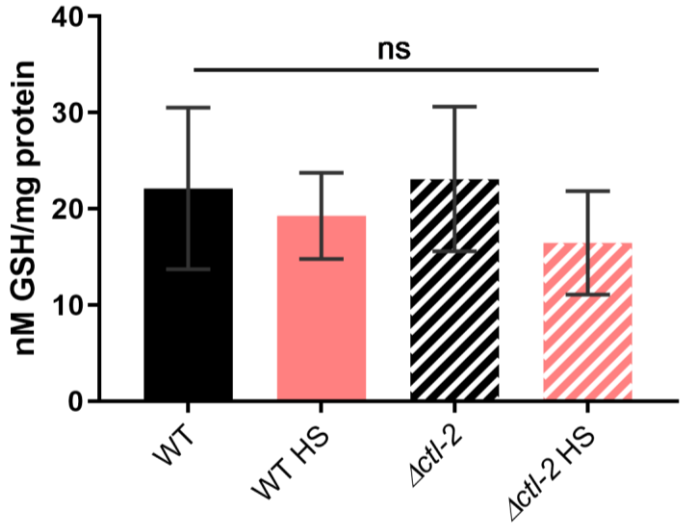

`Figure 3.2.18. GSH levels are not significantly changed during HS. *P* > 0.05 (ANOVA).

3.2.10. TORC1 activity is repressed by HS in WT but not in *Δctl-2* mutant

Finally, we measured TORC1 activity during HS in *C.elegans*. TORC1activity was measured indirectly by qPCR measurement of its downstream targets. When TORC1 is inhibited, its downstream target SKN-1/Nrf is uninhibited and activates transcription of protective genes, as well as TORC1 subunits in a feedback loop. DAF-16/FoxO is also activated. Both DAF-16/FoxO and SKN-1/Nrf are both inhibited by insulin/IGF-like signalling in *C. elegans* (C. Kenyon, 2011; C. J. Kenyon, 2010; Robida-Stubbs et al., 2012). The qPCR measurement revealed that TORC1 was inhibited by both HS and Rapamycin in the WT strain, evidenced by increased transcript levels of both TORC1 transcriptional targets SKN-1 and DAF-16, as well as their own targets, including TORC1 subunit RAGA-1 (Figure 3.2.19.). Surprisingly, HS did not inhibit TORC1 in the peroxisomal *Δctl-2* mutant, while Rapamycin did (Figure 3.2.19.). As Rapamycin can also interfere with TORC2 activity, this may suggest that TORC1 specifically is needed for HS-mediated lifespan extension in *C.elegans*.

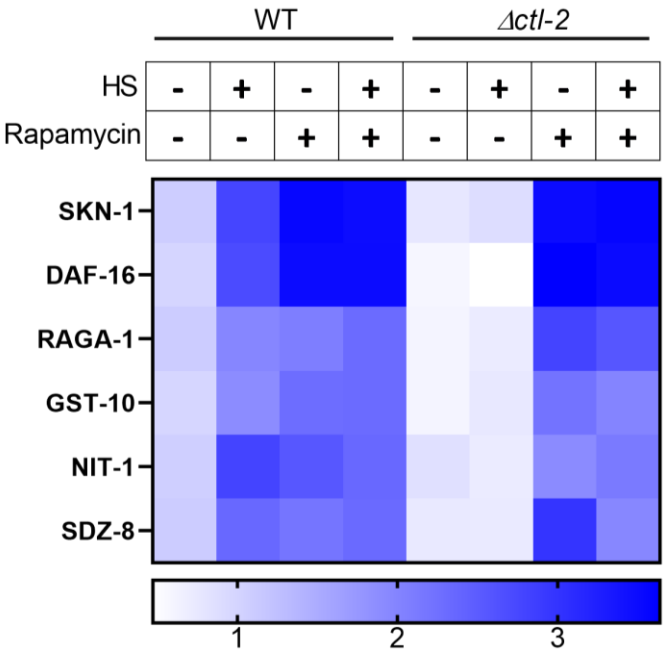

Figure 3.2.19. HS inhibits TORC1 in WT but not in *Δctl-2* mutant. qPCR measurement reveals increased transcript levels of TORC1 downstream targets, indicating TORC1 has been inhibited in the WT but not in the peroxisomal mutant. Color of the squares on the heat map corresponds to the mean value of the log fold change. Individual transcript levels were normalized to *act-1*.

4. DISCUSSION

Hormetic effects of low dose of stressors have been recorded in several organisms so far (Butov et al., 2001; Calabrese et al., 2007; Cypser & Johnson, 2002; Hercus et al., 2003; Kumsta, Chang, Schmalz, & Hansen, 2017; Rattan & Demirovic, 2009; Semchyshyn & Valishkevych, 2016). The mechanism, however, is a matter of contention, and the widely accepted view is that cell defence mechanisms are activated by the heat-induced misfolding of proteins, and that this upregulation of cellular defence machineries is the cause of hormetic lifespan extension (Morimoto, 2011; Richter et al., 2010). While activation of heat shock response is absolutely necessary during stress, both for survival and hormesis, several lines of evidence exist that, while necessary, HSR is not sufficient for HS-induced longevity.

In yeast, it has been shown that in order for the mother cell to benefit from the HS, the diffusion barrier between the mother and the nascent daughter cell needs to be permeated, allowing for relocation of damaged cell components that would otherwise be retained by the mother into the daughter cell (Baldi et al., 2017). Further, damaged cellular components are often found in inclusions or aggregates, together with undamaged molecules such as RNA. While aggregate formation is generally considered toxic, aggregates too have an important biological role. Indeed, presence of aggregates in the cell is a sign of stress and is connected to several pathologies, as well as aging (David et al., 2010; Grune et al., 2004; Saarikangas & Barral, 2015). However, smaller aggregates can be more toxic to the cell compared to larger, more inert aggregates, such as in case of tau (Ghag et al., 2018); therefore, their growth can be a defence mechanism in itself. But not all aggregates are the same. It has been demonstrated that protein aggregates are far more complex than was initially believed; rather than a randomly formed bundle of damaged proteins, proteins are in fact sequestered into aggregates in a controlled and selective manner. JUNQ (juxta nuclear quality control compartment) is a type of protein aggregate that sequesters ubiquitinated proteins and has been shown to exchange its contents with the cytosol, meaning that proteins can be added and taken out from the JUNQ type aggregate. For this purpose, JUNQ concentrates chaperone disagreggases and 26S proteasomes. On the other hand, IPOD (insoluble protein deposit) serves as a final destination for damaged proteins (Kaganovich, Kopito, & Frydman, 2008). Finally, although all proteins are able of forming aggregates upon misfolding, aggregation of only few protein species has been shown to lead to disease (Chiti & Dobson, 2006, 2017), furthering the point that aggregates indeed do have a functional role in cellular homeostasis (Saarikangas & Barral, 2016).

It goes without saying that aggregates need to be properly managed and controlled during stress, not unlike HSR and chaperones; disaggregase Hsp104p has been shown essential for the HS-induced RLS extension in yeast (Sanchez, Taulien, Borkovich, & Lindquist, 1992; Shama, Kirchman, Jiang, & Jazwinski, 1998; Shama, Lai, et al., 1998) and is also found in both IPOD and JUNQ (Kaganovich et al., 2008). Furthermore, sequestering damaged proteins into aggregates means they can be either retained or passed on during asymmetric division, thus enabling cellular rejuvenation (Ogrodnik et al., 2014), similar to the asymmetric inheritance of aging factors such as extra chromosomal circles (Baldi et al., 2017).

These observations demonstrate that any hormetic effect must be a consequence of stress response management and fine-tuning during stress, adapted for the type of stressor, its duration and severity, rather than being a consequence of just massive upregulation of chaperones. However, existence and involvement of other mechanisms and pathways, and their interplay, cannot be excluded. The understanding of the molecular contributions to the hormetic effect is crucial for its potential application.

Our results in yeast suggest that heat stress also causes oxidative stress, as a consequence of increased oxygen consumption and, in turn, mitochondrial superoxide production, and that this is essential for the HS-induced RLS extension i.e. the hormetic effect. Strains unable to make the switch from fermentative to respiratory growth or to increase their respiration rate, petite and *HAP4*Δ, respectively, did not display RLS extension following HS, despite upregulation of HSPs consistent with HSR activation. Furthermore, neutralizing the superoxide produced by respiration eliminated HS-induced RLS extension, despite the switch to respiratory metabolism and upregulation of HSPs. Therefore, we concluded that for heat induced hormesis, upregulation of chaperones is not enough, but that it requires metabolic reprogramming during stress. We do not currently know if the changes we observe are sustained later in life or the metabolism reverts back to utilizing glucose after some recovery period at optimal growth temperature.

In contrast to our finding in yeast, we observe no changes in respiratory metabolism during HS in *C. elegans*. There are other contradictions as well. While the FA oxidation is upregulated in WT yeast during HS, in *C. elegans* the trend is the opposite, and glutathione levels are unchanged. We do not know the exact mechanisms behind the HS-induced lifespan extension in *C. elegans*, however it is already clear that they are different from those employed in *S. cerevisiae*. The reason behind it may

be in how the stress is perceived by the organism and how HSR is regulated. Furthermore, while yeast cells are still dividing during our experiments, adult *C. elegans* are postmitotic organisms: after they reach adulthood the only division happens in the gonad. In the late L4 stage at which our experiments were performed, the majority of the growth is already completed, and the gonad is the only major structure which is not fully matured. Therefore, while in budding yeast it is possible for the mother to be 'rejuvenated' through asymmetrical inheritance, as described in (Baldi et al., 2017), in *C. elegans* not only is this not an option, but they are not even able to replace a cell if it becomes severely damaged. Similar to neurons, being postmitotic means that *C. elegans* must invest energy in protection and preservation. For this reason, it is likely that *C. elegans* would have more incentive to decrease its metabolic rate during stress and preserve its cellular components, while yeast cells reprogram their metabolism.

Adapting membrane fluidity is one of the most important factors in surviving any type of temperature stress. Given that the FA metabolism in *C. elegans* is altered both by HS and by *Δctl-2* mutation, which conferred a certain loss of thermotolerance, maintenance of the optimal membrane composition, and as a consequence, optimal fluidity puts itself forward as a crucial part of the mechanism. It is possible that the observed changes in the lipid metabolism in the *Δctl-2* mutant do not allow it to properly respond to the HS in terms of adjusting its membrane FA contents, making it more susceptible to damage during HS. Therefore, it would be interesting to undertake a series of measurements that would determine how both membrane fluidity/rigidity and FA composition are changed in various conditions of HS and in mutants such as *Δctl-2*.

Furthermore, peroxisomes are crucial as sites of lipid catabolism, providing substrates for other processes including shortened FAs for mitochondria to be used in production of ATP. Therefore, perturbations in peroxisomes are not contained there. For example, the decreased expression of rate limiting POD-2 enzyme could be causing a deficit of malonyl CoA, Malonyl CoA is required for the FA synthesis and it inhibits the transport of FAs to the mitochondria (Figure 1.12.) to prevent cycling between synthesis and oxidation. Furthermore, the FAs oxidized in the mitochondria, in part provided by peroxisomes, provide Acyl CoA to the TCA cycle, thus making it susceptible to any changes in FA availability. Furthermore, mitochondrial fission and fusion machinery is also affected by changes in FA availability: decreased availability of long and very long chain 3-Hydroxy Acyl CoA in mitochondria is associated with accumulation of shorter mitochondria (Hagenbuchner,

Scholl-Buergi, Karall, & Ausserlechner, 2018), similar to what we observed in *Δctl-2* worms. The exact effects of peroxisomal catalase mutations are yet to be determined.

The most obvious difference between the two studied organisms is of course their size, increase in which brings with itself more levels of complexity. In yeast the stress response pathways are cell autonomous, and there is no coordination between two cells. This means that each yeast cell can invest all its energy into preserving itself during stress. *C. elegans*, however, is a more complex organisms, and the stress response needs to be more finely tuned. In *C. elegans*, heat is perceived by AFD thermosensitive neuron, which is needed for the HSR activation in distal tissues (Prahlad et al., 2008; Zhang et al., 2018). Different tissues have different metabolic and energetic needs, and therefore HSR needs to be coordinated not just on cellular level, but also between tissues, imposing additional constraints.

Therefore, different responses between *S. cerevisiae* and *C. elegans* are not unexpected. However, the necessity of increased respiration and the role of mitochondrial superoxide in yeast HS-induced RLS extension have not been described before, and we were interested to see if the lifespan extension has the same requirements in *C. elegans*. One of the drawbacks of our experiments is that we are looking at the response of the whole worm i.e. the average change of all the different cell types and tissues. Consequently, we may be missing some of the metabolic changes that may have been increased in one tissue and decreased in another, as we are always looking at the organism level. Therefore, it is not impossible that the mechanism of the HS induced lifespan extension in *C. elegans* is very similar to the one we hypothesized and experimentally supported in yeast, but that the changes in metabolism are more nuanced and tissue specific.

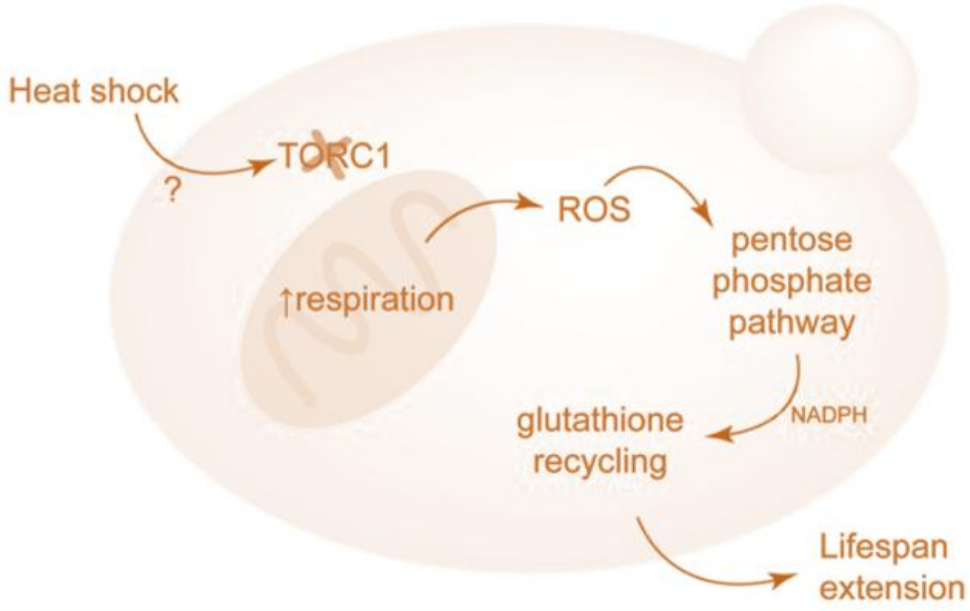

Figure 4.1. Schematic representation of the proposed mechanisms culminating in RLS extension in yeast. Increased respiration, triggered by TORC1 inactivation, leads to increase in superoxide production, which causes activation of antioxidant defenses and redox homeostasis maintenance i.e. glutathione recycling, essential for heat-induced longevity.

Interestingly, inhibition of TORC1 seems to be a common event in both yeast and worm HS-mediated lifespan extension: experiments on both yeast and worms suggested that TORC1 is inhibited by mild HS. However, while we have sufficient evidence to claim TORC1 inhibition is necessary or the HS-mediated lifespan extension in yeast, we cannot claim the same for *C. elegans*, as we were unable to obtain a *C. elegans* strain with constitutively active TORC1. Still, it is reasonable to expect TORC1 has a major role. Therefore, while we were able to elucidate the sequence of events leading to the lifespan extension in yeast, in *C. elegans* the picture is yet to be completed.

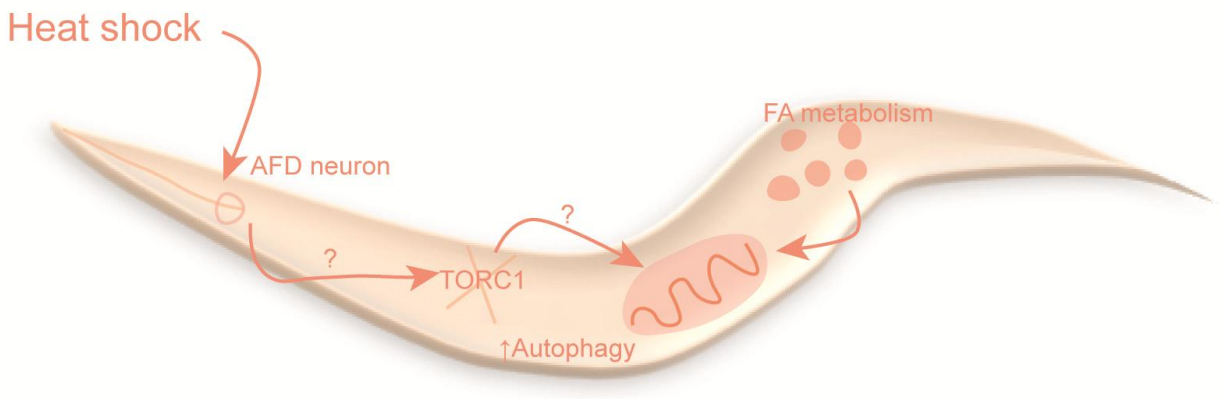

Figure 4.2. Mechanism of lifespan extension following mild HS in *C. elegans*. HS is perceived by AFD thermosensory neuron in the pharynx. Inactivation of TORC1 is one of the necessary events for the lifespan extension to occur. Previous reports also identify autophagy as contributing to the HS-mediated lifespan extension (Kumsta et al., 2017).

It is clear that in *C. elegans* TORC1 plays a vital role in lifespan determination, similar to what we observed in yeast. Furthermore, in all our experiments there were no instances of lifespan being extended while TORC1 was still active. However, we do not know at present why respiration was unaffected by HS despite TORC1 being inhibited. Regardless, TORC1 activity remains one of the mechanistic steps in lifespan extension common to all organisms from yeast to mammals. Another crucial process that has been identified by other groups is autophagy (Kumsta et al., 2017). Importance of autophagy in lifespan extension following hormetic HS underlines the importance of proteostasis maintenance. From our results it seems that even slight perturbations in this process, such as that of removing a catalase from the peroxisomes, is enough to tip the scale and disrupt the balance in the cell.

5. CONCLUSION

Hormetic effects of mild, transient heat shock have been described for a range of organisms from yeast to mammals. Our goal was to describe its mechanisms of action in more robust detail. We find that inhibition of TORC1 is necessary for HS-mediated lifespan extension in yeast *S. cerevisiae*, while in *C. elegans* its importance is strongly implied in our experiments. In yeast, the TORC1 inhibition leads to increase in respiration and increased production of mitochondrial superoxide, and as a consequence increased glutathione recycling as the most downstream event.

In *C. elegans*, however, the mechanisms are more difficult to elucidate given it's a more complex organism whose cellular responses are not cell-autonomous. Still, TORC1 singles itself out as one of the key mediators of longevity, consistent with other reports. Furthermore, lipid metabolism seems to play a key role. Interestingly, in both yeast and *C. elegans*, while upregulation of HSPs is necessary for the lifespan extension, it is not sufficient, contrary to a long standing belief that lifespan extension following stress is due to the increased expression of protective factors.

Therefore, a slight perturbation in the peroxisome in the form of catalase absence, may have triggered a chain reaction in which mitochondria were not able to get all the substrates they need to fully perform their function, and the cell was not able to alter its membrane composition to deal with the HS; in other words, despite the activation of the HSR, the changes necessary to face the HS were not possible to make. Instead, we propose that, in order to benefit from a hormetic stress, a metabolic reprogramming is necessary alongside HSP expression. Taking in consideration that *C. elegans* gut, where majority of the processes and parameters we measured are taking place, is roughly equivalent to mammalian liver, gut, and adipose tissue, our results fall in line with other studies that show that diet is crucial in lifespan and healthspan extension in humans, as well as maintaining a healthy gut microbiome.

6. BIBLIOGRAPHY

Aguilaniu, H., Gustafsson, L., Rigoulet, M., & Nyström, T. (2003). Asymmetric inheritance of oxidatively damaged proteins during cytokinesis. *Science, 299*(5613), 1751-1753. doi:10.1126/science.1080418

Anders, S., Pyl, P. T., & Huber, W. (2015). HTSeq--a Python framework to work with high-throughput sequencing data. *Bioinformatics, 31*(2), 166-169. doi:10.1093/bioinformatics/btu638

Andersson, V., Hanzén, S., Liu, B., Molin, M., & Nyström, T. (2013). Enhancing protein disaggregation restores proteasome activity in aged cells. *Aging (Albany NY), 5*(11), 802-812. doi:10.18632/aging.100613

Babior, B. M. (1984). The respiratory burst of phagocytes. *J Clin Invest, 73*(3), 599-601. doi:10.1172/JCI111249

Baldi, S., Bolognesi, A., Meinema, A. C., & Barral, Y. (2017). Heat stress promotes longevity in budding yeast by relaxing the confinement of age-promoting factors in the mother cell. *Elife, 6*. doi:10.7554/eLife.28329

Bansal, A., Zhu, L. J., Yen, K., & Tissenbaum, H. A. (2015). Uncoupling lifespan and healthspan in Caenorhabditis elegans longevity mutants. *Proc Natl Acad Sci U S A, 112*(3), E277-286. doi:10.1073/pnas.1412192112

Baugh, L. R. (2013). To grow or not to grow: nutritional control of development during Caenorhabditis elegans L1 arrest. *Genetics, 194*(3), 539-555. doi:10.1534/genetics.113.150847

Ben-Zvi, A., Miller, E. A., & Morimoto, R. I. (2009). Collapse of proteostasis represents an early molecular event in Caenorhabditis elegans aging. *Proc Natl Acad Sci U S A, 106*(35), 14914-14919. doi:10.1073/pnas.0902882106

Blackwell, T. K., Steinbaugh, M. J., Hourihan, J. M., Ewald, C. Y., & Isik, M. (2015). SKN-1/Nrf, stress responses, and aging in Caenorhabditis elegans. *Free Radic Biol Med, 88*(Pt B), 290-301. doi:10.1016/j.freeradbiomed.2015.06.008

Blake, M. J., Fargnoli, J., Gershon, D., & Holbrook, N. J. (1991). Concomitant decline in heat-induced hyperthermia and HSP70 mRNA expression in aged rats. *Am J Physiol, 260*(4 Pt 2), R663-667. doi:10.1152/ajpregu.1991.260.4.R663

Bonawitz, N. D., Chatenay-Lapointe, M., Pan, Y., & Shadel, G. S. (2007). Reduced TOR signaling extends chronological life span via increased respiration and upregulation of mitochondrial gene expression. *Cell Metab, 5*(4), 265-277. doi:10.1016/j.cmet.2007.02.009

Brunk, U. T., & Terman, A. (2002). The mitochondrial-lysosomal axis theory of aging: accumulation of damaged mitochondria as a result of imperfect autophagocytosis. *Eur J Biochem, 269*(8), 1996-2002.

Butov, A., Johnson, T., Cypser, J., Sannikov, I., Volkov, M., Sehl, M., & Yashin, A. (2001). Hormesis and debilitation effects in stress experiments using the nematode worm Caenorhabditis elegans: the model of balance between cell damage and HSP levels. *Exp Gerontol, 37*(1), 57-66.

Cadenas, E., & Davies, K. J. (2000). Mitochondrial free radical generation, oxidative stress, and aging. *Free Radic Biol Med, 29*(3-4), 222-230.

Caito, S. W., & Aschner, M. (2015). Quantification of Glutathione in Caenorhabditis elegans. *Curr Protoc Toxicol, 64*, 6.18.11-16. doi:10.1002/0471140856.tx0618s64

Calabrese, E. J., Bachmann, K. A., Bailer, A. J., Bolger, P. M., Borak, J., Cai, L., . . . Mattson, M. P. (2007). Biological stress response terminology: Integrating the concepts of adaptive response and preconditioning stress within a hormetic dose-response framework. *Toxicol Appl Pharmacol, 222*(1), 122-128. doi:10.1016/j.taap.2007.02.015

Charlesworth, B. (2000). Fisher, Medawar, Hamilton and the evolution of aging. *Genetics, 156*(3), 927-931.

Chiti, F., & Dobson, C. M. (2006). Protein misfolding, functional amyloid, and human disease. *Annu Rev Biochem, 75*, 333-366. doi:10.1146/annurev.biochem.75.101304.123901

Chiti, F., & Dobson, C. M. (2017). Protein Misfolding, Amyloid Formation, and Human Disease: A Summary of Progress Over the Last Decade. *Annu Rev Biochem, 86*, 27-68. doi:10.1146/annurev-biochem-061516-045115

Cohen, E., & Dillin, A. (2008). The insulin paradox: aging, proteotoxicity and neurodegeneration. *Nat Rev Neurosci, 9*(10), 759-767. doi:10.1038/nrn2474

Cortopassi, G. A., & Arnheim, N. (1990). Detection of a specific mitochondrial DNA deletion in tissues of older humans. *Nucleic Acids Res, 18*(23), 6927-6933.

Csermely, P. (2001). Chaperone overload is a possible contributor to 'civilization diseases'. *Trends Genet, 17*(12), 701-704.

Cuervo, A. M. (2008). Autophagy and aging: keeping that old broom working. *Trends Genet, 24*(12), 604-612. doi:10.1016/j.tig.2008.10.002

Cypser, J. R., & Johnson, T. E. (2002). Multiple stressors in Caenorhabditis elegans induce stress hormesis and extended longevity. *J Gerontol A Biol Sci Med Sci, 57*(3), B109-114.

Dai, C., Santagata, S., Tang, Z., Shi, J., Cao, J., Kwon, H., . . . Lindquist, S. (2012). Loss of tumor suppressor NF1 activates HSF1 to promote carcinogenesis. *J Clin Invest, 122*(10), 3742-3754. doi:10.1172/JCI62727

Dai, C., Whitesell, L., Rogers, A. B., & Lindquist, S. (2007). Heat shock factor 1 is a powerful multifaceted modifier of carcinogenesis. *Cell, 130*(6), 1005-1018. doi:10.1016/j.cell.2007.07.020

Das, R., Melo, J. A., Thondamal, M., Morton, E. A., Cornwell, A. B., Crick, B., . . . Samuelson, A. V. (2017). The homeodomain-interacting protein kinase HPK-1 preserves protein homeostasis and longevity through master regulatory control of the HSF-1 chaperone network and TORC1-restricted autophagy in Caenorhabditis elegans. *PLoS Genet, 13*(10), e1007038. doi:10.1371/journal.pgen.1007038

David, D. C., Ollikainen, N., Trinidad, J. C., Cary, M. P., Burlingame, A. L., & Kenyon, C. (2010). Widespread protein aggregation as an inherent part of aging in C. elegans. *PLoS Biol, 8*(8), e1000450. doi:10.1371/journal.pbio.1000450

Di Cara, F., Sheshachalam, A., Braverman, N. E., Rachubinski, R. A., & Simmonds, A. J. (2017). Peroxisome-Mediated Metabolism Is Required for Immune Response to Microbial Infection. *Immunity, 47*(1), 93-106.e107. doi:10.1016/j.immuni.2017.06.016

Dobin, A., Davis, C. A., Schlesinger, F., Drenkow, J., Zaleski, C., Jha, S., . . . Gingeras, T. R. (2013). STAR: ultrafast universal RNA-seq aligner. *Bioinformatics, 29*(1), 15-21. doi:10.1093/bioinformatics/bts635

Dues, D. J., Andrews, E. K., Schaar, C. E., Bergsma, A. L., Senchuk, M. M., & Van Raamsdonk, J. M. (2016). Aging causes decreased resistance to multiple stresses and a failure to activate specific stress response pathways. *Aging (Albany NY), 8*(4), 777-795. doi:10.18632/aging.100939

Dukan, S., Farewell, A., Ballesteros, M., Taddei, F., Radman, M., & Nyström, T. (2000). Protein oxidation in response to increased transcriptional or translational errors. *Proc Natl Acad Sci U S A, 97*(11), 5746-5749. doi:10.1073/pnas.100422497

Eldakak, A., Rancati, G., Rubinstein, B., Paul, P., Conaway, V., & Li, R. (2010). Asymmetrically inherited multidrug resistance transporters are recessive determinants in cellular replicative ageing. *Nat Cell Biol, 12*(8), 799-805. doi:10.1038/ncb2085

ELLMAN, G. L. (1959). Tissue sulfhydryl groups. *Arch Biochem Biophys, 82*(1), 70-77.

Ferrington, D. A., Husom, A. D., & Thompson, L. V. (2005). Altered proteasome structure, function, and oxidation in aged muscle. *FASEB J, 19*(6), 644-646. doi:10.1096/fj.04-2578fje

Finkel, T., & Holbrook, N. J. (2000). Oxidants, oxidative stress and the biology of ageing. *Nature, 408*(6809), 239-247. doi:10.1038/35041687

Fransen, M., Nordgren, M., Wang, B., & Apanasets, O. (2012). Role of peroxisomes in ROS/RNS-metabolism: implications for human disease. *Biochim Biophys Acta, 1822*(9), 1363-1373. doi:10.1016/j.bbadis.2011.12.001

Fransen, M., Nordgren, M., Wang, B., Apanasets, O., & Van Veldhoven, P. P. (2013). Aging, age-related diseases and peroxisomes. *Subcell Biochem, 69*, 45-65. doi:10.1007/978-94-007-6889-5_3

Gangloff, Y. G., Mueller, M., Dann, S. G., Svoboda, P., Sticker, M., Spetz, J. F., . . . Kozma, S. C. (2004). Disruption of the mouse mTOR gene leads to early postimplantation lethality and prohibits embryonic stem cell development. *Mol Cell Biol, 24*(21), 9508-9516. doi:10.1128/MCB.24.21.9508-9516.2004

Gershon, H., & Gershon, D. (2000). The budding yeast, Saccharomyces cerevisiae, as a model for aging research: a critical review. *Mech Ageing Dev, 120*(1-3), 1-22.

Ghag, G., Bhatt, N., Cantu, D. V., Guerrero-Munoz, M. J., Ellsworth, A., Sengupta, U., & Kayed, R. (2018). Soluble tau aggregates, not large fibrils, are the toxic species that display seeding and cross-seeding behavior. *Protein Sci, 27*(11), 1901-1909. doi:10.1002/pro.3499

Gietz, R. D., & Schiestl, R. H. (2007). High-efficiency yeast transformation using the LiAc/SS carrier DNA/PEG method. *Nat Protoc, 2*(1), 31-34. doi:10.1038/nprot.2007.13

Goldring, E. S., Grossman, L. I., & Marmur, J. (1971). Petite mutation in yeast. II. Isolation of mutants containing mitochondrial deoxyribonucleic acid of reduced size. *J Bacteriol, 107*(1), 377-381.

Goldstein, A. L., & McCusker, J. H. (1999). Three new dominant drug resistance cassettes for gene disruption in Saccharomyces cerevisiae. *Yeast, 15*(14), 1541-1553. doi:10.1002/(SICI)1097-0061(199910)15:14<1541::AID-YEA476>3.0.CO;2-K

Grune, T., Jung, T., Merker, K., & Davies, K. J. (2004). Decreased proteolysis caused by protein aggregates, inclusion bodies, plaques, lipofuscin, ceroid, and 'aggresomes' during oxidative stress, aging, and disease. *Int J Biochem Cell Biol, 36*(12), 2519-2530. doi:10.1016/j.biocel.2004.04.020

Hagenbuchner, J., Scholl-Buergi, S., Karall, D., & Ausserlechner, M. J. (2018). Very long-/ and long Chain-3-Hydroxy Acyl CoA Dehydrogenase Deficiency correlates with deregulation of the mitochondrial fusion/fission machinery. *Sci Rep, 8*(1), 3254. doi:10.1038/s41598-018-21519-2

Hamilton, W. D. (1966). The moulding of senescence by natural selection. *J Theor Biol, 12*(1), 12-45.

Hars, E. S., Qi, H., Ryazanov, A. G., Jin, S., Cai, L., Hu, C., & Liu, L. F. (2007). Autophagy regulates ageing in C. elegans. *Autophagy, 3*(2), 93-95. doi:10.4161/auto.3636

Hartl, F. U., & Hayer-Hartl, M. (2009). Converging concepts of protein folding in vitro and in vivo. *Nat Struct Mol Biol, 16*(6), 574-581. doi:10.1038/nsmb.1591

Hellemans, J., Mortier, G., De Paepe, A., Speleman, F., & Vandesompele, J. (2007). qBase relative quantification framework and software for management and automated analysis of real-time quantitative PCR data. *Genome Biol, 8*(2), R19. doi:10.1186/gb-2007-8-2-r19

Hercus, M. J., Loeschcke, V., & Rattan, S. I. (2003). Lifespan extension of Drosophila melanogaster through hormesis by repeated mild heat stress. *Biogerontology, 4*(3), 149-156.

Hill, S. M., Hao, X., Liu, B., & Nyström, T. (2014). Life-span extension by a metacaspase in the yeast Saccharomyces cerevisiae. *Science, 344*(6190), 1389-1392. doi:10.1126/science.1252634

https://wiki.yeastgenome.org/. (2018). Retrieved from https://wiki.yeastgenome.org/

Huber, W., Carey, V. J., Gentleman, R., Anders, S., Carlson, M., Carvalho, B. S., . . . Morgan, M. (2015). Orchestrating high-throughput genomic analysis with Bioconductor. *Nat Methods, 12*(2), 115-121. doi:10.1038/nmeth.3252

Jang, J. Y., Blum, A., Liu, J., & Finkel, T. (2018). The role of mitochondria in aging. *J Clin Invest, 128*(9), 3662-3670. doi:10.1172/JCI120842

Janssens, G. E., & Veenhoff, L. M. (2016). Evidence for the hallmarks of human aging in replicatively aging yeast. *Microb Cell, 3*(7), 263-274. doi:10.15698/mic2016.07.510

Johnson, S. C., Rabinovitch, P. S., & Kaeberlein, M. (2013). mTOR is a key modulator of ageing and age-related disease. *Nature, 493*(7432), 338-345. doi:10.1038/nature11861

Johnson, T. E., Mitchell, D. H., Kline, S., Kemal, R., & Foy, J. (1984). Arresting development arrests aging in the nematode Caenorhabditis elegans. *Mech Ageing Dev, 28*(1), 23-40.

Kaeberlein, M., Powers, R. W., Steffen, K. K., Westman, E. A., Hu, D., Dang, N., . . . Kennedy, B. K. (2005). Regulation of yeast replicative life span by TOR and Sch9 in response to nutrients. *Science, 310*(5751), 1193-1196. doi:10.1126/science.1115535

Kaganovich, D., Kopito, R., & Frydman, J. (2008). Misfolded proteins partition between two distinct quality control compartments. *Nature, 454*(7208), 1088-1095. doi:10.1038/nature07195

Kamada, Y., Funakoshi, T., Shintani, T., Nagano, K., Ohsumi, M., & Ohsumi, Y. (2000). Tor-mediated induction of autophagy via an Apg1 protein kinase complex. *J Cell Biol, 150*(6), 1507-1513. doi:10.1083/jcb.150.6.1507

Kauppila, T. E. S., Kauppila, J. H. K., & Larsson, N. G. (2017). Mammalian Mitochondria and Aging: An Update. *Cell Metab, 25*(1), 57-71. doi:10.1016/j.cmet.2016.09.017

Kenyon, C. (2011). The first long-lived mutants: discovery of the insulin/IGF-1 pathway for ageing. *Philos Trans R Soc Lond B Biol Sci, 366*(1561), 9-16. doi:10.1098/rstb.2010.0276

Kenyon, C. J. (2010). The genetics of ageing. *Nature, 464*(7288), 504-512. doi:10.1038/nature08980

Kim, H. E., Grant, A. R., Simic, M. S., Kohnz, R. A., Nomura, D. K., Durieux, J., . . . Dillin, A. (2016). Lipid Biosynthesis Coordinates a Mitochondrial-to-Cytosolic Stress Response. *Cell, 166*(6), 1539-1552.e1516. doi:10.1016/j.cell.2016.08.027

Koga, H., Kaushik, S., & Cuervo, A. M. (2011). Protein homeostasis and aging: The importance of exquisite quality control. *Ageing Res Rev, 10*(2), 205-215. doi:10.1016/j.arr.2010.02.001

Kostál, V. (2006). Eco-physiological phases of insect diapause. *J Insect Physiol, 52*(2), 113-127. doi:10.1016/j.jinsphys.2005.09.008

Krisko, A., & Radman, M. (2010). Protein damage and death by radiation in Escherichia coli and Deinococcus radiodurans. *Proc Natl Acad Sci U S A, 107*(32), 14373-14377. doi:10.1073/pnas.1009312107

Krisko, A., & Radman, M. (2013). Phenotypic and genetic consequences of protein damage. *PLoS Genet, 9*(9), e1003810. doi:10.1371/journal.pgen.1003810

Krisko, A., & Radman, M. (2019). Protein damage, ageing and age-related diseases. *Open Biol, 9*(3), 180249. doi:10.1098/rsob.180249

Kumsta, C., Chang, J. T., Schmalz, J., & Hansen, M. (2017). Hormetic heat stress and HSF-1 induce autophagy to improve survival and proteostasis in C. elegans. *Nat Commun, 8*, 14337. doi:10.1038/ncomms14337

Kurtz, S., Rossi, J., Petko, L., & Lindquist, S. (1986). An ancient developmental induction: heat-shock proteins induced in sporulation and oogenesis. *Science, 231*(4742), 1154-1157.

Labbadia, J., & Morimoto, R. I. (2014). Proteostasis and longevity: when does aging really begin? *F1000Prime Rep, 6*, 7. doi:10.12703/P6-7

Labbadia, J., & Morimoto, R. I. (2015a). Repression of the Heat Shock Response Is a Programmed Event at the Onset of Reproduction. *Mol Cell, 59*(4), 639-650. doi:10.1016/j.molcel.2015.06.027

Labbadia, J., & Morimoto, R. I. (2015b). The biology of proteostasis in aging and disease. *Annu Rev Biochem, 84*, 435-464. doi:10.1146/annurev-biochem-060614-033955

Lee, C. K., Klopp, R. G., Weindruch, R., & Prolla, T. A. (1999). Gene expression profile of aging and its retardation by caloric restriction. *Science, 285*(5432), 1390-1393.

Ley, K. (2018). *Inflammation: Fundamental Mechanisms* (1 edition ed.): World Scientific Publishing Co Pte Ltd.

Lindquist, S. (1980). Varying patterns of protein synthesis in Drosophila during heat shock: implications for regulation. *Dev Biol, 77*(2), 463-479.

Lindquist, S. (1986). The heat-shock response. *Annu Rev Biochem, 55*, 1151-1191. doi:10.1146/annurev.bi.55.070186.005443

Love, M. I., Huber, W., & Anders, S. (2014). Moderated estimation of fold change and dispersion for RNA-seq data with DESeq2. *Genome Biol, 15*(12), 550. doi:10.1186/s13059-014-0550-8

López-Martínez, G., & Hahn, D. A. (2014). Early life hormetic treatments decrease irradiation-induced oxidative damage, increase longevity, and enhance sexual performance during old age in the Caribbean fruit fly. *PLoS One, 9*(1), e88128. doi:10.1371/journal.pone.0088128

López-Otín, C., Blasco, M. A., Partridge, L., Serrano, M., & Kroemer, G. (2013). The hallmarks of aging. *Cell, 153*(6), 1194-1217. doi:10.1016/j.cell.2013.05.039

Ma, X. M., & Blenis, J. (2009). Molecular mechanisms of mTOR-mediated translational control. *Nat Rev Mol Cell Biol, 10*(5), 307-318. doi:10.1038/nrm2672

Mackenzie, I. R., Bigio, E. H., Ince, P. G., Geser, F., Neumann, M., Cairns, N. J., . . . Trojanowski, J. Q. (2007). Pathological TDP-43 distinguishes sporadic amyotrophic lateral sclerosis from amyotrophic lateral sclerosis with SOD1 mutations. *Ann Neurol, 61*(5), 427-434. doi:10.1002/ana.21147

Matecic, M., Smith, D. L., Pan, X., Maqani, N., Bekiranov, S., Boeke, J. D., & Smith, J. S. (2010). A microarray-based genetic screen for yeast chronological aging factors. *PLoS Genet, 6*(4), e1000921. doi:10.1371/journal.pgen.1000921

Mendillo, M. L., Santagata, S., Koeva, M., Bell, G. W., Hu, R., Tamimi, R. M., . . . Lindquist, S. (2012). HSF1 drives a transcriptional program distinct from heat shock to support highly malignant human cancers. *Cell, 150*(3), 549-562. doi:10.1016/j.cell.2012.06.031

Morimoto, R. I. (2011). The heat shock response: systems biology of proteotoxic stress in aging and disease. *Cold Spring Harb Symp Quant Biol, 76*, 91-99. doi:10.1101/sqb.2012.76.010637

Murakami, M., Ichisaka, T., Maeda, M., Oshiro, N., Hara, K., Edenhofer, F., . . . Yamanaka, S. (2004). mTOR is essential for growth and proliferation in early mouse embryos and embryonic stem cells. *Mol Cell Biol, 24*(15), 6710-6718. doi:10.1128/MCB.24.15.6710-6718.2004

Musa, M., Perić, M., Bou Dib, P., Sobočanec, S., Šarić, A., Lovrić, A., . . . Kriško, A. (2018). Heat-induced longevity in budding yeast requires respiratory metabolism and glutathione recycling. *Aging (Albany NY), 10*(9), 2407-2427. doi:10.18632/aging.101560

Musa, M., Radman, M., & Krisko, A. (2016). Decreasing translation error rate in Escherichia coli increases protein function. *BMC Biotechnol, 16*, 28. doi:10.1186/s12896-016-0259-8

Nixon, R. A. (2013). The role of autophagy in neurodegenerative disease. *Nat Med, 19*(8), 983-997. doi:10.1038/nm.3232

Ogrodnik, M., Salmonowicz, H., Brown, R., Turkowska, J., Średniawa, W., Pattabiraman, S., . . . Kaganovich, D. (2014). Dynamic JUNQ inclusion bodies are asymmetrically inherited in mammalian cell lines through the asymmetric partitioning of vimentin. *Proc Natl Acad Sci U S A, 111*(22), 8049-8054. doi:10.1073/pnas.1324035111

Ozawa, T. (1997). Genetic and functional changes in mitochondria associated with aging. *Physiol Rev, 77*(2), 425-464. doi:10.1152/physrev.1997.77.2.425

Pan, Y., Schroeder, E. A., Ocampo, A., Barrientos, A., & Shadel, G. S. (2011). Regulation of yeast chronological life span by TORC1 via adaptive mitochondrial ROS signaling. *Cell Metab, 13*(6), 668-678. doi:10.1016/j.cmet.2011.03.018

Pan, Y., & Shadel, G. S. (2009). Extension of chronological life span by reduced TOR signaling requires down-regulation of Sch9p and involves increased mitochondrial OXPHOS complex density. *Aging (Albany NY), 1*(1), 131-145. doi:10.18632/aging.100016

Papsdorf, K., & Brunet, A. (2018). Linking Lipid Metabolism to Chromatin Regulation in Aging. *Trends Cell Biol*. doi:10.1016/j.tcb.2018.09.004

Perisic, O., Xiao, H., & Lis, J. T. (1989). Stable binding of Drosophila heat shock factor to head-to-head and tail-to-tail repeats of a conserved 5 bp recognition unit. *Cell, 59*(5), 797-806.

Perić, M., Bou Dib, P., Dennerlein, S., Musa, M., Rudan, M., Lovrić, A., . . . Kriško, A. (2016). Crosstalk between cellular compartments protects against proteotoxicity and extends lifespan. *Sci Rep, 6*, 28751. doi:10.1038/srep28751

Perić, M., Lovrić, A., Šarić, A., Musa, M., Bou Dib, P., Rudan, M., . . . Kriško, A. (2017). TORC1-mediated sensing of chaperone activity alters glucose metabolism and extends lifespan. *Aging Cell, 16*(5), 994-1005. doi:10.1111/acel.12623

Perluigi, M., Coccia, R., & Butterfield, D. A. (2012). 4-Hydroxy-2-nonenal, a reactive product of lipid peroxidation, and neurodegenerative diseases: a toxic combination illuminated by redox proteomics studies. *Antioxid Redox Signal, 17*(11), 1590-1609. doi:10.1089/ars.2011.4406

Petriv, O. I., & Rachubinski, R. A. (2004). Lack of peroxisomal catalase causes a progeric phenotype in Caenorhabditis elegans. *J Biol Chem, 279*(19), 19996-20001. doi:10.1074/jbc.M400207200

Prahlad, V., Cornelius, T., & Morimoto, R. I. (2008). Regulation of the cellular heat shock response in Caenorhabditis elegans by thermosensory neurons. *Science, 320*(5877), 811-814. doi:10.1126/science.1156093

Rahman, M. M., Sykiotis, G. P., Nishimura, M., Bodmer, R., & Bohmann, D. (2013). Declining signal dependence of Nrf2-MafS-regulated gene expression correlates with aging phenotypes. *Aging Cell, 12*(4), 554-562. doi:10.1111/acel.12078

Rattan, S. I., & Demirovic, D. (2009). Hormesis can and does work in humans. *Dose Response, 8*(1), 58-63. doi:10.2203/dose-response.09-041.Rattan

Richter, K., Haslbeck, M., & Buchner, J. (2010). The heat shock response: life on the verge of death. *Mol Cell, 40*(2), 253-266. doi:10.1016/j.molcel.2010.10.006

Robida-Stubbs, S., Glover-Cutter, K., Lamming, D. W., Mizunuma, M., Narasimhan, S. D., Neumann-Haefelin, E., . . . Blackwell, T. K. (2012). TOR signaling and rapamycin influence longevity by regulating SKN-1/Nrf and DAF-16/FoxO. *Cell Metab, 15*(5), 713-724. doi:10.1016/j.cmet.2012.04.007

Rosenbloom, K. R., Armstrong, J., Barber, G. P., Casper, J., Clawson, H., Diekhans, M., . . . Kent, W. J. (2015). The UCSC Genome Browser database: 2015 update. *Nucleic Acids Res, 43*(Database issue), D670-681. doi:10.1093/nar/gku1177

Saarikangas, J., & Barral, Y. (2015). Protein aggregates are associated with replicative aging without compromising protein quality control. *Elife, 4*. doi:10.7554/eLife.06197

Saarikangas, J., & Barral, Y. (2016). Protein aggregation as a mechanism of adaptive cellular responses. *Curr Genet, 62*(4), 711-724. doi:10.1007/s00294-016-0596-0

Saarikangas, J., Caudron, F., Prasad, R., Moreno, D. F., Bolognesi, A., Aldea, M., & Barral, Y. (2017). Compartmentalization of ER-Bound Chaperone Confines Protein Deposit Formation to the Aging Yeast Cell. *Curr Biol, 27*(6), 773-783. doi:10.1016/j.cub.2017.01.069

Saez, I., & Vilchez, D. (2015). Protein clearance mechanisms and their demise in age-related neurodegenerative diseases. *AIMS Molecular Science, 2*(1). doi:10.3934/molsci.2015.1.1

Sanchez, Y., Taulien, J., Borkovich, K. A., & Lindquist, S. (1992). Hsp104 is required for tolerance to many forms of stress. *EMBO J, 11*(6), 2357-2364.

Santagata, S., Hu, R., Lin, N. U., Mendillo, M. L., Collins, L. C., Hankinson, S. E., . . . Ince, T. A. (2011). High levels of nuclear heat-shock factor 1 (HSF1) are associated with poor prognosis in breast cancer. *Proc Natl Acad Sci U S A, 108*(45), 18378-18383. doi:10.1073/pnas.1115031108

Santagata, S., Mendillo, M. L., Tang, Y. C., Subramanian, A., Perley, C. C., Roche, S. P., . . . Lindquist, S. (2013). Tight coordination of protein translation and HSF1 activation supports the anabolic malignant state. *Science, 341*(6143), 1238303. doi:10.1126/science.1238303

Scott, B. R., Bruce, V. R., Gott, K. M., Wilder, J., & March, T. (2012). Small γ-Ray Doses Prevent Rather than Increase Lung Tumors in Mice. *Dose Response, 10*(4), 527-540. doi:10.2203/dose-response.12-035.Scott

Semchyshyn, H. M., & Valishkevych, B. V. (2016). Hormetic Effect of H2O2 in Saccharomyces cerevisiae: Involvement of TOR and Glutathione Reductase. *Dose Response, 14*(2), 1559325816636130. doi:10.1177/1559325816636130

Shama, S., Kirchman, P. A., Jiang, J. C., & Jazwinski, S. M. (1998). Role of RAS2 in recovery from chronic stress: effect on yeast life span. *Exp Cell Res, 245*(2), 368-378. doi:10.1006/excr.1998.4276

Shama, S., Lai, C. Y., Antoniazzi, J. M., Jiang, J. C., & Jazwinski, S. M. (1998). Heat stress-induced life span extension in yeast. *Exp Cell Res, 245*(2), 379-388. doi:10.1006/excr.1998.4279

Shcheprova, Z., Baldi, S., Frei, S. B., Gonnet, G., & Barral, Y. (2008). A mechanism for asymmetric segregation of age during yeast budding. *Nature, 454*(7205), 728-734. doi:10.1038/nature07212

Shemesh, N., Shai, N., & Ben-Zvi, A. (2013). Germline stem cell arrest inhibits the collapse of somatic proteostasis early in Caenorhabditis elegans adulthood. *Aging Cell, 12*(5), 814-822. doi:10.1111/acel.12110

Shore, D. E., Carr, C. E., & Ruvkun, G. (2012). Induction of cytoprotective pathways is central to the extension of lifespan conferred by multiple longevity pathways. *PLoS Genet, 8*(7), e1002792. doi:10.1371/journal.pgen.1002792

Sies, H. (1985). *Oxidative stress: introductory remarks* (H. Sies Ed.). London: Academic.

Sies, H., Berndt, C., & Jones, D. P. (2017). Oxidative Stress. *Annu Rev Biochem, 86*, 715-748. doi:10.1146/annurev-biochem-061516-045037

Simonsen, A., Cumming, R. C., Brech, A., Isakson, P., Schubert, D. R., & Finley, K. D. (2008). Promoting basal levels of autophagy in the nervous system enhances longevity and oxidant resistance in adult Drosophila. *Autophagy, 4*(2), 176-184. doi:10.4161/auto.5269

Sinclair, D. A., & Guarente, L. (1997). Extrachromosomal rDNA circles--a cause of aging in yeast. *Cell, 91*(7), 1033-1042.

Sohal, R. S., & Brunk, U. T. (1992). Mitochondrial production of pro-oxidants and cellular senescence. *Mutat Res, 275*(3-6), 295-304.

Sohal, R. S., & Sohal, B. H. (1991). Hydrogen peroxide release by mitochondria increases during aging. *Mech Ageing Dev, 57*(2), 187-202.

Sulston, J. E., & Horvitz, H. R. (1977). Post-embryonic cell lineages of the nematode, Caenorhabditis elegans. *Dev Biol, 56*(1), 110-156.

Szostak, J. W., & Wu, R. (1980). Unequal crossing over in the ribosomal DNA of Saccharomyces cerevisiae. *Nature, 284*(5755), 426-430.

Takasawa, M., Hayakawa, M., Sugiyama, S., Hattori, K., Ito, T., & Ozawa, T. (1993). Age-associated damage in mitochondrial function in rat hearts. *Exp Gerontol, 28*(3), 269-280.

Tanaka, K., & Matsuda, N. (2014). Proteostasis and neurodegeneration: the roles of proteasomal degradation and autophagy. *Biochim Biophys Acta, 1843*(1), 197-204. doi:10.1016/j.bbamcr.2013.03.012

Tomaru, U., Takahashi, S., Ishizu, A., Miyatake, Y., Gohda, A., Suzuki, S., . . . Kasahara, M. (2012). Decreased proteasomal activity causes age-related phenotypes and promotes the development of metabolic abnormalities. *Am J Pathol, 180*(3), 963-972. doi:10.1016/j.ajpath.2011.11.012

Tóth, M. L., Sigmond, T., Borsos, E., Barna, J., Erdélyi, P., Takács-Vellai, K., . . . Vellai, T. (2008). Longevity pathways converge on autophagy genes to regulate life span in Caenorhabditis elegans. *Autophagy, 4*(3), 330-338. doi:10.4161/auto.5618

Valente, A. J., Maddalena, L. A., Robb, E. L., Moradi, F., & Stuart, J. A. (2017). A simple ImageJ macro tool for analyzing mitochondrial network morphology in mammalian cell culture. *Acta Histochem, 119*(3), 315-326. doi:10.1016/j.acthis.2017.03.001

Van Raamsdonk, J. M., & Hekimi, S. (2009). Deletion of the mitochondrial superoxide dismutase sod-2 extends lifespan in Caenorhabditis elegans. *PLoS Genet, 5*(2), e1000361. doi:10.1371/journal.pgen.1000361

Van Raamsdonk, J. M., & Hekimi, S. (2010). Reactive Oxygen Species and Aging in Caenorhabditis elegans: Causal or Casual Relationship? *Antioxid Redox Signal, 13*(12), 1911-1953. doi:10.1089/ars.2010.3215

Vanneste, J., & van den Bosch de Aguilar, P. (1981). Mitochondrial alterations in the spinal ganglion neurons in ageing rats. *Acta Neuropathol, 54*(1), 83-87.
Vernace, V. A., Arnaud, L., Schmidt-Glenewinkel, T., & Figueiredo-Pereira, M. E. (2007). Aging perturbs 26S proteasome assembly in Drosophila melanogaster. *FASEB J, 21*(11), 2672-2682. doi:10.1096/fj.06-6751com
Vihervaara, A., & Sistonen, L. (2014). HSF1 at a glance. *J Cell Sci, 127*(Pt 2), 261-266. doi:10.1242/jcs.132605
Vowinckel, J., Hartl, J., Butler, R., & Ralser, M. (2015). MitoLoc: A method for the simultaneous quantification of mitochondrial network morphology and membrane potential in single cells. *Mitochondrion, 24*, 77-86. doi:10.1016/j.mito.2015.07.001
Wallner, S., & Schmitz, G. (2011). Plasmalogens the neglected regulatory and scavenging lipid species. *Chem Phys Lipids, 164*(6), 573-589. doi:10.1016/j.chemphyslip.2011.06.008
Watts, J. L., & Browse, J. (2000). A palmitoyl-CoA-specific delta9 fatty acid desaturase from Caenorhabditis elegans. *Biochem Biophys Res Commun, 272*(1), 263-269. doi:10.1006/bbrc.2000.2772
Wei, M., Fabrizio, P., Madia, F., Hu, J., Ge, H., Li, L. M., & Longo, V. D. (2009). Tor1/Sch9-regulated carbon source substitution is as effective as calorie restriction in life span extension. *PLoS Genet, 5*(5), e1000467. doi:10.1371/journal.pgen.1000467
Westerheide, S. D., Anckar, J., Stevens, S. M., Sistonen, L., & Morimoto, R. I. (2009). Stress-inducible regulation of heat shock factor 1 by the deacetylase SIRT1. *Science, 323*(5917), 1063-1066. doi:10.1126/science.1165946
Whitesell, L., & Lindquist, S. (2009). Inhibiting the transcription factor HSF1 as an anticancer strategy. *Expert Opin Ther Targets, 13*(4), 469-478. doi:10.1517/14728220902832697
Whitesell, L., Santagata, S., Mendillo, M. L., Lin, N. U., Proia, D. A., & Lindquist, S. (2014). HSP90 empowers evolution of resistance to hormonal therapy in human breast cancer models. *Proc Natl Acad Sci U S A, 111*(51), 18297-18302. doi:10.1073/pnas.1421323111
Williams, P. D., Pollock, D. D., & Goldstein, R. A. (2007). Functionality and the evolution of marginal stability in proteins: inferences from lattice simulations. *Evol Bioinform Online, 2*, 91-101.
Wong, P., & Houry, W. A. (2004). Chaperone networks in bacteria: analysis of protein homeostasis in minimal cells. *J Struct Biol, 146*(1-2), 79-89. doi:10.1016/j.jsb.2003.11.006
Yanase, S., Onodera, A., Tedesco, P., Johnson, T. E., & Ishii, N. (2009). SOD-1 deletions in Caenorhabditis elegans alter the localization of intracellular reactive oxygen species and show molecular compensation. *J Gerontol A Biol Sci Med Sci, 64*(5), 530-539. doi:10.1093/gerona/glp020
Yang, W., & Hekimi, S. (2010). A mitochondrial superoxide signal triggers increased longevity in Caenorhabditis elegans. *PLoS Biol, 8*(12), e1000556. doi:10.1371/journal.pbio.1000556
Yang, W., Li, J., & Hekimi, S. (2007). A Measurable increase in oxidative damage due to reduction in superoxide detoxification fails to shorten the life span of long-lived mitochondrial mutants of Caenorhabditis elegans. *Genetics, 177*(4), 2063-2074. doi:10.1534/genetics.107.080788
Zhang, B., Gong, J., Zhang, W., Xiao, R., Liu, J., & Xu, X. Z. S. (2018). Brain-gut communications via distinct neuroendocrine signals bidirectionally regulate longevity in C. elegans. *Genes Dev, 32*(3-4), 258-270. doi:10.1101/gad.309625.117

CURRICULUM VITAE

MARINA MUSA

EDUCATION

Doctoral Program – Biophysics.....2013 – 2019
University of Split, Croatia

Bachelor of Arts in Biology..... 2012
Grinnell College - Iowa, USA

International Baccalaureate.....2008
United World College in Mostar - Bosnia and Herzegovina (2006- 2008)
Gimnazija Fra Grge Martića - Bosnia and Herzegovina (2004- 2006)

WORK EXPERIENCE

Researcher
Mediterranean Institute for Life Science.....2013 - 2019
Group: Molecular basis of aging

FELLOWSHIPS

FEBS short term fellowship
European Institute for Neuroscience.....April 2018 - May 2018

EMBO short term fellowship
Universitätsmedizin Göttingen/European Institute for Neuroscience …....January 2017 - March 2017

ERASMUS +
Universitätsmedizin Göttingen.....July 2016 - November 2016

RESEARCH TOPICS

- Cellular stress response pathways
- Mechanisms of aging

PUBLICATIONS

1. **Musa M***, Perić M*, Bou Dib P, Sobočanec S, Šarić A, Lovrić A, Rudan M, Nikolić A, Milošević I, Vlahoviček K, Raimundo N & Kriško A (2018) Heat-induced longevity in budding yeast requires the crosstalk between respiratory metabolism and glutathione recycling. Aging, 10, 2407-2427. (* equal contribution)

2. Rudan M, Bou Dib P, **Musa M**, Kanunnikau M, Sobočanec S, Rueda D, Warnecke T & Kriško A (2018) Normal mitochondrial function in Saccharomyces cerevisiae has become dependent on inefficient splicing. Elife 7, 35330.

3. Perić M, Lovrić A, **Musa M**, Bou Dib P, Rudan M, Nikolić A, Sobočanec S, Mikecin A, Dennerlein S, Milošević I, Vlahoviček K, Raimundo N & Kriško A (2017) TORC1-mediated sensing of chaperone activity alters glucose metabolism and extends lifespan. *Aging Cell* 16, 994-1005.

4. **Musa M**, Radman M & Kriško A (2016) Decreasing translation error rate in Escherichia coli increases protein function. *BMC Biotechnol* 16, 28.

5. Mačak Šafranko Ž, Balog T, **Musa M,** Tartaro Buljak I & Sobočanec S (2016) The effect of 17β-estradiol on sex-dimorphic cytochrome P450 expression patterns induced by hyperoxia in the liver of male CBA/H mice. *Mol Cell Biochem* 421,183-91.

6. Perić M, Bou Dib P, Dennerlein S, **Musa M**, Rudan M, Lovrić A, Nikolić A, Šarić A, Sobočanec S, Mačak Ž, Raimundo N & Kriško A (2016) Crosstalk between cellular compartments protects against proteotoxicity and extends lifespan. *Sci Rep* 6, 28751.